THE UNIVERSITY OF QUEENSLAND

AUSTRALIA

Investigating neural connectivity of corticomotor networks in ataxia-telangiectasia: Improving our understanding of the clinical phenotype

Ishani Sachintha Sahama

BSc, BSc (Hons)

A thesis submitted for the degree of Doctor of Philosophy at
The University of Queensland in 2015

The University of Queensland School of Medicine

Abstract

The human genetic disorder ataxia-telangiectasia (A-T) is an autosomal recessive neurodegenerative condition occurring in 3 per million live births. The disease is characterised by neurodegeneration, immunodeficiency, radiosensitivity, cell cycle checkpoint defects, genomic instability and cancer predisposition among patients. The most debilitating aspect of the disease is progressive cerebellar ataxia, which represents the hallmark neuropathological condition of A-T.

At present, long term therapy to cure or prevent progressive symptoms of A-T are not currently available. While short term treatment to alleviate symptoms associated with immunodeficiency and deficient lung function are available to patients, the predisposition to cancer and the progressive neurodegeneration associated with A-T cannot be prevented with such efforts. To gain a more informed understanding of the A-T condition, research has focused on clinical, genetic and immunological aspects of the disorder; however, minimal attention has been directed towards identifying altered brain structure and function using imaging modalities such as magnetic resonance imaging (MRI).

Imaging studies in A-T are limited to structural MRI imaging, where various radiological anomalies in patients are reported as clinical case studies. While these studies provide a detailed focus on the morphological and histopathological conditions of A-T, they provide limited insight into the mechanisms of neurodegeneration and loss of neural motor network connectivity among patients. In other ataxic diseases such as Friedrich's ataxia and spinocerebellar ataxia, the use of high-resolution MRI and diffusion-weighted imaging (DWI) has given valuable insight into the microstructural tissue environment, and the loss of white matter integrity of motor networks due to abnormal neurodevelopmental and/or progressive neurodegenerative conditions associated with the disease. Such imaging approaches have not yet been extended to the study of A-T, and could provide important new information regarding the relationship between the ataxia-telangiectasia gene mutation (ATM) and loss of motor pathway integrity in A-T patients.

The key objective of this PhD programme was to investigate white matter integrity and grey matter volume changes associated with A-T using a combination of structural MRI and diffusion-weighted imaging, to pinpoint potential neurodegenerative biomarkers that can be targeted for therapeutic use among young A-T patients. Performing diffusion imaging in children with A-T presents a significant challenge, as spontaneous movement at resting positions form part of the A-T condition, and non-sedated imaging procedures will contribute to excessive motion artefact and limited image quality in diffusion-weighted images. To effectively detect and correct for motion artefacts, a series of data pre-processing and correction steps were introduced to the DWI processing pipeline of A-T images in this project. Whole brain imaging analysis, specifically voxel-based morphometry (based on structural MRI) was applied to interrogate and compare grey matter volume in young A-T patients and typically developing age-matched control participants as a preliminary starting point in uncovering neurodegenerative biomarkers in A-T. Tract-based spatial statistics (based on diffusion MRI) was employed to elucidate the white matter microstructure differences between groups, using the diffusion metrics fractional anisotropy (FA) and mean diffusivity (MD) as quantitative measures of tissue integrity. Voxel-wise analyses revealed reduced cerebellar grey matter volume and white matter tract degeneration in pathways projecting from the cerebellum into corticomotor regions among young A-T patients, indicating the need to focus on the corticomotor system in A-T.

To assess white matter degeneration quantitatively in A-T corticomotor pathways, white matter fibre tracking and along tract statistical analyses were used to assess FA and MD differences along the length of cortico-ponto-cerebellar, cerebellar-thalamo-cortical, somatosensory and lateral corticospinal pathways between controls and patients. Significant differences in FA and MD were observed along the length of all patient tracts, particularly in locations pertaining to the pre- and postcentral gyrus, thalamus, medial and superior cerebellar peduncles and the spinal cord, suggestive of comprehensive motor pathway degeneration in young A-T patients.

Despite numerous histopathological and anatomical studies of degeneration in A-T, the pattern of A-T neurodegeneration over time has not been effectively captured. To this end, serial analysis using structural MRI, whole brain imaging methodology and automated volumetric analysis of the basal ganglia (caudate and putamen), thalamus and cerebellum were conducted in A-T MRI data sets spanning two years. Significant changes in white and grey matter integrity were absent in the A-T longitudinal data, however concurrent use of the A-T Neuro Examination Scale Toolkit (A-T NEST) clinical scores during the imaging time frame revealed loss in clinical motor functional scores for some participants, indicating neurodegenerative change in early stages of A-T. These findings highlight the need for high-resolution images to capture significant early neurodegenerative changes

in the A-T cohort. In addition, the inclusion of the spinal cord, a prominent area of A-T pathology, for study, and the incorporation of a larger, international collaborative cohort for imaging analysis should be considered in future A-T imaging studies.

Declaration by author

This thesis is composed of my original work, and contains no material previously published or written by another person except where due reference has been made in the text. I have clearly stated the contribution by others to jointly-authored works that I have included in my thesis.

I have clearly stated the contribution of others to my thesis as a whole, including statistical assistance, survey design, data analysis, significant technical procedures, professional editorial advice, and any other original research work used or reported in my thesis. The content of my thesis is the result of work I have carried out since the commencement of my research higher degree candidature and does not include a substantial part of work that has been submitted to qualify for the award of any other degree or diploma in any university or other tertiary institution. I have clearly stated which parts of my thesis, if any, have been submitted to qualify for another award.

I acknowledge that an electronic copy of my thesis must be lodged with the University Library and, subject to the policy and procedures of The University of Queensland, the thesis be made available for research and study in accordance with the Copyright Act 1968 unless a period of embargo has been approved by the Dean of the Graduate School.

I acknowledge that copyright of all material contained in my thesis resides with the copyright holder(s) of that material. Where appropriate I have obtained copyright permission from the copyright holder to reproduce material in this thesis.

Publications during candidature

Peer-reviewed journal papers

Sahama I, Sinclair K, Pannek K, Lavin M, Rose S. Radiological imaging in ataxia-telangiectasia: a review. Cerebellum 2014;13(4):521-530. Impact Factor (IF) = 2.595; Citations = 6.

Sahama I, Sinclair K, Fiori S, Pannek K, Lavin M, Rose S. Altered corticomotor-cerebellar integrity in young ataxia-telangiectasia patients. Movement Disorders : official journal of the Movement Disorder Society 2014;29(10):1289-1298. Impact Factor (IF) = 4.558; Citations = 3.

Sahama I, Sinclair K, Fiori S, Doecke J, Pannek K, Reid L, Lavin M, Rose S. Motor pathway degeneration in young ataxia-telangiectasia patients: A diffusion tractography study. NeuroImage Clinical 2015;9:206-215. Impact Factor (IF) = 2.526.

Journal papers under peer-review

Sahama I, Sinclair K, Fripp J, Pannek K, Lavin M, Rose S. Serial investigation of neurodegeneration in young ataxia-telangiectasia patients. Submitted to Paediatric Neurology. Impact Factor (IF) = 1.695.

Conference abstracts and presentations

Sahama I, Sinclair K, Fiori S, Pannek K, Reid L, Lavin M, Rose S. Altered corticomotor-cerebellar integrity in young patients. Bi-Annual Ataxia-telangiectasia Clinical Research Conference. Nijmegen, Netherlands, 2014.

Publications included in this thesis

Peer-reviewed journal papers

Chapter 2:

Sahama I, Sinclair K, Pannek K, Lavin M, Rose S. Radiological imaging in ataxia-telangiectasia: a review. Cerebellum 2014;13(4):521-530. Impact Factor (IF) = 2.595; Citations = 6.

	IS	KS	KP	ML	SER
Conception and design of project	20%	25%	5%	25%	25%
Collection of data					
Analysis of data					
Interpretation of results					
Drafting of article	100%				
Critical revision of article for intellectual input		10%	10%	25%	55%

Chapter 3:

Sahama I, Sinclair K, Fiori S, Pannek K, Lavin M, Rose S. Altered corticomotor-cerebellar integrity in young ataxia-telangiectasia patients. Movement Disorders : official journal of the Movement Disorder Society 2014;29(10):1289-1298. Impact Factor (IF) = 4.558; Citations = 3.

	IS	KS	SF	KP	ML	SER
Conception and design of project	30%			20%		50%
Collection of data	90%			5%		5%
Analysis of data	100%					
Interpretation of results	50%	5%	25%	5%		15%
Drafting of article	100%					
Critical revision of article for intellectual input		10%	15%	10%	10%	55%

Chapter 4: Sahama I, Sinclair K, Fiori S, Doecke J, Pannek K, Reid L, Lavin M, Rose S. Motor pathway degeneration in young ataxia-telangiectasia patients: A diffusion tractography study. NeuroImage Clinical 2015;9:206-215. Impact Factor (IF) = 2.526.

	IS	KS	SF	JD	KP	LR	ML	SER
Conception and design of project	30%				10%	20%		40%
Collection of data	90%				5%			5%
Analysis of data	90%			10%				
Interpretation of results	50%	5%	10%	10%	5%	5%		15%
Drafting of article	100%							
Critical revision of article for intellectual input		10%	10%	10%	10%	10%	10%	40%

Chapter 5: Sahama I, Sinclair K, Fripp J, Pannek K, Lavin M, Rose S. Serial investigation of neurodegeneration in young ataxia-telangiectasia patients. Submitted to Paediatric Neurology. Impact Factor (IF) = 1.695.

	IS	KS	JF	KP	ML	SER
Conception and design of project	30%		20%	10%		40%
Collection of data	90%		10%			
Analysis of data	50%		50%			
Interpretation of results	50%	5%	25%	5%		15%
Drafting of article	100%					
Critical revision of article for intellectual input		10%	10%	10%	10%	60%

Contributions by others to the thesis

Prof Stephen Rose and Prof Martin Lavin were involved in the conception, organisation and execution of this research project, as well as the design, review and critique of the statistical analyses of the project. They also provided editorial comments and critical revision for all research papers included in this thesis. Dr. Kate Sinclair was involved in the conception and organisation of the research project, including the organisation of the ataxia-telangiectasia (A-T) imaging clinics held in The University of Queensland (UQ) Centre for Advanced Imaging, Brisbane, Australia and The Lady Cliento Children's Hospital, Brisbane Australia. Prof Roslyn Boyd provided control subject data for comparison with patients for this project. Dr. Kerstin Pannek and Mr. Lee Reid provided guidance and critique of general statistical analyses of the project. Dr. James Doecke provided extensive statistical and computational advice for analyses, particularly for Chapter 4. Dr. Jurgen Fripp provided analytical expertise, particularly for Chapter 5. Dr. Cynthia Rothblum-Oviatt and Dr. Tom Crawford provided insight into the clinical aspects and scoring of patients to supplement imaging findings and Dr. Simona Fiori's knowledge of neuroanatomy was instrumental to the analysis and interpretation of the research data. All co-authors reviewed the final draft of peer-reviewed articles enclosed within this thesis. Specific contributions of each author for peer-reviewed articles are presented in tabular format under the section 'Publications included in this thesis'.

Statement of parts of the thesis submitted to qualify for the award of another degree

None.

Acknowledgements

The PhD journey I have undertaken these past three years have been immensely enjoyable, insightful and by far the most challenging educational pursuit I have ever endeavoured to complete. For this I owe my sincerest gratitude to my Principal Supervisor Prof Stephen Rose and my Associate Supervisor Prof Martin Lavin. In the same vein, I would like to thank Dr. Kate Sinclair for her exceptional organisation of the A-T patient clinics and her dedicated support of my research. A special mention also goes to Ms. Kate Munro, for organising the clinics and the clinical scoring data. I would also like to express my thanks to Dr. Cynthia Rothblum-Oviatt and Dr. Tom Crawford of the A-T Children's Project and John Hopkins Hospital, USA, for their continued funding support and appreciation of my work.

As a newcomer to the field of diffusion MRI, I would like to thank Dr. Kerstin Pannek for being an indispensable source of expertise in the field. Likewise, I would like to thank Lee Reid for his support in the computational side of my project and Dr. Andrew Janke for his continued support in maintaining our less than stable computers! A special mention goes to Dr. Christina Knuepffer and Dr. Nancy Cloake for their invaluable advice to me during my PhD journey.

To all the co-authors of the papers I have included in this thesis, my sincerest thanks. I could not have done it without you. A special mention goes to Dr. Simona Fiori, whose expertise in neuroanatomy was of paramount importance in shaping three chapters of this thesis. I would also like to thank Dr. James Doecke and Dr. Jurgen Fripp for their invaluable support and assistance in the statistical and computational parts of the analysis, highlighted in Chapter 4 and 5 of this thesis, respectively. I also extend my gratitude to Mr. Aiman Al Najjar and Ms. Anita Burns, for their dedicated support of imaging the A-T patients and data delivery.

Lastly, I would like to thank my family, to whom I dedicate this thesis to. Without all of you, I could never have completed my studies as comfortably as I have done. Dad for always being my pillar of strength and advisor in absolutely everything I have done in my life, including undertaking this PhD. Mum for being the most understanding and patient person in my life, who has always believed in my work, even if she doesn't understand a word of it. And finally to Ishara, my sister, to whom I hope I haven't put off doing a PhD of her own.

Keywords

ataxia-telangiectasia, cerebellum, cerebrum, diffusion magnetic resonance imaging.

Australian and New Zealand Standard Research Classifications (ANZSRC)

The content of this thesis falls under the following disciplines and discipline clusters in the Federal Government's Excellence in Research for Australia (ERA) initiative:

ANZSRC code: 110904, Neurology and Neuromuscular Diseases, 50%
ANZSRC code: 080106, Image Processing, 50%

Fields of Research (FoR) Classification

The Fields of Research (FoR) Classification for the research project and content contained in this thesis is specified below:

FoR code: 1109, Neurosciences, 50%
FoR code: 0801, Artificial Intelligence and Image Processing, 50%

Table of Contents

List of Figures

List of Tables

List of Abbreviations

ACT	Anatomically Constrained Tractography
ADC	Apparent Diffusion Coefficient
AFD	Apparent Fibre Density
ANTS	Advanced Normalisation Tools
A-T	Ataxia-telangiectasia
ATM	Ataxia-telangiectasia Mutated gene
Atm	mouse homologue of Ataxia-telangiectasia Mutated gene
A-T NEST	Ataxia-telangiectasia Neuro Examination Scale Toolkit
ATP	Adenosine Triphosphate
BET	Brain Extraction Tool
Cho	Choline
CPC	Cortico-Ponto Cerebellar
Cr	Creatine
CSD	Constrained Spherical Deconvolution
CSF	Cerebrospinal Fluid
CST	Corticospinal Tract
CT	Computerised Tomography
CTC	Cerebellar-Thalamo-Cortical
decFA	Directionally Encoded Colour Fractional Anisotropy
dMRI	Diffusion Magnetic Resonance Imaging
DNA	Deoxyribonucleic Acid
DROP-R	Detection and Replacement of Outliers Prior to Sampling
DSP	Dexamethasone Sodium Phosphate
DTI	Diffusion Tensor Imaging
DWI	Diffusion-Weighted Imaging

EPI	Echo-Planar Imaging
F	Fluorine
FA	Fractional Anisotropy
FAST	FMRIB’s Automated Segmentation Tool
FDG	Fluorodeoxyglucose
FIRST	FMRIB’s Integrated Registration and Segmentation Tool
FMAM	Fit Model to All Measurements
fMRI	Functional Magnetic Resonance Imaging
FNIRT	FMRIB's Non-linear Image Registration Tool
FOD	Fibre Orientation Distribution
FSL	FMRIB’s Software Library
FUGUE	FMRIB’s Utility for Geometrically Unwarping EPIs
GM	Grey Matter
HARDI	High Angular Resolution Diffusion Imaging
HASTE	Half Fourier Acquisition Single Shot Turbo Spin Echo
HOMOR	Higher Order Model Outlier Rejection
ICV	Intracranial Volume
JHU-ICBM-DTI-81	John Hopkins University White Matter Atlas
K+	Potassium
KO	Knock Out
L.	Left (Hemisphere)
MCP	Medial Cerebellar Peduncle
MD	Mean Diffusivity
MNI	Montreal Neurological Institute
MPRAGE	Magnetisation Prepared Rapid Gradient Echo
MP2RAGE	Magnetisation Prepared Rapid Gradient Echo 2
MRI	Magnetic Resonance Imaging
NAA	N-acetylaspartate
Na+	Sodium
NO	Nitric Oxide
PET	Positron Emission Tomography
PLIC	Posterior Limb of the Internal Capsule

PRELUDE	Phase Region Expanding Labeller for Unwrapping Discrete Estimates
R	R Statistical Environment
R.	Right (Hemisphere)
ROI	Region of Interest
SCP	Superior Cerebellar Peduncle
SIFT	Spherical-deconvolution Informed Filtering of Tractograms
TBSS	Tract-Based Spatial Statistics
VBM	Voxel-Based Morphometry
WM	White Matter

CHAPTER 1

Introduction

Imaging in Ataxia-telangiectasia

Ataxia-telangiectasia (A-T), an autosomal recessive neurodegenerative disorder, occurs at a rate of 3 per million live births.[1] The multi-system characteristics of this disorder are caused by genetic mutation of the ATM (ataxia-telangiectasia mutated) gene,[2, 3] and involve progressive cerebellar ataxia, immunodeficiency, sinopulmonary infections, oculocutaneous telangiectasia,[4, 5] and elevated serum alpha-fetoprotein levels.[6] The ATM gene encodes for the protein kinase ATM, which plays a key role in the cellular response to DNA double-stranded breaks.[7, 8] It is also involved in the response to oxidative damage, in ATM activation by oxidative stress,[9] and may have more general roles in cell homeostasis. Upon activation, the ATM protein kinase phosphorylates a multitude of proteins that control various cellular processes, including different cell cycle checkpoint pathways.[10] ATM gene mutation is linked to increased radiosensitivity in A-T patients[11, 12] and in cells from these patients in culture.[13, 14] To date, there is no long-term cure for cancer susceptibility or progressive neurodegeneration among A-T patients. To this end, the cause of death among most patients is lymphoreticular malignancy or recurrent chronic respiratory infections.[4, 5]

The hallmark neuropathological condition of A-T is progressive cerebellar atrophy, which can extend to cerebral motor areas and the spinal cord with advanced age (reviewed in Sahama[15]). Extensive study of these neuropathological features have been conducted in both histopathological and post-mortem anatomy study, however non-invasive study of A-T neuropathology using structural imaging modalities in living patients is limited. Indeed, conventional T1- and T2-weighted magnetic resonance imaging (MRI) remains the predominant imaging modality used in A-T to date (reviewed in Sahama[15]). Additional information regarding these studies can be viewed in Table 2.1 (Chapter 2)

and Table 2.2 (Appendices) in this thesis. Although these morphological studies have been useful from a radiological perspective, they provide limited information of A-T neurodegeneration and its associations to the loss in neural motor network integrity among patients. To capture A-T brain and brainstem structural integrity and identify altered structure and function of these areas accurately, further investigation using comprehensive imaging modalities in A-T must be conducted. In this regard, diffusion-weighted MRI (dMRI), particularly diffusion tensor imaging (DTI), has been demonstrated to provide a more accurate depiction of brain and brainstem structural integrity than standard MRI.[16]

Diffusion-weighted MRI

Diffusion-weighted magnetic resonance imaging (dMRI) measures the random motion of water molecules (diffusion) in the brain to infer white matter (WM) microstructure organisation of neural tissue. In the cellular environment of the brain, cell membranes, cytoskeletal and macromolecular structures hinder and restrict the movement of water molecules. In neural environments, water movement is hindered in the extra-axonal environment (i.e. Gaussian diffusion), whereas in the intra-axonal environment, water movement is restricted (i.e. non-Gaussian diffusion). If diffusion is completely unimpeded, the mean square displacement (χ^2) of particles during diffusion time Δ is directly related to the diffusion coefficient (D)[17]:

$$(\chi^2) = 2D\Delta$$

Hindered and restricted diffusion lower the mean square displacement of water in the brain and in turn, lower the apparent diffusion coefficient (ADC). In addition, the tight structural organisation of the neural axons causes greater hindered water diffusion in the direction perpendicular to the WM fibre bundle than in the parallel direction, causing diffusion anisotropy. It is this diffusion restriction and anisotropy that is used to indirectly assess the underlying microstructural organisation of neural tissue using dMRI in a non-invasive manner.[18]

Diffusion image acquisition

When acquiring diffusion-weighted magnetic resonance (MR) images of target subjects, diffusion sensitising gradients are added to the pulse sequence, allowing magnetic labelling of the spins of individual protons, and a diffusion-weighting of MR images to be achieved. The attenuation of the MR signal intensity (A) is observed as the diffusion component parallel to the applied diffusion gradients, and is given by the following equation[19]:

$$A(TE) = e^{-\gamma^2 G^2 \delta^2 \left(\Delta - \frac{\delta}{3}\right).D} = e^{-b.D}$$

where γ represents the gyromagnetic ratio, and G, δ and Δ are the strength, duration and separation of the diffusion gradient, respectively. The echo time is given by TE whereas the diffusion coefficient is denoted by D. A single b-value is typically used to summarise $\gamma^2 G^2 \delta^2 \left(\Delta - \frac{\delta}{3}\right)$. It should be noted that in practice, cross-terms of a combination of imaging and diffusion gradients need to be considered during image acquisition, thus the above equation for MR signal intensity is inaccurate. Exact cross-terms are numerically calculated and incorporated into a revised b-value. An echo-planar imaging (EPI) sequence is typically used to acquire diffusion MRI data, however other pulse sequences can also be employed.

As previously mentioned, voxel-wise signal attenuation of the MR image is derived from diffusion gradients, in which the diffusion direction is the same as the diffusion sensitising gradient that is applied. Different contrasts can be derived for diffusion-weighted images, compared to images without diffusion weighting, where the contrast varies depending on the orientation of the diffusion gradient. In effect, the degree of diffusion restriction, corresponding anisotropy and underlying orientation of WM architecture can all be deduced using this property of diffusion contrasts. For instance, upon left-right application of the diffusion gradient, signal intensities of pathways that travel from left to right in the brain (i.e. commissural pathways such as the corpus callosum) are attenuated. Application in the anterior-posterior orientation yields signal intensities of association pathways (e.g. anterior limb of the internal capsule). Finally, application of the diffusion gradient in the inferior-superior orientation attenuates signal intensities of projection pathways (e.g. posterior limb of the internal capsule) (Figure 1.1).

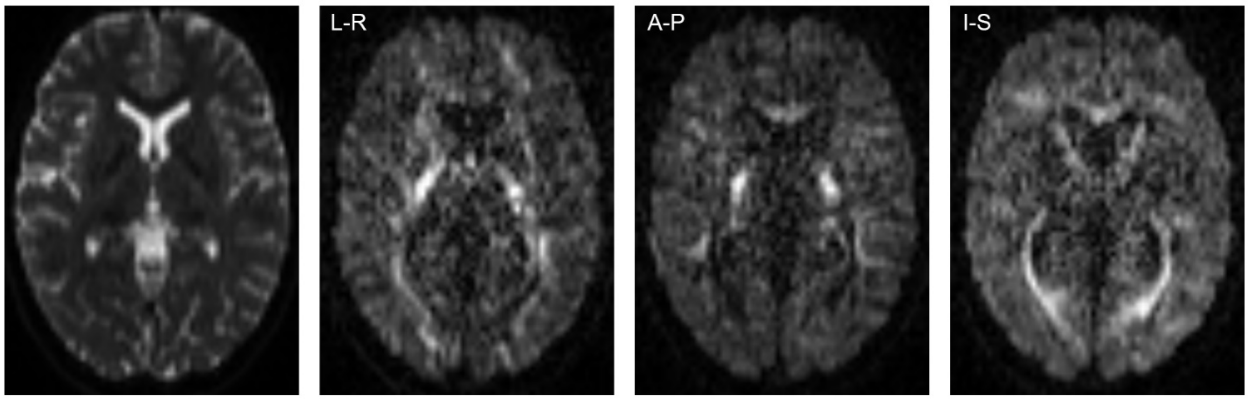

Figure 1.1. The dependency of diffusion-weighted image contrasts on the direction (orientation) of applied diffusion encoding gradients. Axial plane images from left to right: B0 image with no diffusion weighting applied; left-right application of diffusion weighting (L-R) allowing signal attenuation of callosal pathways; anterior-posterior application of diffusion weighting (A-P) allowing signal attenuation of association pathways (e.g. anterior limb of the internal capsule); inferior-

superior application of diffusion weighting (I-S) allowing signal attenuation of projection pathways (e.g. posterior limb of the internal capsule).

A number of challenges exist with respect to acquiring diffusion images, particularly in a non-sedated manner, from A-T patients. The degree of motion artefact, caused by uncontrolled head movement, in acquired diffusion images presents a significant challenge in imaging A-T patients, due to the effect on data quality and corresponding accuracy of downstream statistical analysis. Specifically, head motion in the acquired scan leads to misalignment of brain structures between diffusion images and loss of signal in the image slices (volumes) of the brain where that movement artefact occurred (reviewed in Pannek[20]). In this respect, robust data pre-processing and correction methods to detect and remove image distortions and motion artefact in raw A-T diffusion data must be implemented before subsequent analysis of diffusion images.

Diffusion data pre-processing

In this project, pre-processing of raw diffusion data was conducted to detect and correct for motion artefacts before subsequent data analysis (Chapters 3-5) (Figure 1.2). In this protocol, raw diffusion data (Step 1) volumes were rejected from further downstream analysis based on within-volume movement (Step 2). Within the remaining image slices, signal intensity outlier voxels were detected and an outlier mask was created for subsequent voxel-wise processing (Step 3). Following this procedure, image distortions caused by susceptibility inhomogeneities were corrected and reduced using the diffusion data field map (Step 4). Intensity inhomogeneities within the image were removed (Step 5) and distortions caused by head movement were corrected within images (Step 6). Finally, the slice-wise outlier mask created in Step 3 was used as input to detect signal intensity outlier voxels (i.e. caused by cardiovascular pulsation, bulk head motion, etc.), which were replaced within images (Step 7) to acquire corrected diffusion data (Step 8) for subsequent downstream statistical analysis (Figure 1.2). For a detailed review of this pre-processing protocol, the reader is referred to the journal article by Pannek et al. (2012).[20]

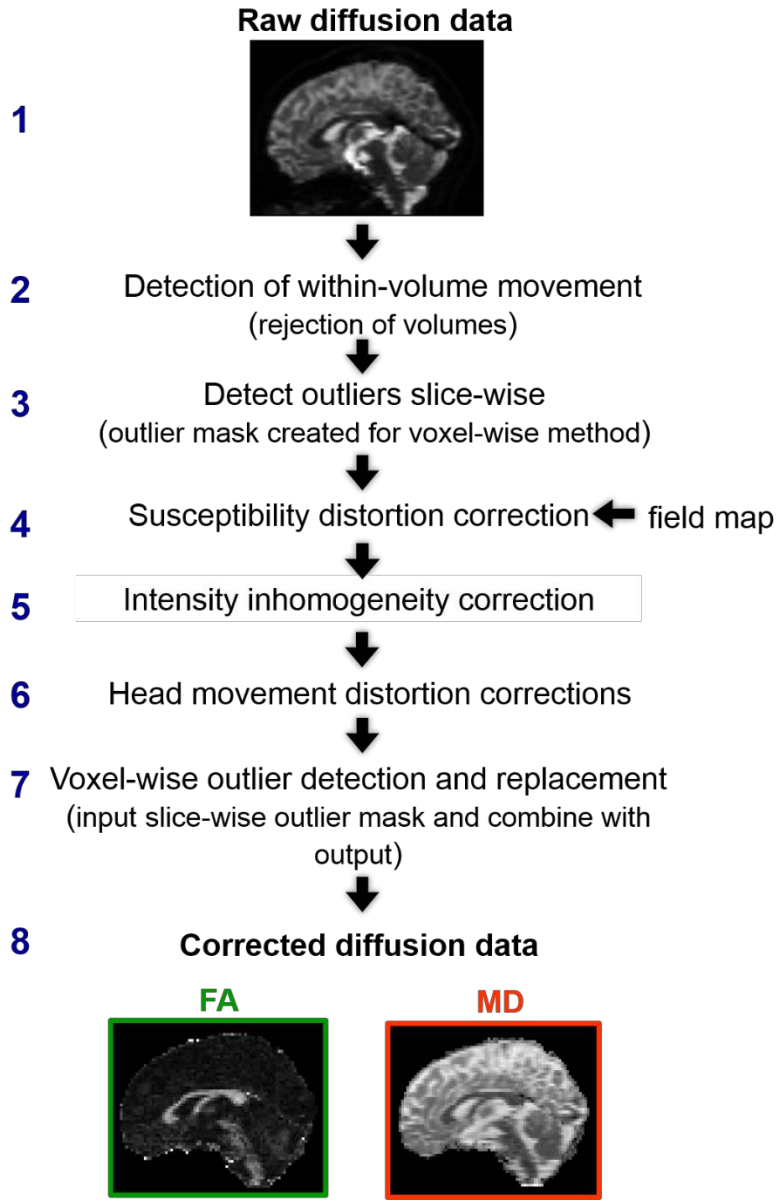

Figure 1.2. Raw diffusion data pre-processing pipeline. Raw diffusion data (Sagittal image, Step 1) was used as input for this protocol. Within-volume movement was detected in raw diffusion data volumes, and volumes were rejected from further downstream analysis (Step 2). Within the remaining image slices, signal intensity outlier voxels were detected and an outlier mask was created for subsequent voxel-wise processing (Step 3). Image distortions caused by susceptibility inhomogeneities were corrected and reduced using the diffusion data field map (Step 4). Intensity inhomogeneities within the image were removed (Step 5) before distortions caused by head movement were corrected within images (Step 6). Slice-wise outlier masks (output from Step 3) were used as input to detect and replace signal intensity outlier voxels (i.e. caused by cardiovascular pulsation, bulk head motion, etc.) in images (Step 7) to acquire corrected diffusion data (Step 8) in the form of fractional anisotropy (FA; green) and mean diffusivity (MD; orange) maps (pictured here in the sagittal plane).

Diffusion tensor imaging

To comprehensively probe corticomotor-cerebellar integrity in ataxic conditions,[21-28] diffusion tensor imaging (DTI),[29] a model of dMRI, is used. The diffusion tensor describes the molecular displacement (D) of water in the brain in three dimensions (x, y and z) and is comprised of a 3×3 matrix as shown:

$$\mathrm{D} = \begin{pmatrix} D_{xx} & D_{xy} & D_{xz} \\ D_{xy} & D_{yy} & D_{yz} \\ D_{xz} & D_{yz} & D_{zz} \end{pmatrix}$$

These six independent elements of the above diffusion tensor matrix (D_{xx}, D_{yy}, D_{zz}, D_{xy}, D_{xz} and D_{yz}) are calculated by acquiring six diffusion weighted images at the minimum, with application of diffusion gradients in noncollinear directions. Despite this convention, acquisitions that utilise a minimum of 30 unique orientations that are distributed using the electrostatic approach[30] have been required for robust tensor orientation estimation.[31] Recent acquisition methods have also incorporated the use of multiple diffusion weightings or 'multi-shell' methods to capture the main tissue types of the brain (WM, grey matter (GM) and cerebrospinal fluid (CSF)) more effectively. This method aims to overcome the limitations of the single constant diffusion weighting acquisition or 'single shell' method, to elucidate information in tissue types that cannot be distinguished using the standard single-shell approach.[32] The diffusion tensor is visualised as an ellipsoid, where the axes of the ellipsoid $\left(\underset{\varepsilon_1}{\rightarrow}, \underset{\varepsilon_2}{\rightarrow}, \underset{\varepsilon_3}{\rightarrow}\right)$ are given by the eigenvectors of the diffusion tensor and the length is given by the eigenvalues $(\lambda_1, \lambda_2, \lambda_3)$ of the diffusion tensor (Figure 1.3).

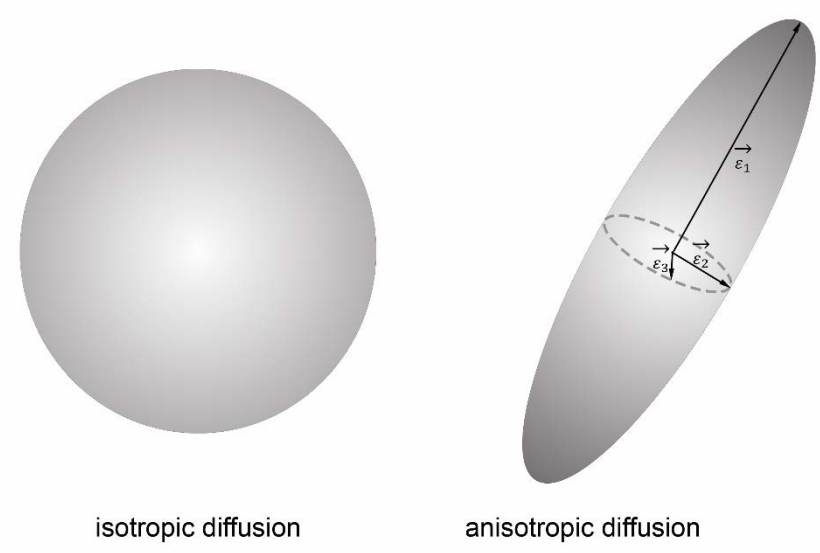

Figure 1.3. The ellipsoid visualisation of the diffusion tensor. In isotropic environments, the eigenvector length of the diffusion tensor is equal and the tensor is represented by a sphere (Left). In anisotropic environments, the principal eigenvector $\underset{\varepsilon_1}{\rightarrow}$ length is greater than the lengths of the other eigenvectors $\left(\underset{\varepsilon_2}{\rightarrow}, \underset{\varepsilon_3}{\rightarrow}\right)$ and the corresponding tensor shape is a 'cigar' (Right).

Based on the eigenvalues of the diffusion tensor, a number of quantitative diffusion metrics can be calculated in DTI. The diffusion metrics used in this thesis are fractional anisotropy (FA) and mean diffusivity (MD), respectively. FA, a unit-less scalar value between 0 (isotropic water diffusion) and 1 (anisotropic water diffusion), measures the organisation of specific WM axonal pathways in the brain.[33] FA is given by the following equation, where λ is the average of the three diffusion tensor eigenvalues:

$$\text{FA} = \sqrt{\frac{3}{2}} \cdot \sqrt{\frac{(\lambda_1 - \lambda)^2 + (\lambda_2 - \lambda)^2 + (\lambda_3 - \lambda)^2}{\lambda_1^2 + \lambda_2^2 + \lambda_3^2}}$$

FA is dependent on the uniform direction of water movement (degree of anisotropy) in WM pathways.[33] In areas of unrestricted water diffusion in the brain, low FA values are recorded, whereas high FA values are observed in areas containing highly organised WM microstructure (Figure 1.4). Colour coded FA maps are used for visualisation as part of the dMRI image processing pipeline, and incorporate the directional information of the principal eigenvector $\underset{\varepsilon_1}{\rightarrow}$.[34] Indeed, in single fibre voxels (pixels of the MRI image), the principal eigenvector is believed to coincide with the orientation of WM architecture, allowing easier identification and improved analysis of major WM tracts.[35]

MD or the Apparent Diffusion Coefficient (ADC) provides a measure of the mean motion of water in all directions in the given space[36, 37]:

$$\text{MD} = \frac{1}{3}(\lambda_1 + \lambda_2 + \lambda_3)$$

It is equivalent to $^1/_3$ of the Trace of the diffusion tensor. MD values share an inverse relationship to FA values. In areas of high WM microstructure organisation, low MD values are observed whereas relatively high levels of MD are recorded in areas where fewer fibres restrict water movement (reviewed in Mori[38]) (Figure 1.4). This inverse relationship is used to characterise WM degeneration. Specifically, a decrease in FA and an increase in MD, where lower FA is indicative of reduced uniform diffusion direction and by extension, WM fibre alignment,[33] indicates WM degeneration.

Other diffusion metrics that are calculated in DTI are axial ($\lambda\|$) and radial ($\lambda\perp$) diffusivity, respectively. Axial diffusivity is equal to the primary eigenvector magnitude (parallel diffusion) whereas radial diffusivity represents the average of the two tertiary eigenvectors (diffusion direction that is perpendicular to the primary vector). Typically, in areas of unrestricted water diffusion, an increase in radial diffusivity and either increases, decreases or relatively no change in axial diffusivity are recorded.[39] These measures were not utilised for this project.

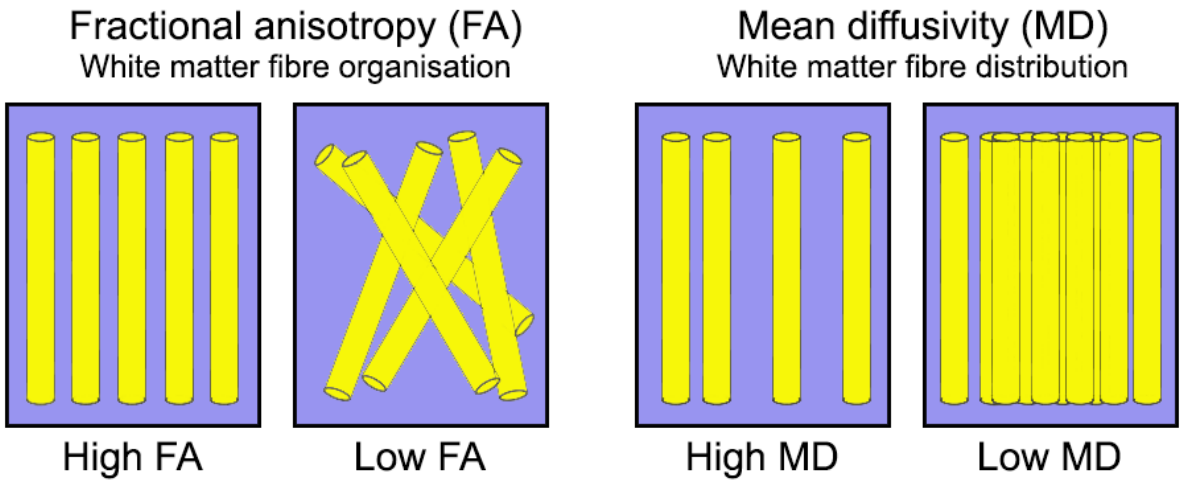

Figure 1.4. Fractional anisotropy (FA) and mean diffusivity (MD). FA and MD changes respective of white matter (WM) fibre organisation and distribution.

Image processing methodology

Following pre-processing of diffusion data, the following analysis pipelines were used in this project to statistically analyse imaging data. The image processing pipelines are presented in order of the type of input data needed for the analysis. In this project, T1-weighted structural images and pre-processed diffusion data (FA and MD images) were used as input images for analysis, respectively.

Structural T1-weighted images

T1- (and T2)-weighted structural images are image contrasts acquired by using pulse sequences in MR image acquisition. T1-weighted images are used to differentiate anatomical structures, where tissue with high fat content (i.e. WM) appear bright and water-filled compartments (i.e. CSF) appear dark. Conversely, in T2-weighted images, compartments filled with water appear light, whereas tissue with high fat content appear dark. In this project, both T1- and T2-weighted images, that provide high-resolution structural information of brain anatomy and pathology (cortical morphology), were used to characterise degeneration in A-T patients (Figure 1.5).

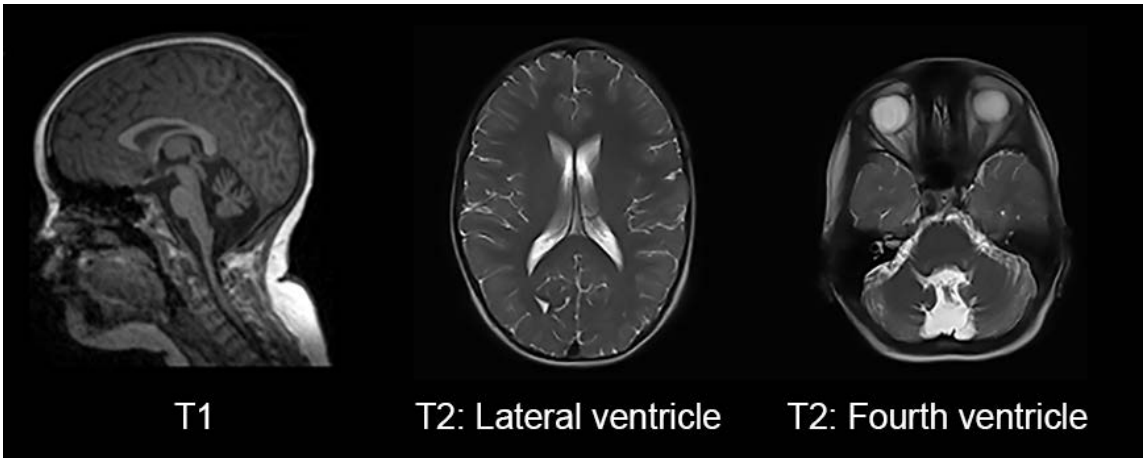

Figure 1.5. Sagittal T1-weighted (Left) and axial T2-weighted (Middle and Right) structural images of an ataxia-telangiectasia patient. T2-weighted images picture the lateral and fourth ventricles of the brain respectively.

As previously mentioned, the main challenge of analysing brain images in A-T is the prevalence of motion artefacts in the image. In contrast to established pre-processing protocols for diffusion data (see 'Diffusion data pre-processing' section in this Chapter), based on detecting and correcting for motion artefact in multiple diffusion image volumes of the brain, there is no method by which motion artefact can be removed from T1 structural images, to reduce the impact of data quality on downstream processing and statistical analysis. Despite this limitation, careful visual examination of images derived from processing pipelines that use T1 images as input, and manual editing of structural errors where they were detected in such images ensured the accuracy of analyses in this project.

Voxel Based Morphometry

A number of elegant methods, whereby structural changes are measured in the whole brain of subjects in a voxel-wise manner, have been developed. One such method is Voxel Based Morphometry (VBM), where the GM volumetric changes between two conditions (i.e. control and diseased cohorts) are measured using T1-weighted structural images (Step 1, Figure 1.6).[40, 41] In the VBM analysis used in this project, T1-weighted images were skull-stripped (the brain is extracted from the structural image), GM segmented (WM and CSF spaces of the image were removed) (Step 2), and resulting images were registered to a standard space (Step 3) before images were averaged and flipped along the x-axis to create a GM template with specific left-right symmetry (Step 4). After non-linear registration of GM segmented images to this template, voxels within the resulting image were smoothed (according to VBM recommendations)[40-42], to ameliorate residual misalignments of images (Step 5), before voxel-wise statistical analyses were conducted (Step 6). Significant changes between

groups were marked on the GM template in the corresponding brain area (Figure 1.6, shown in yellow). For this project, an optimised VBM protocol using FMRIB's Software Library (FSL) tools was used (Chapter 3).

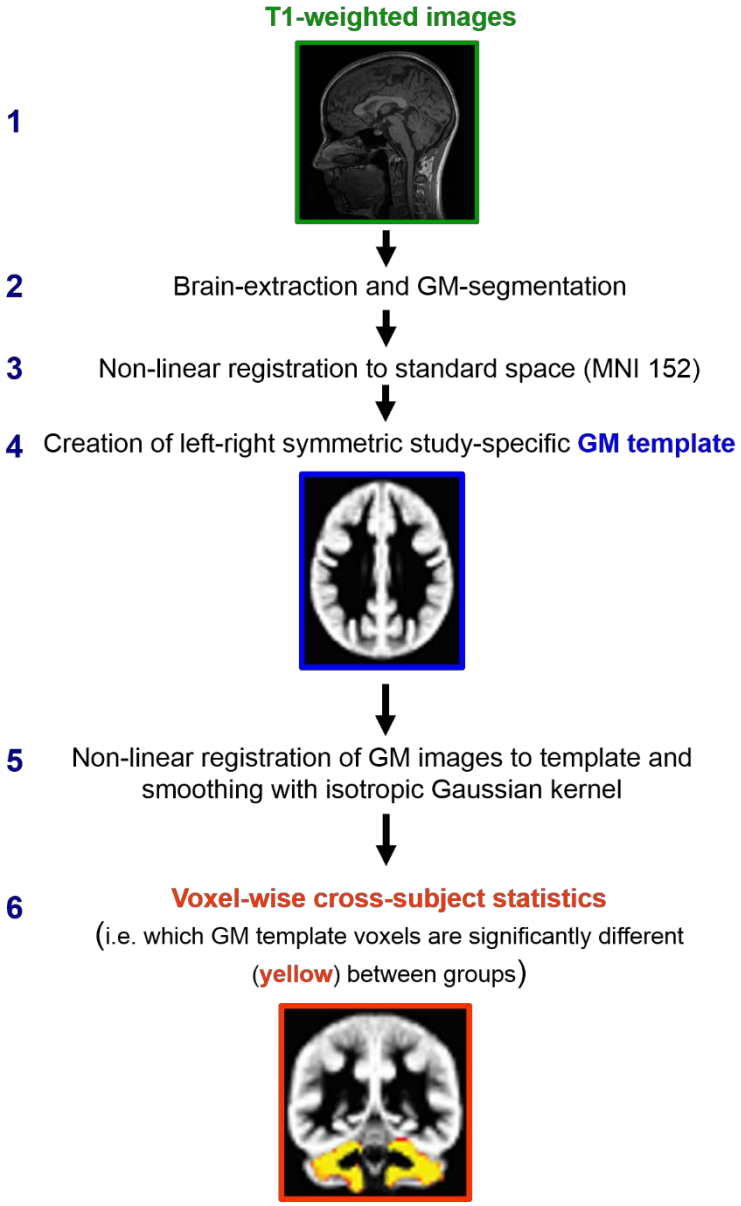

Figure 1.6. Voxel Based Morphometry (VBM) processing pipeline. This processing pipeline uses T1-weighted structural images (Sagittal image, Step 1) from control and patient groups. T1 images underwent brain extraction and grey matter (GM) segmentation (Step 2), before registration to standard space (Montreal Neurological Institute (MNI) 152 standard space was used, Step 3). A GM template was created with specific left-right symmetry (Step 4), followed by non-linear registration of GM segmented images to this template (Step 5). Voxels within the resulting image were smoothed, to ameliorate residual misalignments of images (Step 5), before voxel-wise statistical analyses were conducted (Step 6). Significant GM volumetric changes between control and patient groups are indicated on the GM template in the corresponding brain area (Yellow, Step 6).

The main advantages of a VBM-style analysis is that it is fully automated and only requires structural T1 data for analysis. One significant challenge however, is the inherent alignment issues of the atlas space (i.e. Montreal Neurological Institute (MNI) 152 standard space for VBM) that occur during processing for statistical analysis. Specifically, it is not possible to say for certain that any given voxel in the space in which voxel-wise statistics will be carried out, accurately represents corresponding data from all subjects in a given anatomical region.[43, 44] The second limitation in VBM-style analyses, is the arbitrary choice of smoothing designated for the analysis. Final results have been found to depend very strongly on the choice of smoothing.[45] In addition, smoothing can also increase the partial voluming problem, where it is difficult to observe whether estimated structural changes are due to genuine changes in volume and structure, rather than by changes in the amount of tissue types (reviewed in Smith[44]). To address these limitations in the current project, visual cross-checking of alignment issues[46] and manual editing of resultant volumes, followed by careful post-statistics analysis, was conducted at all stages of the VBM processing pipeline to ensure the accuracy of the automated VBM alignment process.

Cortical and Subcortical Segmentation

As whole brain analysis methods are automated, selection or segmentation of specific cortical brain regions is relatively easy. One prominent model-based segmentation/registration tool in VBM to conduct GM segmentation of structural images is FMRIB's Integrated Registration and Segmentation Tool (FIRST),[47] which can also be used as a standalone tool to segment individual areas of interest in the brain (Chapter 5). Within the FIRST protocol used in this project (Figure 1.7), T1-weighted structural images were cropped at the neck and skull-stripped (Step 2) before applying the FIRST script to segment all sub-cortical structures of the brain (Step 3). The output of this script were mesh and volumetric structural (colour coded template masks, Figure 1.7) outputs of the selected brain regions (Step 4, Figure 1.7). It should be noted however, that certain brain areas (i.e. cerebellum) are particularly sensitive to image resolution[48] and that the quality of T1 structural images determines the effectiveness by which target brain areas are segmented using FIRST. In this project, motion artefact and image distortions in T1 images presented a challenge in the automated segmentation of brain structures for analysis. Indeed, in instances where the cerebellum was selected, careful manual segmentation of structures was required to ensure the accuracy of downstream volumetric measurements and subsequent statistical analysis of the cerebellum (Chapter 5).

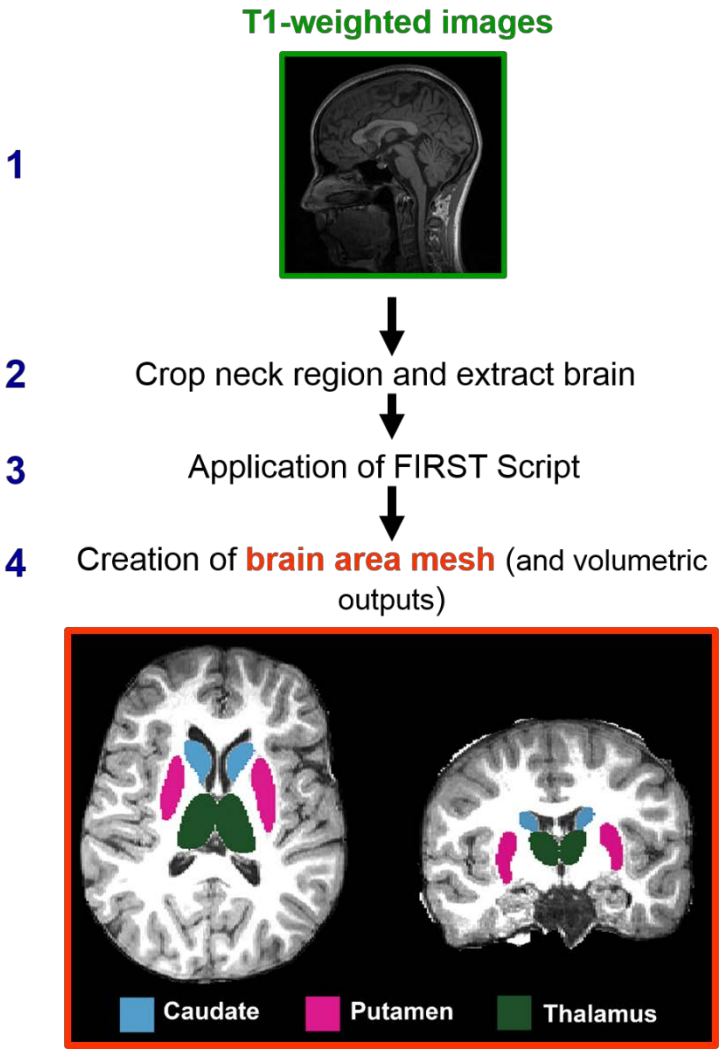

Figure 1.7. FMRIB's Integrated Registration and Segmentation Tool (FIRST) processing pipeline. Within this protocol, T1-weighted structural images (Sagittal image, Step 1) were cropped at the neck and skull-stripped (Step 2) before the FIRST script was applied to segment all sub-cortical structures of the brain (Step 3), and provide mesh and volumetric structural outputs of the selected brain regions (Step 4). Volumetric structural outputs of the caudate (blue), putamen (pink) and thalamus (green) are represented on skull-stripped T1-weighted images in the axial (left) and coronal (right) planes, respectively (Step 4).

Diffusion images

Tract-Based Spatial Statistics

Whole brain voxel-wise analysis of diffusivity measures (FA and MD) is conducted using Tract-Based Spatial Statistics (TBSS, Figure 1.8).[42, 44] TBSS is a sensitive analysis used in this project where FA and MD images from multiple subjects in control and patient cohorts were aligned via registration (non-linear) to a standard space (Step 2), and subsequently projected onto an alignment-invariant tract representation (or 'mean FA skeleton') (Steps 3-4). Following this image projection,

voxel-wise statistical comparisons of WM microstructure change were made between controls and A-T patients (Step 5). Significant WM changes between groups were marked on the FA skeleton in the corresponding brain area (Figure 1.8, shown in red).

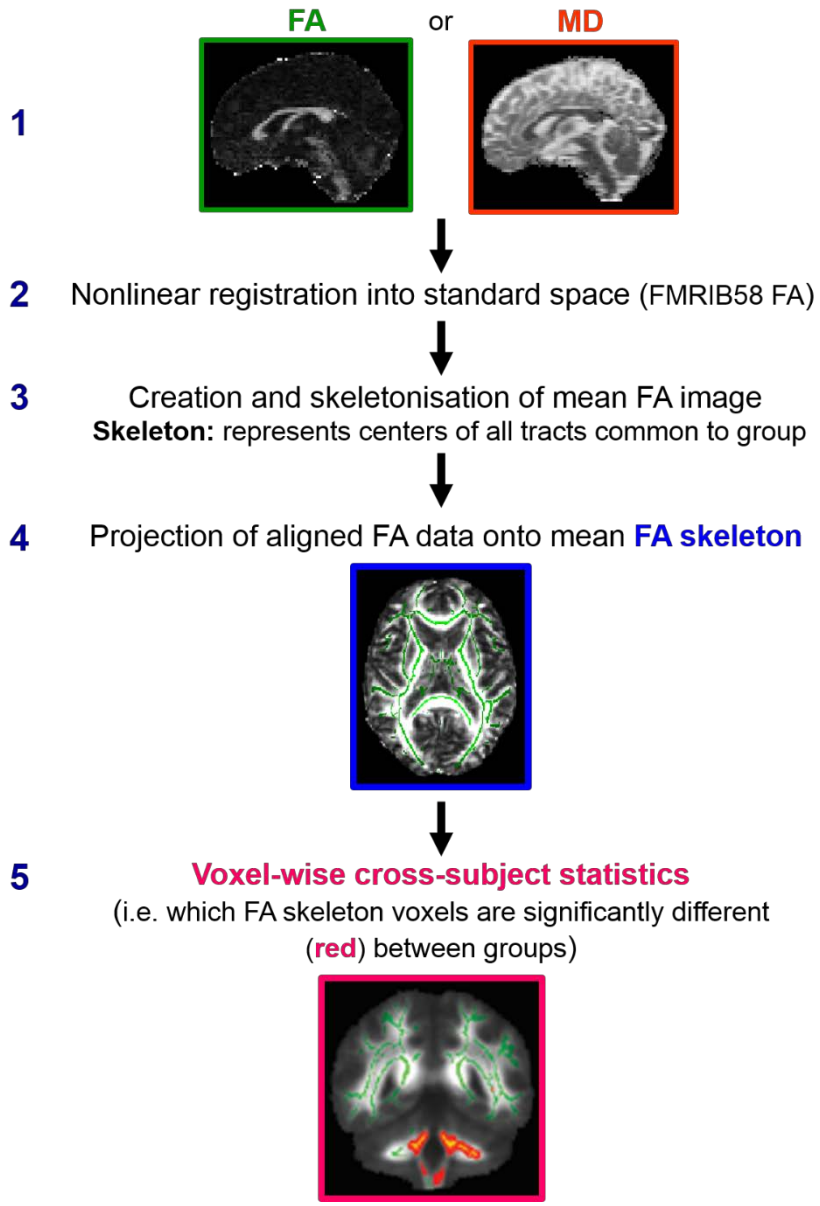

Figure 1.8. Tract-Based Spatial Statistics (TBSS) processing pipeline. In the TBSS processing pipeline, fractional anisotropy (FA) and mean diffusivity (MD) images from multiple subjects in control and patient cohorts were non-linearly registered for image alignment to a standard space (FMRIB58 FA space, Step 2), and subsequently projected onto an alignment-invariant tract representation (or 'mean FA skeleton') (Steps 3-4). Voxel-wise statistical comparisons of white matter (WM) microstructure change were made between controls and patient cohorts, where significant WM changes between groups where highlighted (red) in the FA skeleton by brain region.

Like all VBM-style analyses, TBSS is fully automated and only requires pre-processed diffusion data for analysis. It is limited by the inherent alignment issues of the atlas space (FMRIB58 FA space)

during processing, specifically, it is not guaranteed that the same region of the same WM tract from each analysed subject has been accurately captured per voxel in the space in which voxel-wise statistics will be carried out.[43, 44] In addition, limited information about the specific WM tracts that traverse the area of affectation is revealed using TBSS, enforcing the need for specialised and comprehensive analysis of specific WM tracts of interest in areas of structural change (i.e. tractography). The aforementioned quality of TBSS image registration also confounds the anatomical specificity of specific tracts within this analysis.[49] Similar to VBM analysis, the smoothing choice made during TBSS processing has a strong influence on the final results,[45] and can increase partial voluming problems.[44] To resolve these issues, visual cross-checking of alignment issues[46] followed by careful post-statistics analysis was conducted at all stages of the TBSS processing pipeline to ensure the accuracy of subsequent results.

Tractography

In addition to providing information about the microstructural organisation of the brain, DTI, specifically the directional information within the diffusion signal (direction of water diffusion), can be used to track WM pathways (Figure 1.9), in a process known as tractography. To track WM tracts from voxel to voxel, early tractography methods used the direction of the principal eigenvector $\underset{\varepsilon_1}{\rightarrow}$ of the diffusion tensor.[50-52]

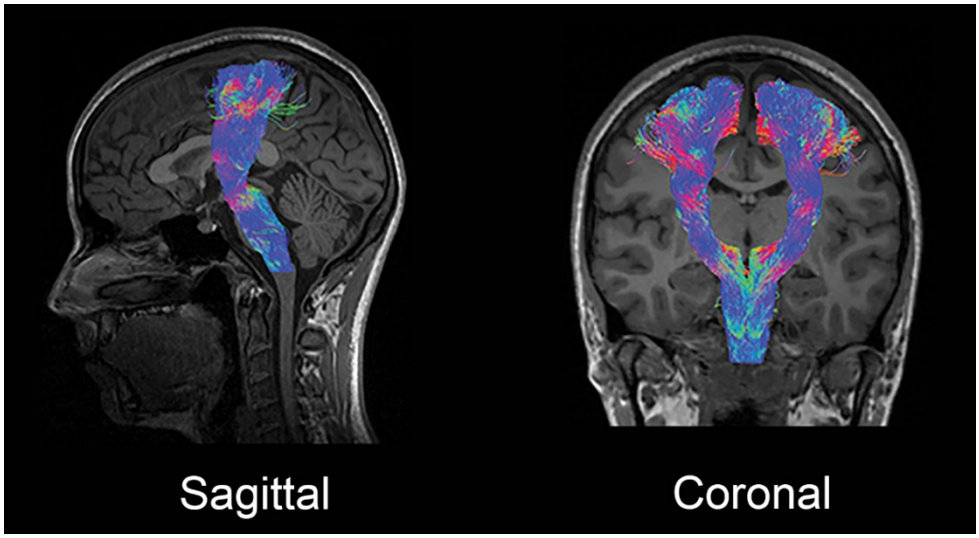

Figure 1.9. Tractography of the corticospinal tracts in the sagittal (left) and coronal (right) views. Bilateral tracts were extracted using probabilistic tractography based on constrained spherical deconvolution, in a typically developing subject.

Limitations of DTI and Tractography

In diffusion images, almost 90% of WM voxels comprise of complex WM architecture and crossing fibres.[53] DTI is limited in resolving this complex architecture and crossing fibre pattern.[54] Unintuitive DTI measures are derived from voxels containing multiple crossing fibres, particularly in neurodegenerative diseases where increased FA measures can be observed in degenerative regions.[55] In cases of Wallerian degeneration, changes in diffusion anisotropy may not be observed in degenerated pathways crossing other tracts.[56] In addition, false-positive (i.e. presence of non-existent tracts) and false-negative (i.e. inability to delineate existing tracts) errors may accumulate in tractography-derived WM pathways when crossing fibres are analysed using diffusion tensor tractography. This is due to a lack of correspondence in orientation between the principal eigenvector of the diffusion tensor and WM architecture.

In the cases outlined above, changes in the diffusion tensor can be interrogated by using more than one DTI metric (i.e. both FA and MD as in this project) to observe neuropathology in neurodegenerative disease states (reviewed in Alexander[57]). To resolve multiple crossing fibres within voxels, a number of higher order models of the diffusion signal can be used. For this project, constrained spherical deconvolution (CSD)[58] implemented in the MRtrix software package[59] was used to estimate fibre orientations and improve the resolution of multiple crossing fibre tracts in a given voxel.[60, 61] To estimate the fibre orientation distribution (FOD) by spherical deconvolution,[62] the response function (diffusion signal of single fibre voxels) is measured before applying it as a convolution kernel with the diffusion signal in all voxels. In effect, FOD reconstructions display the orientations of underlying WM tracts as multiple ‘lobes’ (Figure 1.10). A more robust FOD reconstruction is achieved with an additional non-negativity constraint[58] that ensures positive volume fractions of contributing fibre populations. The information contained within the MRtrix-derived FOD can be used in tractography to drive WM fibre delineation, with greater accuracy than diffusion tensor based tractography methods without a higher order model approach,[54] and is the method implemented in this project.

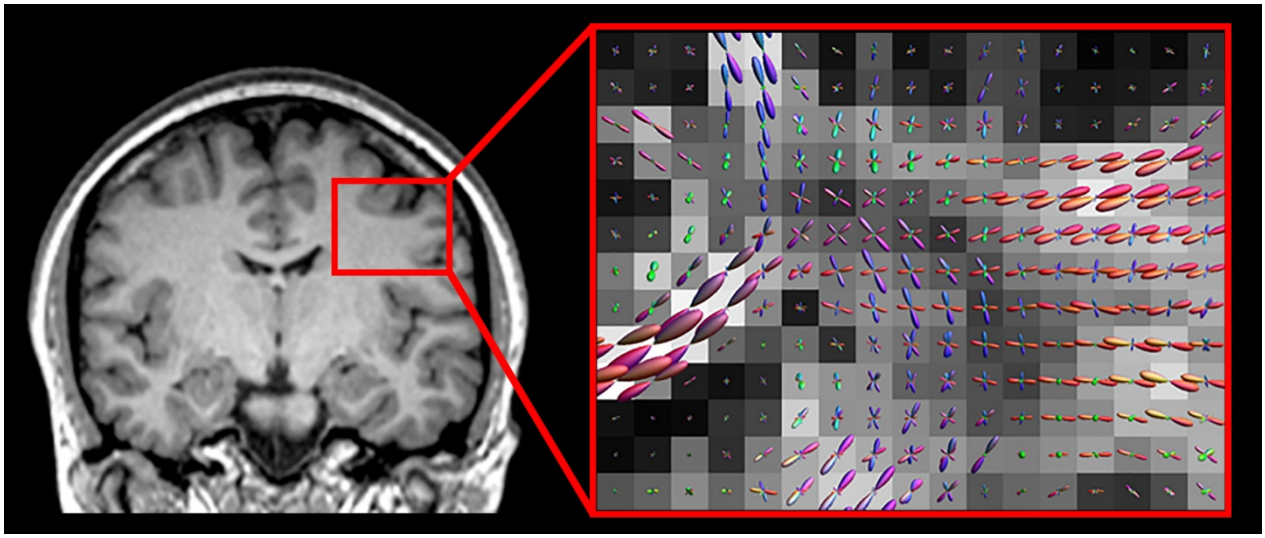

Figure 1.10. Fibre orientation distribution (FOD) estimated using constrained spherical deconvolution (CSD). In regions of crossing fibres, multiple 'lobes' as depicted (right) are used to represent the underlying white matter orientations.

MRTrix3 Tractography

In this project, a newly released demonstrative version of the MRtrix program, MRTrix3, was implemented for probabilistic tractography analysis. In comparison to MRtrix, MRTrix3 offers two novel features that assist in the extraction of tracts that are anatomically constrained to the brain space of individual subjects, and that improve quantitative whole brain streamline reconstruction for subsequent tract extraction. The first feature is called anatomically constrained tractography (ACT)[63] and is a framework used to confine tracts in the brain to the brain space of individual subject images. Tractography operates by following the local water diffusion direction from voxel to voxel from a start (seed) point, until the tractography streamline terminates according to pre-defined criteria. One important criterion for termination is when streamlines attempt to leave the brain region (brain mask). The ACT framework ensures that streamlines are anatomically constrained to the brain mask.

In this project, structural T1-images registered to the diffusion image (FA image) were used as input for the MRTrix3 processing pipeline, specifically for the ACT protocol (Step 1, Figure 1.11). T1 images were skull-stripped and segmented using the FSL Brain Extraction Tool (BET) and segmentation tools (FIRST and FMRIB's Automated Segmentation Tool (FAST)) respectively, to remove the encasing skull in the image and segment the brain into five tissue types (i.e. cortical grey matter, sub-cortical grey matter, white matter, cerebrospinal fluid and pathological tissue). The resulting image was a 'five tissue types' mask (Step 2) which was subsequently used to produce whole brain tractography maps (tractograms) (Step 3).

1 **T1 image registered to diffusion image**

2 Anatomically Constrained Tractography (ACT): **5 tissue types mask**

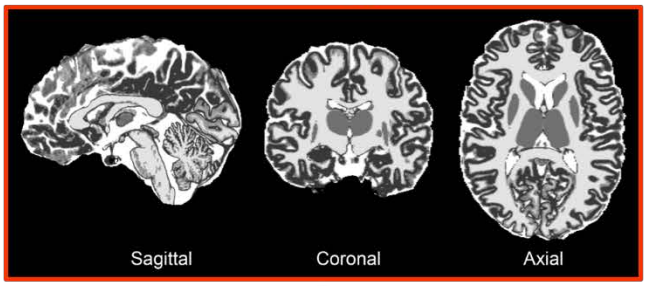

3 Generation of **wholebrain tractogram**

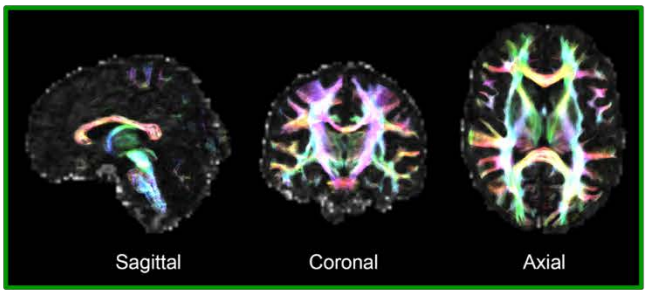

4 Spherical-deconvolution Informed Filtering of Tractograms (**SIFT**)

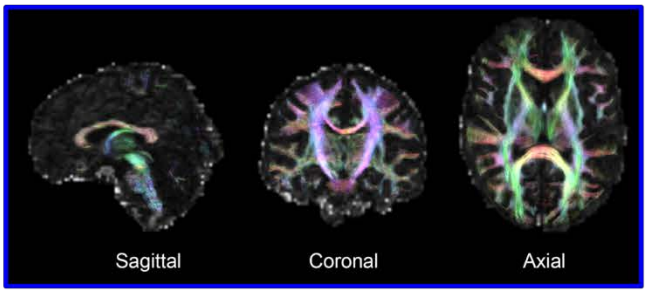

5 Region of interest (ROI) implementation to SIFTed tractograms

6 Extraction of **white matter (WM) tracts**

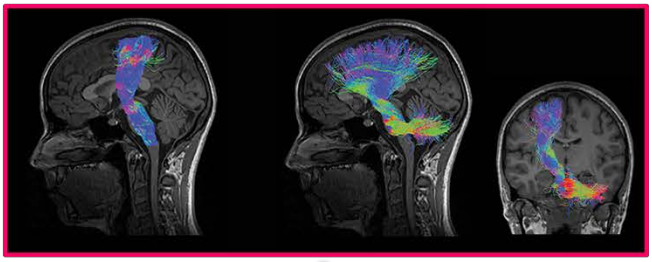

7 WM tract measurement

Diffusion metrics (FA and MD)

Streamline Number, Tract Volume & Apparent Fibre Density

Figure 1.11. MRTrix3 processing pipeline. T1-weighted structural images registered to diffusion image space (Fractional Anisotropy (FA) image, Step 1) were skull-stripped and segmented using the FSL Brain Extraction Tool (BET) and segmentation tools (FMRIB's Integrated Registration and Segmentation Tool (FIRST) and FMRIB's Automated Segmentation Tool (FAST)) respectively, to create 'five tissue types' masks as part of the Anatomically Constrained Tractography (ACT) framework (Representative 'five tissue types' mask presented in the sagittal, coronal and axial planes respectively, Step 2). The resulting mask was used to produce whole brain tractography maps (tractograms) (Representative whole brain tract images are overlaid on the FA map in the sagittal, coronal and axial planes respectively, Step 3). The Spherical-deconvolution Informed Filtering of Tractograms (SIFT) framework was utilised on whole brain tractograms (Representative SIFTed whole brain tract images are overlaid on the FA map in the sagittal, coronal and axial planes respectively, Step 4) before subsequent extraction of white matter (WM) tracts of interest using region of interest (ROI) selection of tracts from whole brain tracts (Steps 5-6). Finally, quantitative methods to extract fractional anisotropy (FA) and mean diffusivity (MD) metrics and identify structural differences along fibre bundles were conducted using resultant tracts.

Following generation of whole brain tractograms in the MRTrix3 probabilistic tractography pipeline, tractograms were processed using the second new feature of the new MRtrix software. This feature is termed Spherical-deconvolution Informed Filtering of Tractograms (SIFT) (Step 4, Figure 1.11).[64] SIFT ensures that within the produced tractography reconstruction, the number of connecting streamlines between two brain regions match spherical deconvolution estimated WM fibre densities (cross-sectional areas) between these regions. In effect, SIFT ensures that the derived tracts are captured as they would appear in true biological constraints within the subject.

Following SIFT processing of whole brain tractograms, ROIs were manually selected in directionally encoded colour (dec) FA maps, derived from pre-processing raw diffusion data. The decFA colour scheme displays the fibre orientation in the image; specifically red represents left-right orientation, blue represents inferior-superior orientation and green represents anterior-posterior orientation of fibres. ROI placement and subsequent tract extraction relies on anatomical expertise of brain structures within the decFA image (Figure 1.12). In this project, ROIs were selected and subsequently used to extract tracts of interest from SIFTed whole brain tractograms (Steps 5-6, Figure 1.11).

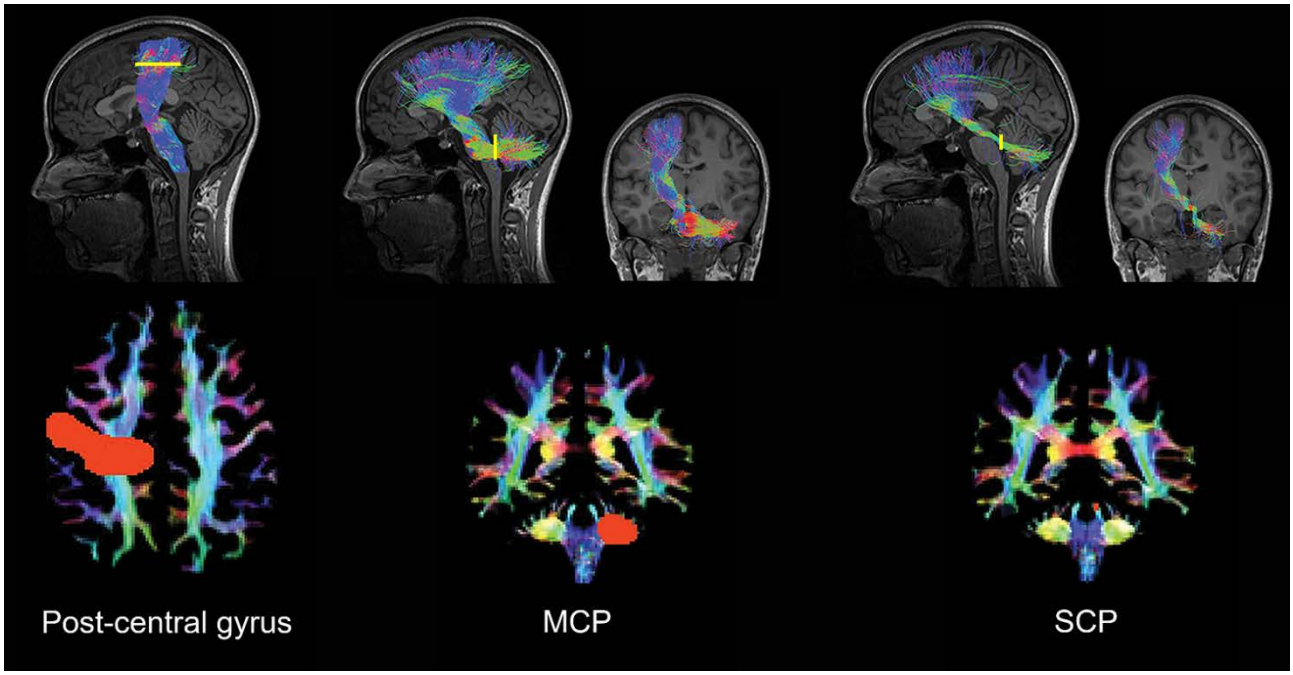

Figure 1.12. First row: Tractography of white matter (WM) corticospinal (left) and corticomotor-cerebellar (middle and right) tracts from a typically developing control subject in the sagittal T1-weighted image. Coronal images (middle and right) show decussation of corticomotor-cerebellar tracts. Yellow lines indicate corresponding region of interest (ROI) placement. Second row: ROI selection of the postcentral gyrus (left), medial cerebellar peduncle (MCP; middle) and superior cerebellar peduncle (SCP; right) marked on a directionally encoded colour fractional anisotropy (decFA) image in the axial (left) and coronal (middle and right) planes, respectively. The decFA colour scheme is represented as follows: red (left-right fibre orientation), blue (inferior-superior fibre orientation) and green (anterior-posterior fibre orientation).

In contrast to automated voxel-wise image processing methods, the use of ROIs to select WM tracts of interest from whole brain tractography can be time consuming, especially when many structures require manual selection and/or a large number of participants are involved in the analysis. The ROI approach is largely operator-dependent, thus to ensure adequate intra- and inter-rater reproducibility, ROIs should be drawn consistently each time by the same operator and different operators. Despite these challenges, ROI analysis is recommended in cases where changes in specific brain regions need to be observed.

Quantitative Tract Measurements

Along Tract Analysis

Following the extraction of WM tracts of interest in this project, a number of methods to derive quantitative tract measurements from the tracts were used (Step 7, Figure 1.11). The first method is

called ‘Along Tract Analysis’, which was used to measure diffusion tensor metrics (FA and MD) along the length of selected tracts (Figure 1.13). In this protocol, motor pathways were first defined by ‘start’ and ‘end’ ROIs (placed in the cerebral cortex and culminating at the brainstem level, respectively) (Step 1) and cropped at ‘end’ ROIs to ensure similar tract length of all tracts within the circuit (Step 2). Spurious tracts were removed by rejecting the longest tracts in motor circuits (Step 3). Diffusion metrics (FA and MD) were subsequently sampled in the remaining selection of tracts by automated segmentation of individual tracts into a pre-determined number of locations (bins) of equal streamline point count, to ensure minimal data variance in metrics along the tract (Steps 4-5, Figure 1.13). This approach ensured anatomically coincident bins to be sampled along each tract of interest for each individual subject (Figure 1.14). The advantage of the along tract protocol is its ability to capture the immense amount of anatomical variability in WM microstructure along the length of selected tracts.[65] An alternative to the along tract method is the more commonly used ‘tract-averaged’ approach, whereby FA and MD values are derived along the length of the tract selection and averaged to provide one single point spread estimate of FA or MD per tract. Using this second method, potential variances in WM microstructure are lost, therefore this project takes advantage of the along tract protocol to effectively capture WM microstructural variability in the heterogeneous A-T cohort under study.

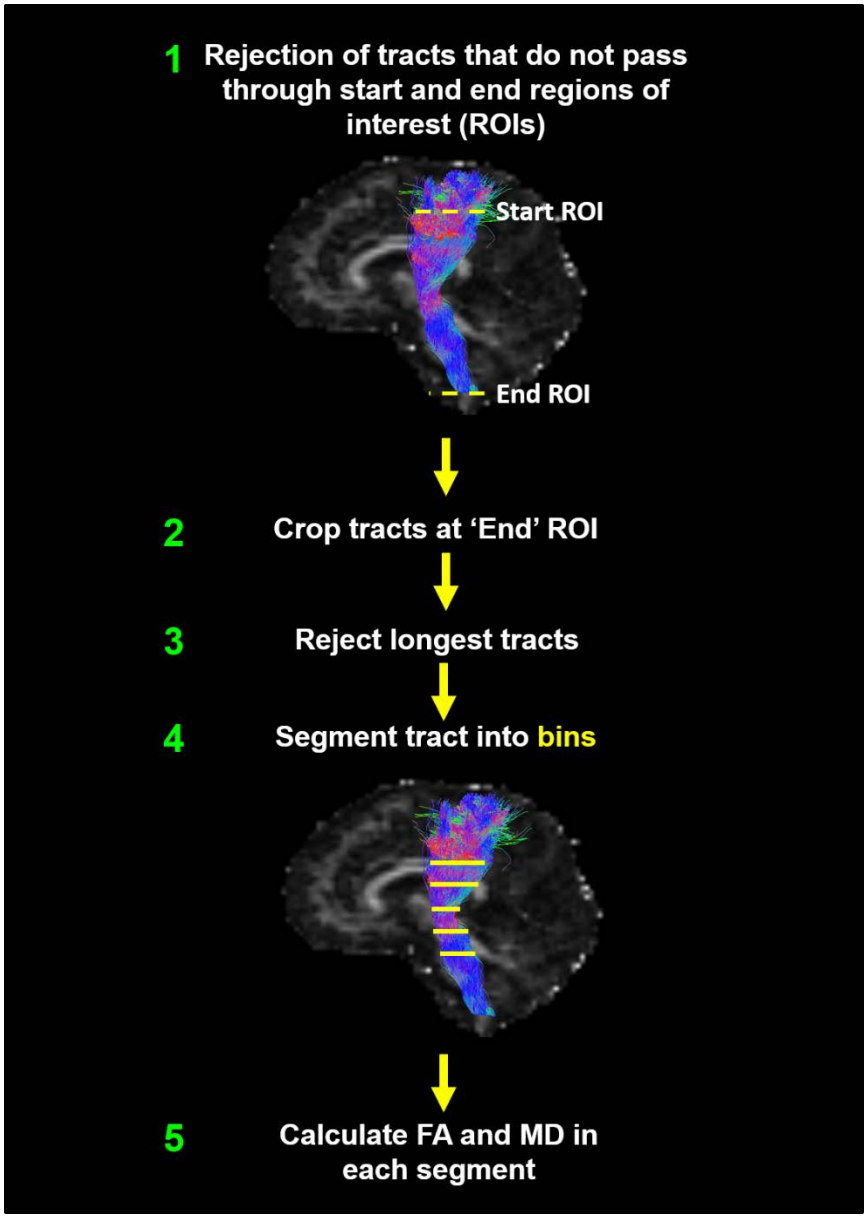

Figure 1.13. Along Tract Analysis pipeline. Motor pathways were first defined by 'start' and 'end' regions of interest (ROIs) (placed in the cerebral cortex and culminating at the brainstem level respectively, Step 1). In this figure, representative corticospinal tracts overlaid on a sagittal fractional anisotropy (FA) image are presented in Steps 1 and 4, where fibre orientation of tracts in the left-right direction are highlighted in red, in the inferior-superior direction are highlighted in blue and in the anterior-posterior direction are highlighted in green, respectively. Tracts were cropped at 'end' ROIs to ensure similar tract length of all tracts within the circuit (Step 2). Spurious tracts were removed by rejecting the longest tracts in motor circuits (Step 3). Diffusion metrics (FA and mean diffusivity (MD)) were subsequently sampled in the remaining selection of tracts by automated segmentation of individual tracts into a pre-determined number of locations (Bins, represented by yellow markings on corticospinal tracts, Step 4) of equal streamline point count, to ensure minimal data variance in metrics along the tract (Steps 4-5).

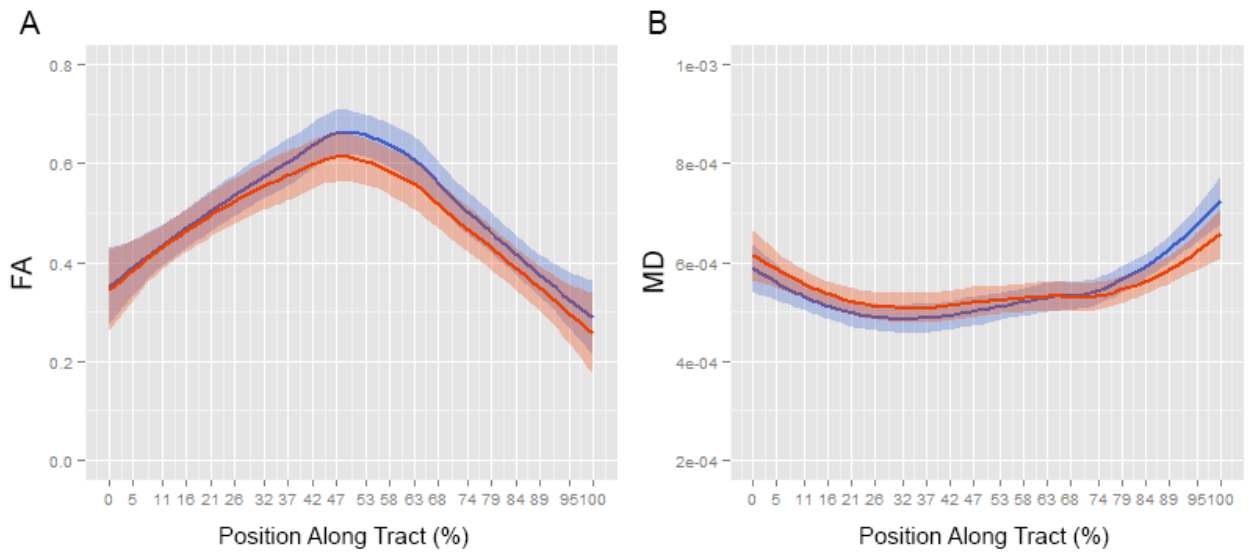

Figure 1.14. Representative graphs from the Along Tract Analysis pipeline. A) Smooth estimates of the average fractional anisotropy (FA) of a representative control (blue) and patient (red) corticospinal tract in the left cerebral hemisphere are plotted versus position from tract origin (cerebral motor cortex (0%) – brainstem level spinal cord (100%)), ± pointwise 99% confidence range (blue: control, red: patient)). B) Smooth estimates of the average mean diffusivity (MD) of a representative control (blue) and patient (red) corticospinal tract in the left cerebral hemisphere are plotted versus position from tract origin (cerebral motor cortex (0%) – brainstem level spinal cord (100%)), ± pointwise 99% confidence range (blue: control, red: patient)). Tract position at 0-5% represents precentral and postcentral gyrus layers, at 47-58% represents thalamic layers and at 95-100% represents the spinal cord at the level of the brainstem in corticospinal tracts, respectively.

Streamline Number, Tract Volume and Apparent Fibre Density

Additional measurements taken from selected tracts in this project were streamline number, tract volume and apparent fibre density (AFD). Streamline number and tract volume, derived directly from the tract using robust FSL statistical tools, can be used to identify structural differences along fibre bundles. Similarly, AFD, which is derived from the FOD lobe parallel to the streamline direction, allows the structural differences along single fibre bundles and the corresponding connectivity between two anatomic regions between a tract to be identified.[66] Specifically, it combines information from intra-voxel fibre density and tract cross-sectional area (anatomic region) to identify tracts with reduced fibre density, an analysis component that is useful when studying WM microstructure in neurodegenerative diseases.

Thesis Aims and Objectives

Performing diffusion imaging in children with ataxias presents a significant challenge. A-T patients particularly, display spontaneous movement at resting positions and imaging procedures where non-sedated scanning is conducted will contribute to excessive motion artefact in diffusion-weighted images. This presents a considerable limitation to data quality which, through a series of data pre-processing and correction steps, have been largely addressed in this thesis (Chapters 3-5). Second, young A-T patients display competing effects of white and grey matter maturation and degeneration in structural integrity studies, therefore data from this project should be viewed in consideration of this competing effect. Finally, heterogeneous neurodegeneration and clinical observations in the A-T cohort can and should be expected. Analysis and interpretation of A-T diffusion imaging data should ideally be conducted on a case-by-case basis, with strong linkage to individual clinical observations where possible. Despite these challenges, diffusion imaging studies are urgently needed to fully elucidate the relationship between ATM gene mutation and loss in integrity of motor circuitry in A-T patients.

In this context, this PhD project aims to:

1. Assess whole brain cortex and subcortical WM and GM morphological changes between A-T patients and typically developing participants

2. Investigate if A-T neuropathy is localised to the cerebellum or extends to the entire motor cortex in select WM pathways in A-T

3. Investigate if A-T neuropathy is localised to the cerebellum or extends to the entire motor cortex in serial study of patients

Thesis Format

The above listed aims are presented in three of the six chapters of this thesis. This thesis consists primarily of publications, where chapters 2, 3, 4 and 5 are manuscripts that have either been published or have been submitted for peer review to an international journal. Each manuscript in general, consists of an introduction, methods, results, discussion and if applicable, a conclusions section. Each manuscript was written to be a standalone publication, therefore there may be repetition of information, particularly of the methodology in this thesis. The specifics of each chapter following the current chapter are detailed below.

Chapter 2 contains a literature review published in the journal *Cerebellum* in 2014. This chapter reviews A-T anatomical and histopathological findings, the involvement of MR modalities and identification of disease conditions using these modalities in A-T, and future imaging work that is needed in the area.

Chapter 3 addresses the first aim of this project and contains a research article published in the journal *Movement Disorders* in 2014. This paper implements whole brain WM and GM imaging in A-T patients for the first time, to analyse GM volume alterations and WM microstructure differences between healthy controls and patients, to understand the differences in structural integrity underlying A-T.

Chapter 4 addresses the second aim of this project and contains a research article published in the journal *NeuroImage Clinical* in 2015. This paper details the computational analysis of diffusion tensor metrics (FA and MD) along the length of somatosensory, corticospinal and select corticomotor cerebellar tracts in control and patient data. The paper highlights the effectiveness of along tract methodology in studying brain WM connectivity, specifically by calculating FA and MD at consistent intervals along tract length, thereby providing a comprehensive view of the anatomical variation in WM integrity along the assessed neural pathways.

Chapter 5 addresses the third aim of this project and contains a research article submitted for peer review to the journal *Paediatric Neurology* in 2015. This report details the results of longitudinal whole brain WM and GM analysis, used to track neurodegenerative progression in patients over the first, second and third years of MRI scanning in this project. Additional volumetric analysis of key corticomotor areas of the brain are also included to provide a complete picture of the progress of neurodegeneration over two years in A-T patients.

Finally, Chapter 6 contains a summary of findings detailed in Chapters 3-5 and presents limitations specific to each study. General limitations of the project are also discussed and future implications and avenues of research for this project are presented.

CHAPTER 2

Radiological Imaging in Ataxia-telangiectasia: a Review

The second chapter consists of a systematic literature review published in the journal *Cerebellum* in 2014. The review presents a broad introduction to the multi-faceted nature of ataxia-telangiectasia (A-T) symptomology followed by a concise review of the cerebral, cerebellar and spinal cord histopathology of the disease. The biochemical and physiological causes of A-T neurodegeneration and relevant short-term therapies are presented. The prevalence of predominately radiological imaging in A-T is discussed and contrasted to the lack of diffusion imaging application in the A-T imaging arena. The paper concludes with the potential benefits of applying diffusion imaging to A-T, which are improvements to the investigation of the microstructural tissue environment, and the ability to uncover the mechanics behind loss of motor network integrity in A-T non-invasively. It should be noted that since the publication of this review article, a number of studies utilising structural brain imaging modalities in young A-T patients have been published and are recorded in Table 2.2 in the Appendices of this thesis.

As the first author of this paper, I drafted and primarily edited the article. My co-author Stephen Rose assisted in the drafting and critical editing of the manuscript. My co-authors Kate Sinclair, Kerstin Pannek and Martin Lavin contributed to the conception and design of this project and to the critique of this manuscript.

Radiological Imaging in Ataxia-telangiectasia: a Review

Ishani Sahama, Kate Sinclair, Kerstin Pannek, Martin Lavin and Stephen Rose

Cerebellum 2014;13(4):521-530. DOI: 10.1007/s12311-014-0557-4.

Submitted: 20 Jan 2014
Revised: 16 Mar 2014
Accepted: 16 Mar 2014
Available online: 29 March 2014
Journal impact factor (at publication): 2.595

Abstract

The human genetic disorder ataxia-telangiectasia (A-T) is characterised by neurodegeneration, immunodeficiency, radiosensitivity, cell cycle checkpoint defects, genomic instability and cancer predisposition. Progressive cerebellar ataxia represents the most debilitating aspect of this disorder. At present, there is no therapy available to cure or prevent the progressive symptoms of A-T. While it is possible to alleviate some of the symptoms associated with immunodeficiency and deficient lung function, neither the predisposition to cancer nor the progressive neurodegeneration can be prevented. Significant effort has focused on improving our understanding of various clinical, genetic and immunological aspects of A-T; however, little attention has been directed towards identifying altered brain structure and function using MRI. To date, most imaging studies have reported radiological anomalies in A-T. This review outlines the clinical and biological features of A-T along with known radiological imaging anomalies. In addition, we briefly discuss the advent of high-resolution MRI in conjunction with diffusion-weighted imaging, which enables improved investigation of the microstructural tissue environment, giving insight into the loss in integrity of motor networks due to abnormal neurodevelopmental or progressive neurodegenerative processes. Such imaging approaches have yet to be applied in the study of A-T and could provide important new information regarding the relationship between mutation of the ataxia-telangiectasia mutated (ATM) gene and the integrity of motor circuitry.

A-T and Genetic Origins

Ataxia-telangiectasia (A-T, Louis–Bar syndrome) is an autosomal recessive neurodegenerative disorder that occurs in 1 per 88,000 live births in the USA.[67] In the UK, an estimated fourfold lower incidence of approximately three per million live births has been reported.[1] The disease was first characterised in 1941[68] and localised to chromosome 11 q22-q23 in 1988.[2] Multi-system characteristics associated with A-T were subsequently shown to be a result of mutation in a single gene, ATM (ataxia-telangiectasia mutated)[3] and include progressive cerebellar ataxia, immunodeficiency, sinopulmonary infections, oculocutaneous telangiectasia[4, 5] and elevated serum alpha-fetoprotein levels.[6] The ATM gene encodes for the protein kinase ATM, a key player in the cellular response to double-stranded DNA damage[69] and multiple cell cycle checkpoint pathways.[10] As such, ATM gene mutation is associated with increased radiosensitivity in A-T patients.[13, 70-81] The causes of death in most patients are lymphoreticular malignancy or recurrent chronic respiratory infections.[4, 5]

A-T Neuropathology

Since the localisation of the ATM gene to chromosome 11, over 500 different ATM mutations have been identified that give rise to unique A-T case symptoms;[82-84] some of which are characteristic from family to family.[85-87] This genetic variation extends to the neurological symptoms of A-T, which differ on a case-by-case basis and can be grouped by anatomic region. Known neuropathology based on post-mortem studies in A-T is summarised below.

Cerebrum

Anatomical studies in A-T have reported widely distributed cerebral tissue vascular changes. The presence of numerous Lewy bodies and moderate nerve cell loss in the substantia nigra represent part of these changes.[87-91] Haemosiderin scarring in frontal lobe white matter (WM), the parietal area, including the parietal operculum, in the temporal lobe, in the subcortical area of both occipital lobes and capsula externa has been reported.[91, 92] Smaller scarring has been observed in the WM of the precentral and postcentral gyrus[92] as well as moderate cortical gliosis of the central and parietal gyri.[88] Lesions within the thalamus have been reported.[88, 90] Basal ganglia pathology in A-T has also been described, particularly glial scarring and demyelination in the frontal plane sections of both basal ganglia hemispheres.[92]

Cerebellum

Cerebellar pathology in A-T includes cerebellar atrophy of the frontal and posterior vermis and atrophy of both cerebellar hemispheres, particularly in the middle and superior cerebellar peduncles (brachia pontis and conjunctiva, respectively).[87, 88, 90-98] On a microscopic scale, the loss of Purkinje cells and loss or reduction of granular cell layers, especially in the anterior cerebellar vermis, is a hallmark feature in A-T.[11, 88, 89, 91-94, 97-100] Abnormal nuclear and dendritic arborisations in Purkinje neurons have also been reported.[88, 94] A number of generalised findings relating to the loss of occipital cortex pyramidal cells, smaller than average dentate nucleus, larger than average inferior olivary nucleus venules, where the inferior olivary nuclei showed nerve cell loss and reduced myelinated fibres in the nervus hypoglossas and enlarged venules in the cerebellar meninges have been described.[87-89, 97, 98]

Brainstem

Brainstem abnormalities in A-T are dependent on individual patients and age. In some studies, no brainstem abnormalities were seen.[95, 98] In other cases, glial nodules in pyramidal tracts and the medial lemnisci and gliosed gracile nuclei were observed.[94] Sectional demyelination of the pons and midbrain in the brachia conjunctiva and pontis has also been reported.[92] Other more comprehensive case studies observed atrophy in the rostral mesencephalic nucleus of the trigeminus, poorly pigmented neurons of the locus coeruleus, medial/inferior vestibular nuclei and medullary reticular formation, smaller medullary pyramids with gliosed dorsal portions; and gliosed Goll's and Burdach's nuclei.[87, 88, 91]

Other pathological findings include neuroaxonal dystrophy in the medulla oblongata tegmentum, particularly in the gracilis and cuneatus nuclei.[89, 97] Nuclei of the 5th, 6th, 7th and 12th cranial nerves have also been shown to display varying neuronal loss and gliosis.[89]

Spinal Cord

Pathology in lower motor neurons of the spinal cord is generally reported in A-T patients that live past their third decade.[88, 96, 97] The earliest study to discuss spinal cord pathology in A-T reported severe spinal dorsal tract demyelination and fibrillary gliosis, especially in the cervical area and the cuneate and gracile fascicle. Proximal spinal root demyelination and fibrosis, focal necroses in the anterior spinal cord and abnormal grey matter (GM) structures in the cervical and lumbar spinal cord have also been recorded.[93] Pallor regions and demyelination in the posterior spinal column have been described, particularly in the fasciculus gracilis, to a lesser degree in the fasciculus cuneatus, in the crossed pyramidal tracts and in dorsal spinocerebellar tracts.[87-91, 94-97] Demyelination of the entire

posterior funiculi,[92] the fasciculus proprius, the lateral corticospinal tracts[89] and the gliosis of the anterior funiculi have also been recorded.[88] Anterior horn cell degeneration in patients (30–40 years) has also been observed.[87-92, 97, 100, 101] Other affected areas of the spinal cord are the dorsal root ganglia, with morphological and histological abnormalities that differ between individuals.[88, 90, 94, 100] In peripheral nerves, extensive myelin and axon loss have been recorded in the sural, anterior tibial, femoral and sciatic nerves and cervico-brachial and lumbosacral plexus.[87, 89]

A-T Neurodegeneration: Oxidative Stress

As mentioned above, neurodegeneration in A-T is highly dependent on the age and individual patient. The primary cause of A-T neurodegeneration is the inability of the ATM protein to regulate oxidative stress levels in the cerebellum, leading to the apoptosis of oxidative stress sensitive Purkinje cells. Early studies using human and rodent models have shown that ATM protein expression is highest in the cerebellum,[102, 103] particularly in the cytoplasm of Purkinje cells.[104] Recent studies have shown ATM protein localisation to cerebellar Purkinje neuron nuclei in human brain tissue.[105]

The earliest paper to report reactive oxygen species involvement in A-T describes G2 phase sensitivity to hydrogen peroxide in A-T cells.[106] The ATM protein is a sensor of DNA damage and a regulator of cellular homeostasis under oxidative stress;[69, 107] thus, ATM deficiency causes the build-up of reactive oxygen species intermediates and Purkinje cell apoptosis due to these intermediates.[108-111] Purkinje cell degeneration is also attributed to the overproduction of nitric oxide (NO), which is a neurotransmitter to the cells.[108] NO can react with the high levels of superoxide anions in ATM deficient cerebella[103] to form the strong oxidant peroxynitrite,[108, 112, 113] leading to an increase in cerebellar oxidative species and subsequent DNA and protein damage to Purkinje cells.

To manage A-T neurodegenerative symptoms, investigation into therapies focusing on the use of the glucocorticoids dexamethasone and betamethasone have been undertaken.[111, 114-121] In mouse models, dexamethasone has been found to inhibit redox activities in both thymocytes and splenocytes with or without Atm, arrest the cell cycle of Atm knockout thymic lymphoma cells at the G1 phase and cause apoptosis in ATM knockout thymocytes, preventing thymic lymphoma in mice.[122-125] Of the two glucocorticoids, betamethasone has undergone preliminary clinical testing in A-T. In an early study, betamethasone was reported to improve neurological symptoms in a child diagnosed with A-T, 2 to 3 days after initial treatment. This improvement continued 2 weeks into treatment, where ataxic stance and gait were reduced and head and neck control as well as skilled movement control were improved. At 4 weeks, the only adverse side effects were increased appetite, body weight and moon face; however, after 4 weeks, no beneficial effects were observed. At this point, drug therapy was switched

to the glucocorticoid methylprednisolone, and after 6 months without therapy, the child showcased severe impairment of the central nervous system. The serum α-fetoprotein level was unchanged during and after treatment.[126] An extension of this study using six patients produced similar results.[127] A separate multi-centre, double-blind, randomised, placebo-controlled crossover trial using 13 A-T affected children and oral betamethasone and placebo also yielded a reduction of ataxia symptoms among A-T subjects.[128] For these studies, cerebellar improvement and antioxidant increase was found to be drug dependent.[128, 129] Lower doses of betamethasone (30% of what is given to patients) were found to be effective and result in milder steroid side effects; however, α-fetoprotein levels do not change.[130]

These preliminary studies have demonstrated that improved response from betamethasone is associated with age, with younger patients showing better resolution of the clinical ataxia measures.[127] These findings suggest that a threshold level of cerebellar degeneration may be a prerequisite to successful steroid therapy in A-T.[131, 132] Such a threshold level may be determined using non-invasive imaging with MRI, especially diffusion-weighted imaging, which enable the extent of degeneration of cerebellar–corticomotor pathways to be quantitatively assessed in a number of ataxic conditions.[21-28]

Interestingly, a recent fMRI pilot study where A-T patients received a 10-day cycle of oral betamethasone has shown increased activation within corticomotor regions after treatment using simple motor tasks.[133] This preliminary work suggests that steroid treatment could improve motor performance, facilitating cortical compensatory mechanisms. Importantly, this pilot study gives evidence that non-invasive fMRI studies may be useful to monitor treatment effects.

Summary of Radiological Findings in A-T

Early work in understanding radiological changes associated with A-T involved the use of CT to detect cerebellar atrophy.[134-137] These studies reported no cerebral, pons or cerebellar vermis atrophy;[138] however, brainstem calcifications were observed in patients in their fourth decade.[137] Despite the high spatial resolution, such findings highlight the significant challenges of using CT to delineate subtle neuropathological changes associated with A-T (reviewed in Wick[139]). Limits to radiation dosimetry measures also impact on the use of CT to study A-T. MRI is the preferred imaging modality due to its high spatial resolution, superior soft tissue contrast affording exquisite detail of anatomical structures and lack of radiation. In addition, MRI can be employed in a serial fashion to not only target morphological changes but also measure physiologic parameters, including cellular diffusion[140, 141] and permeability,[142] making this modality ideally useful for neurological research.

To date, only 18 MRI studies focusing on A-T patients have been reported in the English language.[84, 133, 143-158] Further details of these studies are summarised in Table 2.1. In general, MRI findings in A-T patients have reported cerebellar atrophy, specifically of superior cerebellar hemispheres or vermis, inferior cerebellar vermis hypoplasia, enlarged fourth ventricles and large cisterna magna, with variations among individuals.[84, 143-145, 148, 150, 151, 153, 156, 158] These findings support post-mortem clinical observations, with slight differences in anatomical detail. As mentioned previously, post-mortem studies have reported specific cerebellar pathology in the frontal and posterior vermis, in the middle and superior cerebellar peduncles of both cerebellar hemispheres[87, 88, 90-98] and other generalised findings (see 'Cerebellum' section).[87-89, 97, 98] These variations in post-mortem and radiological findings can be attributed to the genetic variation of ATM mutations in the A-T population, which further extend to the disease neuropathology such that A-T symptoms in the same anatomic region differ on a case-by-case basis.

Table 2.1. Summary of CT/MRI studies in A-T

Reference	Image type (CT/T1/T2/fMRI)	Age Range (years)	Gender (M/F)	Major findings
Huang and colleagues[84]	N/A but possibly CT/T1	4-14	2/6	**Findings:** cerebellar atrophy via CT and MRI examinations.
Quarantelli and colleagues[133]	T1/T2/fMRI	7-17	2/2*	**Aim^:** to test if steroid (betamethasone) induced motor performance changes in A-T is associated with fMRI modifications. **Findings:** increase in the number of activated voxels within the motor cortex under the on-therapy condition compared with the cortical activity under baseline condition in two patients.
Demaerel and colleagues[143]	CT/T1/T2	3-22	3/2	**Findings:** cerebellar atrophy in four patients, with discrete calcification on CT in the lentiform nuclei, WM low density and cortical thickening consistent with pachygyria. Cerebellar atrophy detected in MRI in one patient.
Farina and colleagues[144]	CT/T1/T2	4-22	6/6+	**Findings:** cerebellar atrophy, decreased thickness of superior cortex of cerebellar hemispheres, hypoplasia of inferior vermis and large cisterna magna observed in A-T patients.

Sardanelli and colleagues[145]	T1/T2/T2*	9-28	5/0	**Findings:** vermian atrophy, enlarged fourth ventricles and cisterna magna noted in all patients. Four patients had cerebellar hemisphere atrophy and two had enlarged infracerebellar subarachnoid spaces. Diffuse symmetrical high signal seen in central WM of cerebral hemispheres on T2-weighted images of oldest patient. Brainstem and basal ganglia changes not seen.
Ciemins and colleagues[146]	T1/T2	31	0/1	**Findings:** multiple small foci of decreased WM observed.
Opeskin and colleagues[147]	T1/T2	34	1/0	**Findings:** gross cerebellar atrophy, lesions consistent with vascular malformations in cerebral WM with surrounding abnormal tissue consistent with gliosis found. MRI scans 6 months apart from the age of 32 years showed progression of lesions.
Kamiya and colleagues[148]	T1/T2	24	1/0	**Findings:** coagulated necrosis of brain WM and vascular abnormalities in the brain parenchyma found.
Huang and colleagues[149]	CT/T1/T2	7-8	1/1	**Findings:** in male A-T subject, MRI and CT revealed no abnormalities. Brain MR in female A-T subject revealed cerebellar atrophy.

Tavani and colleagues[150]	T1/T2	2-12; eldest: 35 and 38	10/9	**Findings:** 2-year-old was normal. In the five next youngest patients (3–7 years), lateral cerebellar and superior vermis atrophy were seen. Five patients who were unable to walk had diffuse atrophy in both the vermis and cerebellar hemispheres.
Firat and colleagues[151]	T1/T2	9-13	5/1	**Findings:** clear differences in cerebellar atrophy in A-T patients compared to controls. In early MRI diagnosis of A-T, diffuse atrophy of the superior cerebellar cortex was found. Cerebellar mean apparent diffusion coefficient (ADC) values of patients and controls were statistically different (p<0.011–0.0001).
Lin and colleagues[152]	T2/MR spectroscopy	9-27	3/5	**Aim^:** to measure regional metabolite levels in the posterior fossa and basal ganglia of A-T patients. **Findings:** in A-T, there was loss of all metabolites in the cerebellar vermis and decreased metabolites in the cerebellar hemispheres. No abnormalities in the basal ganglia were seen.
Wallis and colleagues[153]	T1/T2/T2*/MR spectroscopy	23-47	7/5	**Findings:** cerebellar atrophy of vermis and hemispheres were observed in all A-T patients.

				Cerebellar analysis revealed significantly lower NAA/Cho and higher Cho/Cr ratios in A-T compared to controls (*N*-acetylaspartate (NAA), choline (Cho), and creatine (Cr)).
Habek and colleagues[154]	T1/T2/T2*	34	0/1	**Findings:** extensive and diffuse WM demyelination, T1 and T2 hypointense lesions, T1 hypointense but T2 hyperintense lesions and dilated telangiectases seen in A-T.
Kieslich and colleagues[155]	T1/T2	8–26	6/5	**Findings:** marked hyperintense lesions in the cerebral WM of T2-weighted MR images and spinal atrophy and MRI abnormalities of the basal ganglia in one patient were found. MRI in patients with normal IGF-1 levels showed cerebellar lesions in four patients and spinal atrophy in only two patients. No affectation was seen of the cerebral WM or basal ganglia in this group.
Al-Maawali and colleagues[156]	T1/T2	Age of onset: 1-3	N/A	**Findings:** isolated cerebellar atrophy in A-T MRI scans, with no extracerebellar findings.
Chung and colleagues[157]	T2	4	0/1	**Findings:** MRI scans showed leukoencephalopathy which matches leukodystrophy, a neuroimaging feature of A-T not described before.

Lin and colleagues[158]	T1/T2	19-34	4/6	**Findings:** manifest cerebellar atrophy was seen in A-T; supratentorial brain showed no sign of volume loss. Intracerebral telangiectasia with multiple punctate haemosiderin deposits were identified in 60% of subjects.

* Two patients were excluded because of insufficient compliance.[133]

+ One subject was a heterozygote parent.[144]

^ Aims are listed in studies that were not entirely anatomy-based.

In addition, radiological and post-mortem studies involved patients at different progressive stages of the disease; thus, differences in A-T neuropathology between the two study modalities can be expected.

T1- and T2-weighted images have shown multiple WM small foci of signal hypo-intensities in A-T patients, which were hypothesised to be haemosiderin areas related to haemorrhage from capillary telangiectasias or gliovascular nodules.[146] Asymptomatic supratentorial vascular abnormalities in the cerebrum have also been reported in a recent study using 10 adult A-T patients, where intracerebral telangiectasia with multiple punctate haemosiderin deposits were identified in 60% of the imaged patients.[158] These more recent findings reflect post-mortem observations of cerebral pathology in A-T[91, 92] with slight pathological differences due to individual patient differences and differences in the progressive stage of disease.

The number of published MRI studies in A-T is limited; however, it can be seen that abnormal radiological findings reported from MRI were subtle for A-T patients until age 10; after which, cerebellar atrophy becomes more evident.[150] However substantial variation in cerebellar atrophy with age does exist as evidenced in Figure. 2.1. In this case, significant cerebellar atrophy is clearly present in a 7-year-old child with A-T. Again, these observations may differ between case studies and between different A-T cohorts.

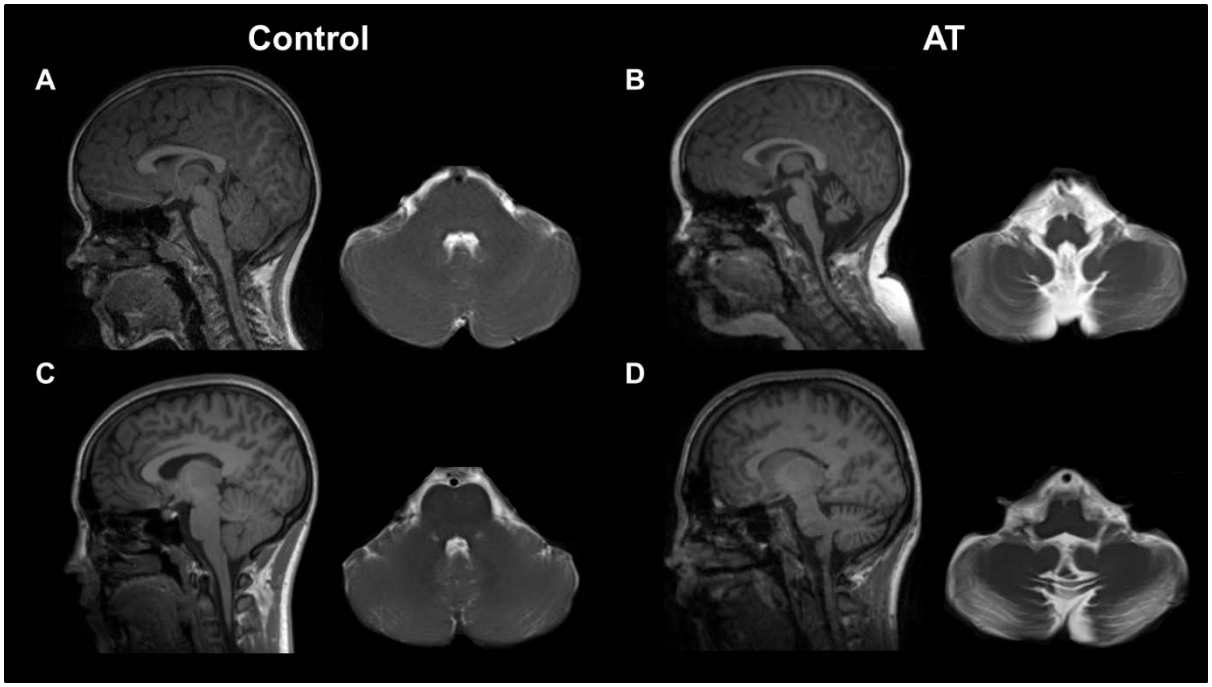

Figure 2.1. Age-matched sagittal T1 and axial T2 MRI scans acquired from control (A, C) and A-T patients (B, D). The representative images have been acquired from 7- (A, B) and 23-year-old

participants (C, D). The A-T images show marked cerebellar atrophy with involvement of both hemispheres including the cerebellar vermis.

The evolution of neuropathological changes in very young children with A-T is not well understood. One case study reported MRI findings of a 4-year-old child who was scanned at 17 months of age. The early images showed leukoencephalopathy compatible with leukodystrophy, a neuroimaging finding that has not been described in A-T.[157] This eludes to the possibility of diffuse WM signal intensity on T2-weighted MRI,[159] which indicates progressive demyelination may occur in the early stages of A-T. The specificity of this finding has yet to be established. MRI scans in older patients in their second and third decade also show varied findings in the cerebellar and cerebral lesion progression, such as corpora amylacea,[147] diffuse symmetrical high signal in the central WM of cerebral hemispheres on T2- weighted images,[145] scattered calcified deposits in the cerebrum WM and space occupying lesions in the right frontal lobe WM and left paraventricular WM.[148, 154] Both of these lesions were displayed with low intensity on T1-weighted images and high intensity on T2-weighted images.[148] General spinal atrophy and abnormalities in the basal ganglia have also been reported in older A-T patients,[155] supporting post-mortem spinal study findings in older A-T patients, but lacking specific anatomical detail (see 'Spinal Cord' section).

Discussion

Very few studies have focused on reporting radiological findings in A-T.[133, 143-148, 150-157] Of these, studies using standard T1- and T2-weighted MRI sequences have consistently shown diffuse cerebellar atrophy, predominantly within the vermis and cerebellar hemispheres. This reflects the loss of Purkinje cells on a histological level, which is a well-established neuropathological hallmark of A-T. Foci of T2-weighted WM hypo- and hyper-intensity have also been observed and attributed to capillary telangiectasia and focal extracerebellar demyelination.[146]

While these morphological studies have been useful from a radiological perspective, they provide limited information regarding the association between neurodegeneration and the loss in integrity of neural motor networks. A growing body of work has demonstrated that diffusion-weighted MRI (dMRI), particularly diffusion tensor imaging (DTI), allows a more accurate depiction of the integrity of brain and brainstem structures than that afforded by standard MRI.[16]

An extension of dMRI is the use of fibre tracking to delineate WM fibre bundles in the brain. The advantage of this approach is that the integrity of specific WM tracts in conjunction with the connectivity of pathways linking multiple brain regions can be assessed.[160, 161] Such technology has

been applied to study cerebellar–corticomotor networks in a number of ataxic conditions.[21-28] A recent study in particular has observed cerebello-cerebral WM connectivity disruptions in Friedreich's ataxia with diffusion MRI, tractography and super-resolution track density imaging, which has explained some of the non-ataxic symptoms observed with this disease.[162] To date, there are no published studies investigating degeneration of cerebellar–corticomotor tracts using WM fibre tracking in A-T. Future work using this modality needs to be directed towards understanding the spatial extent of degeneration along each WM pathway, specifically in terms of the connectivity between the cerebellum and cerebrum, to ascertain whether degeneration occurs predominately within the cerebellum and propagates to cerebral regions or occurs along the entire length of the cortico-cerebellar motor pathway. Such studies are urgently required to fully understand the impact of mutation of the ATM gene and loss in connectivity of motor circuits in A-T.

Future studies should also investigate the degeneration of motor pathways involving subcortical structures such as the basal ganglia, which are known to be involved with motor disorders. Although basal ganglia pathology has been associated with mutation of the ATM gene,[92] it is currently not known whether striatal–corticomotor pathways are affected in A-T. The integrity of such motor networks is of interest due to a recent study reporting improved neurological measures in A-T patients after treatment with amantadine sulphate.[163] Although the mechanism of amantadine is not well understood, it is believed to act on striatal dopaminergic systems.[164, 165] Future work should also focus on the relationship between clinical measures and the integrity of motor pathways to develop useful biomarkers for monitoring disease progression and assessing the efficacy of new therapies.

Our understanding of the very early neuropathological changes in A-T is limited. Imaging data from infants with A-T is extremely difficult to acquire due to delayed onset of clinical phenotypes, and thus, we can only speculate on the integrity of the WM and GM areas, particularly those associated with the cerebellum, which may be compromised at the very early stages of development. Obtaining imaging data from an infant cohort would be extremely beneficial but rather challenging due to the difficulty and complexity of gaining an early diagnosis of A-T. Nonetheless, such information may shed light on the neurodevelopmental origins of A-T.

Conclusion

The various clinical, genetic and immunological aspects of A-T have been reported extensively in past literature, with imaging studies in A-T using CT and MRI to report predominately radiological anomalies. Little attention has been directed towards identifying altered brain structure and function using dMRI, and as such, there are no published studies investigating degeneration of cerebellar–

corticomotor tracts using WM fibre tracking in A-T to date. Future work in A-T using dMRI will assist in understanding the spatial extent of degeneration along each WM pathway, specifically the connectivity between the cerebellum and cerebrum, to ascertain whether degeneration occurs predominately within the cerebellum and propagates to cerebral regions or occurs along the entire length of the cortico-cerebellar motor pathway. Such studies are a key first step to fully understand the impact of mutation of the ATM gene and loss in connectivity of motor circuits in A-T.

CHAPTER 3

Altered Corticomotor-Cerebellar Integrity in Young Ataxia-telangiectasia Patients

This chapter includes the second manuscript published during PhD candidature in *Movement Disorders*, 2014. The paper details grey and white matter imaging conducted between A-T patients and healthy control participants, under the first aim of the PhD project, to: 'assess whole brain cortex and subcortical WM and GM morphological changes between A-T patients and typically developing participants'.

The paper highlights the whole brain methodology involved in uncovering these changes between control and patient groups and presents the voxel-wise WM and GM changes that are seen in young A-T patients compared to controls. In addition, clinical scoring details of each A-T patient are included in the paper to provide a comprehensive picture of heterogeneous neurodegeneration and ataxic symptomology in A-T.

As first author of this paper, I collected, analysed and interpreted the data and drafted and edited the manuscript. My co-authors Stephen Rose and Kerstin Pannek contributed to data collection and the interpretation of results. My co-authors Kate Sinclair, Simona Fiori and Martin Lavin contributed to the clinical interpretation of results. All co-authors provided critique of the article.

Altered Corticomotor-Cerebellar Integrity in Young Ataxia-telangiectasia Patients

Ishani Sahama, Kate Sinclair, Simona Fiori, Kerstin Pannek, Martin Lavin and Stephen Rose

Mov Disord. 2014;29(10):1289-1298. DOI: 10.1002/mds.25970.

Submitted: 28 January 2014
Revised: 15 May 2014
Accepted: 16 June 2014
Available online: 17 July 2014
Journal impact factor (at publication): 4.558

Abstract

Magnetic resonance imaging (MRI) research in identifying altered brain structure and function in ataxia-telangiectasia, an autosomal recessive neurodegenerative disorder, is limited. Diffusion-weighted MRI were obtained from 11 ataxia-telangiectasia patients (age range, 7-22 years; mean, 12 years) and 11 typically developing age-matched participants (age range, 8-23 years; mean, 13 years). Grey matter volume alterations in patients were compared with those of healthy controls using voxel-based morphometry, whereas tract-based spatial statistics was employed to elucidate white matter microstructure differences between groups. White matter microstructure was probed using quantitative fractional anisotropy and mean diffusivity measures. Reduced grey matter volume in both cerebellar hemispheres and in the precentral-postcentral gyrus in the left cerebral hemisphere was observed in ataxia-telangiectasia patients compared with controls (p<0.05, corrected for multiple comparisons). A significant reduction in fractional anisotropy in the cerebellar hemispheres, anterior/posterior horns of the medulla, cerebral peduncles, and internal capsule white matter, particularly in the left posterior limb of the internal capsule and corona radiata in the left cerebral hemisphere, was observed in patients compared with controls (p<0.05). Mean diffusivity differences were observed within the left cerebellar hemisphere and the white matter of the superior lobule of the right cerebellar hemisphere (p<0.05). Cerebellum-localised grey matter changes are seen in young ataxia-telangiectasia patients along with white matter tract degeneration projecting from the cerebellum into corticomotor regions. The lack of cortical involvement may reflect early-stage white matter motor pathway degeneration within young patients.

Introduction

Ataxia-telangiectasia (A-T) is an autosomal recessive neurodegenerative disorder that occurs in 1 per 88,000 live births in the United States[67] and in approximately 3 per million live births in the United Kingdom.[1] Multi-system disease characteristics are attributed to genetic mutation of the ATM (ataxia-telangiectasia mutated) gene[2, 3] and include progressive cerebellar ataxia, immunodeficiency, sinopulmonary infections, oculocutaneous telangiectasia,[4, 5] and elevated serum alpha-fetoprotein levels.[6] The ATM gene encodes the protein kinase ATM, a key player in the cellular response to DNA double-stranded breaks.[7, 8] This protein is also involved in the response to oxidative damage, ATM activation by oxidative stress,[9] and it may have a more general role in cell homeostasis. Once activated, ATM phosphorylates a multitude of proteins that control various cellular processes, including different cell cycle checkpoint pathways.[10] Mutation of this gene is linked to increased radiosensitivity in A-T patients[11, 12] and in cells from these patients in culture.[13, 14] Lymphoreticular malignancy or recurrent chronic respiratory infections[4, 5] is the cause of death in most patients.

To date, imaging studies using conventional T1- and T2-weighted magnetic resonance imaging (MRI) have been used to highlight the hallmark neuropathological features associated with A-T, namely progressive cerebellar atrophy.[84, 144, 148, 150, 158] Although this has been useful from a radiological perspective, such morphological studies provide limited information of the association between neurodegeneration and the loss in neural motor network integrity. Diffusion-weighted MRI (dMRI), particularly diffusion tensor imaging (DTI), has been demonstrated to allow a more accurate depiction of brain and brainstem structure integrity than that afforded by standard MRI.[16]

In contrast to conventional MRI, DTI measures the random motion of water in cerebral tissue. When this random motion is preferentially restricted to movement in one direction, as occurs along axonal bundles, such diffusion is referred to as anisotropic. Fractional anisotropy (FA) is a quantitative measure of the degree of anisotropy, and mean diffusivity (MD) measures the mean motion of water considered in all directions. White matter (WM) fibre degeneration is typically reflected by decreases in FA, and increases in MD (reviewed in Beaulieu[37]). These measures are used to interrogate pathological changes in regard to myelination, in cerebral tissue.[57] A number of elegant approaches have been developed that enable the voxel-wise analysis of diffusivity measures (FA and MD), such as tract-based spatial statistics (TBSS).[42, 44] Furthermore, grey matter (GM) volume can be assessed using voxel-based morphometry (VBM).[40, 41] Such analysis strategies have yet to be applied in A-T clinical populations.

Within the research setting, diffusion imaging studies of children with ataxias presents a significant challenge. The most prominent challenge is the presence of excessive image artefacts caused by uncontrolled head motion during non-sedated scanning procedures on diffusion-weighted images. These technical issues have in part been addressed through a series of data pre-processing and correction steps to reduce image distortions inherent to the acquisition technique, as well as those caused by involuntary head movement,[20] allowing dMRI studies to be performed in A-T. Such studies are urgently needed to fully elucidate the relationship between mutation of the ATM gene and loss in the integrity of motor circuitry. The aim of this paper is to highlight the potential of WM and GM imaging, by demonstrating that DTI can be performed successfully on children with A-T. We present novel findings depicting the loss in integrity of key cerebellar-corticomotor pathways with respect to normal brain development in A-T.

Methods

Participants

Magnetic resonance imaging data were acquired from 11 patients with A-T (6 male: age mean ± SD, 12.18±5.56; age range, 7-22 years) and 11 age-matched typically developing participants (4 male: age mean ± SD, 12.82±5.51; age range, 8-23 years). All of the patients have been clinically diagnosed for human A-T in accordance with the recent World Health Organisation recommendations,[166] including genetic testing. All subjects and parents gave informed consent in accordance with our Human Ethics Institutional Review Board and the Declaration of Helsinki.

Clinical Scoring

The clinical scoring of A-T patients was conducted using a modified version of the A-T Neuro Examination Scale Toolkit (A-T NEST), an A-T scaling system that has been refined from a quantitative 10-point scale since its introduction in 2000.[167] The modified A-T NEST accounts for the multi-dimensional nature of A-T characteristics and compensates for the disease's complexity and heterogeneity, making for an effective and sensitive method to precisely measure A-T neurological deficits (personal communication with Dr. Thomas Crawford, Professor of Neurology and Paediatrics at the John Hopkins Hospital).

Image Acquisition

Imaging data were acquired using a 3T MRI scanner (Siemens Trio, Erlangen, Germany) with TQ gradients (45 mT/m, slew rate 200 T/m/s), using a 12-element Tim head array. A high-resolution structural image was acquired using a 0.9 mm isotropic 3D T1 Magnetisation Prepared Rapid

Gradient Echo (MPRAGE) sequence. The imaging parameters were: field of view, 23×23×17.3 cm; TR/TE/TI 1,900/2.32/900 ms; flip angle, 9 degrees; matrix size, 192×512×512×1 cm. Diffusion MRI acquisition consisted of a high angular resolution diffusion imaging (HARDI) sequence with the following parameters: 60 axial slices; 2.5 mm slice thickness; field of view 30×30 cm; TR/TE 9500/116 ms; acquisition matrix 128×128, resulting in an in-plane resolution of 2.34×2.34 mm. Parallel imaging with an acceleration factor of 2 was employed to reduce susceptibility distortions. Sixty-four diffusion-weighted images were acquired at b=3,000 s mm^{-2}, along with one minimally diffusion-weighted image (b=0). The acquisition time for the diffusion dataset was 9:40 minutes. A field map for diffusion data was acquired using two 2-dimensional gradient-recalled echo images (36 axial slices; 3 mm slice thickness with 0.75 mm gap; field of view 19.2×19.2 cm; TR/TE1/TE2 488/4.92/7.38 ms; acquisition matrix 64×64) to assist correction for distortions caused by susceptibility inhomogeneity.

Diffusion Processing

An extensive pre-processing procedure was followed to detect and correct for image artefacts caused by head motion and image distortions,[20] thereby enabling the use of all patient subjects for analysis. Image volumes affected by within-volume movement were detected using the discontinuity index[168] and excluded from further analysis. Image distortions caused by susceptibility inhomogeneities were reduced using the field map, using tools available with FMRIB's Software Library (FSL[169]). Intensity inhomogeneities were removed using N3.[170] Subsequently, signal intensity outlier voxels (caused by cardiovascular pulsation, bulk head motion, and so forth) were detected and replaced using the detection and replacement of outliers prior to resampling (DROP-R) approach.[171] This involves between-volume registration to account for head movement during the scan time using a fit model to all measurements (FMAM) method,[172] including adjustment of the b-matrix.[173, 174] DROP-R was modified from the originally proposed method to employ a model for the detection and replacement of outliers termed higher order model outlier rejection (HOMOR[175]). FA and MD maps were then generated using the MRtrix package.[59]

Tract-Based Spatial Statistics

To investigate WM degeneration between A-T patients and healthy controls, WM microstructure was compared by carrying out voxel-wise statistical analysis of the FA and MD data using TBSS,[44] part of FSL.[42] After alignment of all subjects' FA data into FMRIB58 FA standard space using the nonlinear registration tool FNIRT,[176, 177] the mean FA image was created and thinned to create a mean FA skeleton representing the centres of all tracts common to the group. The aligned FA data of each subject was projected onto this skeleton and the resulting data fed into voxel-wise cross-subject

statistics. Permutation based testing (independent samples t-test) was carried out using the 'randomise' program included in FSL, which also corrected for multiple comparisons in space, using threshold-free cluster enhancement with 5,000 iterations.[178] Sex was included as a covariate in the analysis. Structures with significantly different FA or MD between subject groups (p<0.05) were identified using the John Hopkins University WM atlases included in FSL.[179]

Voxel-Based Morphometry

Grey matter changes between A-T subjects and healthy controls were analysed with FSL-VBM,[40] an optimised VBM protocol[41] carried out with FSL tools.[42] No A-T subjects were excluded from the analysis based on visual assessment of images for head motion artefacts. Structural images were first brain-extracted and GM segmented before being nonlinearly registered to the Montreal Neurological Institute (MNI) 152 standard space.[177] A left-right symmetric, study-specific GM template was created using the resulting images, which were averaged and flipped along the x-axis. All native GM images were then nonlinearly registered to this study-specific template and 'modulated' for local expansion (or contraction) correction because of the nonlinear component of the spatial transformation. Smoothing with an isotropic Gaussian kernel with a sigma of 3 mm was applied to the modulated GM images. A statistical voxel-wise analysis (independent samples t-test) was then performed, using permutation based nonparametric testing with 5,000 iterations, adjusted for multiple comparisons across space, using threshold-free cluster enhancement.[178] Sex was included as a covariate in the analysis. Voxels were considered significant at corrected p<0.05. We use the terminology GM volume, which refers to the likelihood of GM within a voxel, not a physical property of the underlying GM.

Results

Clinical and T2-Weighted MRI Observations

T2-weighted MRI axial scans revealed cerebellar atrophy without major pathological conditions in the cerebrum of A-T patients used in this study. WM hyper-intensity and telangiectasias (thickening of blood vessels) were not present on T2-weighted MRI (Figure 3.4, Appendices). Overall, clinical observations indicate heterogeneity of A-T characteristics among patients. Ataxia, movement disorder, and neuropathy were highly individualised in each subject, irrespective of age. Indeed, in the clinical scoring of the A-T cohort, three young patients displayed marked/mixed neuropathy, with a loss of ankle, knee, and bicep tendon reflexes and loss of proprioception in toes (Patients 2, 7, and 9, 7-10 years of age, Table 3.1), indicating advanced WM degeneration at a young age in the cohort.

Table 3.1. Summary of clinical observations of A-T patients

Patient	Age	A-T Nest Score	Observed symptoms
1	16	**Eye movements:** 6/30[a] **Ataxia:** 7/28 **Movement Disorder:** 2/6 Bradykinesia 16/16 Hyperkinesia 8/12 Dystonia **Neuropathy:** N/A[b]	**Eye movements:** off-foveal gaze tendency (vertical or horizontal) is frequent and persistent. Nystagmus on lateral gaze unsustained. **Ataxia:** sitting requires no support but sways slightly. Standing needs total vertical support. Walking requires vertical support. **Movement Disorder:** hypomimea (dystonic) facial expression and abnormal persistence of large facial expressions. Limb posturing dystonia present with either social/cognitive or motor activation. **Neuropathy:** absence of ankle tendon, bicep tendon and knee tendon reflexes. Normal proprioception in toes.
2	7	**Eye movements:** 22/30[a] **Ataxia:** 20/28 **Movement Disorder:** 3/6 Bradykinesia 13/16 Hyperkinesia N/A Dystonia **Neuropathy:** N/A[b]	**Ataxia:** sitting requires no support but sways slightly. Stands with feet together but sways. Walking has the normal path width without corrective steps. **Neuropathy:** absence of ankle tendon reflexes. Presence of bicep tendon and knee tendon reflexes. Proprioception in toes and vibration sense at ankles present.
3	12	**Eye movements:** 9/18 **Ataxia:** 8+/26 **Movement Disorder:** 3.5/8 Bradykinesia 6/15 Hyperkinesia 10/14 Dystonia **Neuropathy:** N/A[b]	**Eye movements:** oculo-motor apraxia sometimes observed. **Ataxia:** sits with self-support of arms. Standing requires no support but takes corrective steps. Walking requires massive lateral support. **Movement Disorder:** Retro-Colic spasms with motor or stance activation observed. Hypomimea (dystonic) facial expression present. Head/trunk posturing/tilt/turn mild at rest and mild with movement/posture. Trunk posturing/tilt/turn mild at rest and normal with movement/posture.

4	9	**Eye movements:** 19/30 **Ataxia:** 14/28 **Movement Disorder:** 1/6 Bradykinesia 10/16 Hyperkinesia 7/11 Dystonia **Neuropathy:** N/A[b]	**Eye movements:** off-foveal gaze tendency (vertical or horizontal) present only with certain activities. Oculo-motor apraxia present on most (>50%) gaze shifts. Post-rotary nystagmus persists more than 10 seconds. Period alternating nystagmus present. **Ataxia:** sitting requires no support but sways markedly. Standing takes no support but takes corrective steps. Walking requires no support but wide base or corrective stagger steps taken. **Movement Disorder:** distal/hand tremor present at rest. Proximal (face/head/trunk) tremor present at rest. Hypomimea (dystonic) facial expression present with abnormal persistence of large facial expressions. **Neuropathy:** normal with proprioception in toes, where movement sensibility is intact.
5	7	**Eye movements:** 29/30 **Ataxia:** 18/28 **Movement Disorder:** 2/6 Bradykinesia 10/16 Hyperkinesia 7/11 Dystonia **Neuropathy:** 6/6 (Normal)	**Eye movements:** off-foveal gaze tendency (vertical or horizontal) present only with certain activities. **Ataxia:** sitting requires no support but sways slightly/occasionally. Stands with feet together but slight sway. No support required while walking. Walks with normal speed with mild path deviations or corrective steps. **Movement Disorder:** face/head/trunk/distal limb tremor present at rest. Hypomimea (dystonic) facial expression present with abnormal persistence of large expressions.
6	21	Patient had no clinical attendance.	Patient had no clinical attendance.
7	10	**Eye movements:** 17/30 **Ataxia:** 6/28 **Movement Disorder:**	**Eye movements:** off-foveal gaze tendency (vertical or horizontal) present only with certain

		2/6 Bradykinesia 6/16 Hyperkinesia 8/11 Dystonia **Neuropathy:** N/A[b]	activities. Oculo-motor apraxia present on all gaze shifts. **Ataxia:** sitting requires no support but sways markedly. Standing requires lateral support. Walking requires massive lateral support. **Movement Disorder:** face/head/trunk/distal limb tremor present with both social/cognitive and motor activation. Hypomimea (dystonic) facial expression present with abnormal persistence of large expressions. Head/trunk posturing present with either social/cognitive or motor activation. **Neuropathy:** absence of ankle tendon, bicep tendon and knee tendon reflexes.
8	15	**Eye movements:** 20/30 **Ataxia:** 7/28 **Movement Disorder:** 1/6 Bradykinesia 13/16 Hyperkinesia 6/11 Dystonia **Neuropathy:** N/A[b]	**Eye movements:** horizontal nystagmus unsustained. Nystagmus on lateral gaze unsustained. Off-foveal gaze tendency (vertical or horizontal) present only with certain activities. Oculo-motor apraxia present on most (>50%) gaze shifts. Post-rotary nystagmus persists more than 10 seconds. **Ataxia:** sitting requires no support but sways markedly. Standing requires vertical support. Walking requires vertical support. **Movement Disorder:** face/head/trunk tremor present with both social/cognitive and motor activation. Hypomimea (dystonic) facial expression present with abnormal persistence of large expressions. Limb posturing present with both social/cognitive and motor activation. Head/trunk posturing present with either social/cognitive or motor activation. **Neuropathy:** absence of ankle tendon, bicep tendon and knee tendon reflexes. Proprioception in

			toes have movement sensibility intact. Some vibration sense present in ankles.
9	7	**Eye movements:** 16/30[a] **Ataxia:** 19/28 **Movement Disorder:** 4/6 Bradykinesia 10/14[a] Hyperkinesia 8/12 Dystonia **Neuropathy:** 1.5/6	**Ataxia:** sitting requires no support but sways slightly. Stands with feet together but sways. Walking requires no support. Walks at normal speed with mild deviations in path or corrective steps. **Movement Disorder:** hypomimea (dystonic) facial expression present with abnormal persistence of large expressions. Head posturing and limb posturing present with either social/cognitive or motor activation. **Neuropathy:** presence of knee tendon reflexes. Absence of ankle tendon reflexes. Proprioception in toes is not completely absent (between scores 0 and 1).
10	22	**Eye movements:** 6/30 **Ataxia:** 5/28 **Movement Disorder:** 2/6 Bradykinesia 8/16 Hyperkinesia 3/12 Dystonia **Neuropathy:** N/A[b]	**Eye movements:** sustained horizontal nystagmus. Sustained nystagmus on lateral gaze. Off-foveal gaze tendency is frequent and persistent. Oculo-motor apraxia is present on all gaze shifts. Post-rotary nystagmus persists more than 10 seconds. **Ataxia:** sitting requires no support but sways slightly. Standing needs support. Walking requires vertical support. **Movement Disorder:** distal limb movement present at rest. Face/head/trunk tremor present with both social/cognitive and motor activation. Hypomimea (dystonic) facial expression present with abnormal persistence of large expressions. Head posturing and limb posturing present with both social/cognitive and motor activation. **Neuropathy:** absence of ankle tendon, bicep tendon and knee tendon reflexes. Scored 3 on proprioception and 1 on vibration sense (because

			proprioception is unreliable), showing that some vibration sense at ankles is intact.
11	8	**Eye movements:** 21/30 **Ataxia:** 7/28[a] **Movement Disorder:** 2/6 Bradykinesia N/A[b] Hyperkinesia N/A[b] Dystonia **Neuropathy:** 6/6 (normal)	**Eye movements:** nystagmus on lateral gaze unsustained. Oculo-motor apraxia occasionally present. Post-rotary nystagmus persists more than 10 seconds. Periodic alternating nystagmus present. **Ataxia:** sitting requires no support but sways markedly. Standing requires no support but takes corrective steps. Walking requires some lateral support.

a Not all clinical tests were completed.

b Scores are absent/were not recorded.

Grey Matter Analysis

The VBM analysis revealed areas of reduced GM volume in both the cerebellar hemispheres of the A-T subjects compared with the control participants ($p<0.05$) (Figure 3.1). GM changes were also present in the precentral-postcentral gyrus in the left cerebral hemisphere, indicating possible extension of GM degeneration to the cerebrum. The dentate nucleus was not part of the GM map and was not included in the analysis. The observed changes do not reflect progression of GM degeneration with age and are comparisons made from grouped data from control and A-T data sets.

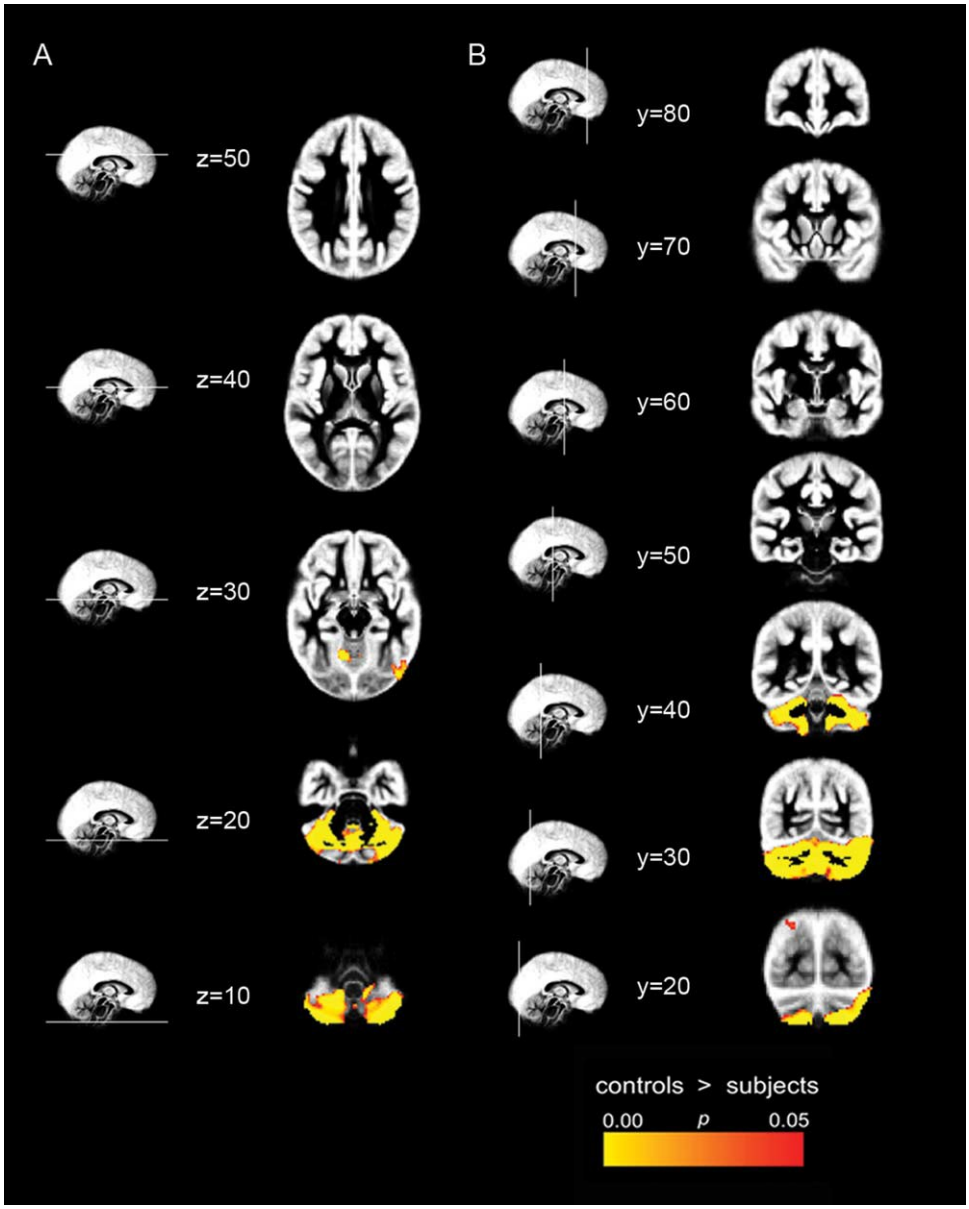

Figure 3.1. Axial (**A**) and coronal (**B**) view of voxels with significantly reduced grey matter (GM) volume in ataxia-telangiectasia subjects compared with healthy participants. Data are shown at axial and coronal slices of GM template, at Y and Z coordinates as labelled.

White Matter Analysis

The TBSS analysis showed a significant reduction in FA in a number of WM tracts in the A-T subjects compared with the control participants. As shown in Figure 3.2, these regions included the cerebellar hemispheres, anterior/posterior horns of the medulla, cerebral peduncles, and WM of the internal capsule, particularly involving the left posterior limb of the internal capsule and corona radiata in the left cerebral hemisphere ($p<0.05$); see Table 3.2 for a summary of imaging findings. Differences in MD were observed within the left cerebellar hemisphere and the WM of the superior lobule of the right cerebellar hemisphere ($p<0.05$) (Figure 3.3). Significant loss in integrity of cerebellar WM and degeneration of WM tracts projecting from the cerebellum into corticomotor regions is collectively

seen. The observed changes do not reflect progression of WM degeneration with age and are comparisons made from grouped data from control and A-T data sets.

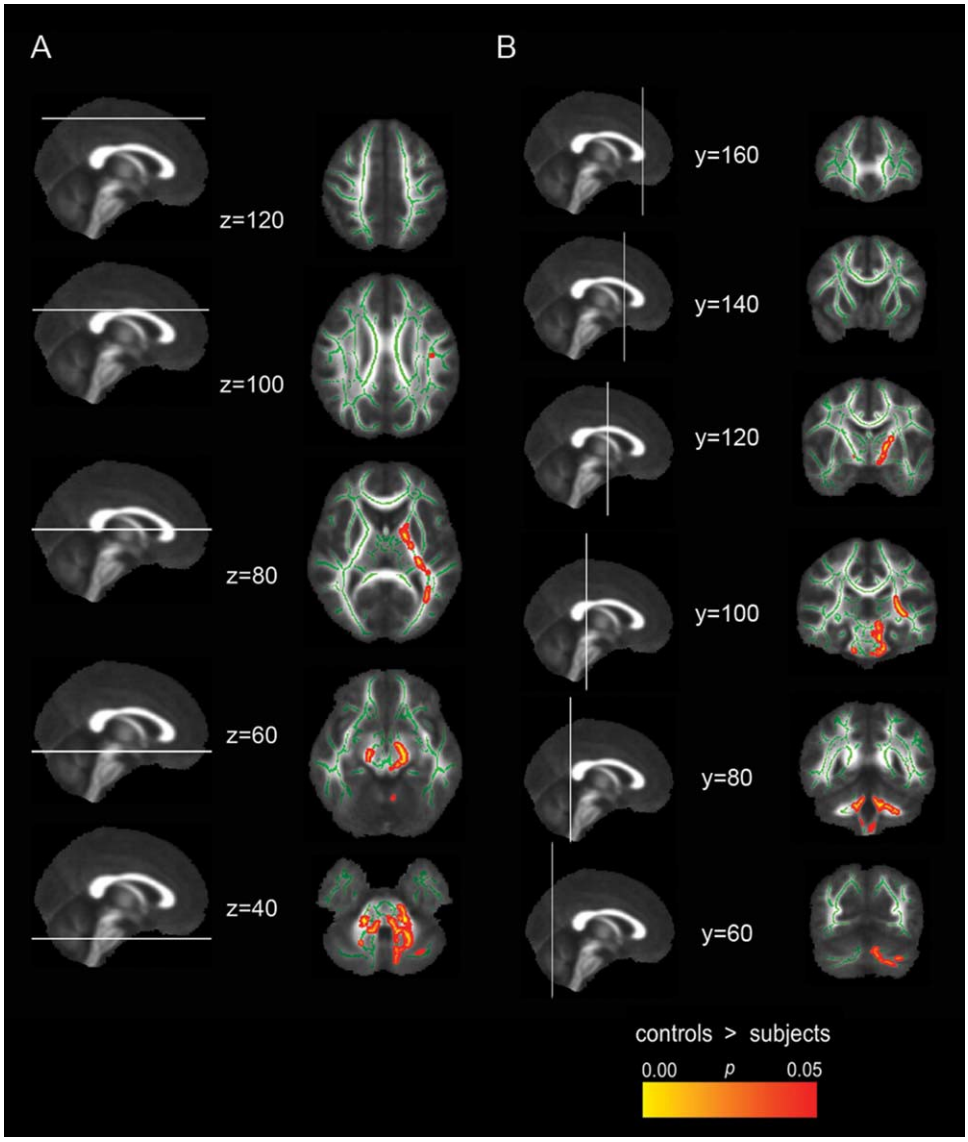

Figure 3.2. Axial (**A**) and coronal (**B**) view of voxels with significantly reduced fractional anisotropy (FA) in ataxia-telangiectasia subjects compared with healthy participants. Data are shown at labelled MNI-152 Y and Z coordinates overlaid on the mean FA map. Mean FA skeleton is shown in green.

Table 3.2. Regions that were significantly abnormal in patients with A-T (n=11) compared with controls (n=11) after correction for multiple comparisons

DTI Parameters	MNI coordinates			Cluster size (voxels)	*p*-value	Corresponding white matter cortical label (JHU-ICBM-DTI-81 white-matter labels atlas)
	x	y	z			
Reduced FA	x = 129	y = 110	z = 103	7	0.05	Superior longitudinal fasciculus L
	x = 116	y = 106	z = 96	315	0.043	Superior corona radiata L
	x = 111	y = 136	z = 95	3482	0.023	Superior fronto-occipital fasciculus (could be a part of anterior internal capsule) L
	x = 116	y = 102	z = 95	315	0.043	Posterior corona radiata L
	x = 116	y = 102	z = 90	315	0.043	Posterior limb of internal capsule L
	x = 112	y = 137	z = 90	3482	0.023	Anterior limb of internal capsule L
	x = 119	y = 112	z = 90	315	0.043	External capsule L
	x =121	y = 67	z = 89	83	0.048	Posterior thalamic radiation (include optic radiation) L
	x = 118	y = 94	z = 87	315	0.043	Retrolenticular part of internal capsule L
	x = 75	y = 117	z = 69	107	0.045	Posterior limb of internal capsule R
	x = 76	y = 117	z = 67	107	0.045	Cerebral peduncle R

	x = 106	y = 112	z = 67	3482	0.023	Cerebral peduncle L
	x = 95	y = 95	z = 56	3482	0.023	Superior cerebellar peduncle L
	x = 99	y = 73	z = 51	3482	0.023	Inferior cerebellar peduncle L
	x = 99	y = 104	z = 50	3482	0.023	Corticospinal tract L
	x = 79	y = 76	z = 49	14	0.05	Inferior cerebellar peduncle R
	x = 85	y = 82	z = 49	254	0.041	Superior cerebellar peduncle R
	x = 84	y = 93	z = 47	254	0.041	Medial lemniscus R
	x = 104	y = 102	z = 47	3482	0.023	Middle cerebellar peduncle
	x = 97	y = 92	z = 47	3482	0.023	Medial lemniscus L
	x = 95	y = 94	z = 37	3482	0.023	Pontine crossing tract (a part of MCP)
Increased MD	x = 109	y = 74	z = 43	1402	0.009	Middle cerebellar peduncle
	x = 79	y = 78	z = 51	224	0.032	Inferior cerebellar peduncle R
	x = 96	y = 75	z = 50	1402	0.009	Inferior cerebellar peduncle L

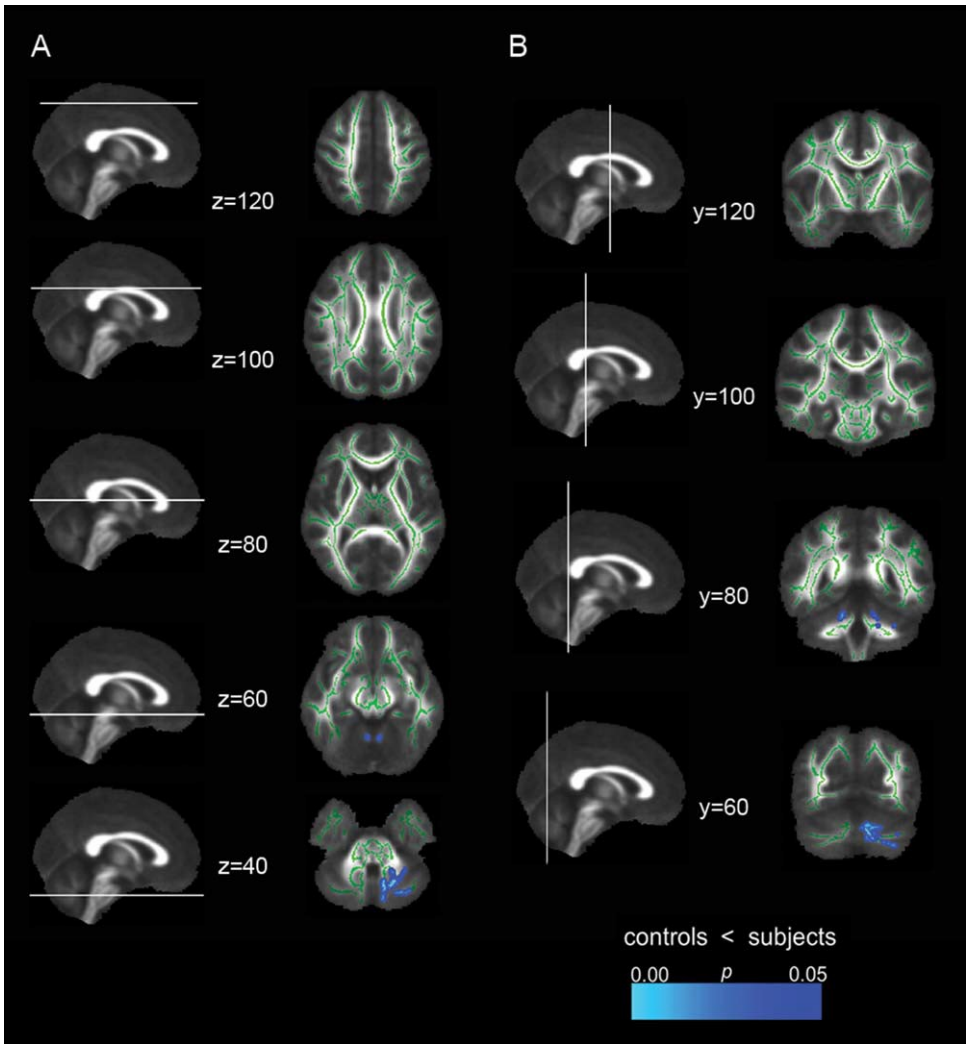

Figure 3.3. Axial (**A**) and coronal (**B**) view of voxels with significantly different mean diffusivity (MD) between healthy and ataxia-telangiectasia subjects. Data are shown at labelled MNI-152 Y and Z coordinates overlaid on the mean FA map. Mean FA skeleton is shown in green.

Discussion

Diffusion-weighted MRI, the method of choice for investigating cerebellar WM degeneration associated with multi-spectrum ataxic disorders,[22, 25, 28] has not yet been extended to the study of A-T. An important outcome of the current study is to highlight that, with use of an appropriate analysis pipeline, it is possible to study the WM microstructure of key cerebellar-corticomotor pathways within a sizeable A-T patient age range. Furthermore, voxel-wise TBSS and VBM analyses enabled delineation of WM and GM changes in the cerebrum and cerebellum of A-T subjects compared with control participants that are similar to neuropathological features reported in post-mortem studies.[87, 88, 91-93, 96, 97] The novel finding from this study identifies the degeneration of important cerebellar-corticomotor pathways responsible for coordinated motor function in all A-T patients analysed. The results of the VBM analysis demonstrate that GM changes are localised primarily to the cerebellum

in these patients. Note that our analysis consisted of young children with A-T, in whom, generally, GM changes are rarely seen.[88, 93, 96, 97] Serial qualitative analysis of high-resolution MRI data was not performed in this study and so trajectories of GM changes with age is yet to be established in A-T. In addition, correlation of VBM results with clinical scores was not performed, because scoring was incomplete (Table 3.1). Additional studies using VBM should focus on the inclusion of older A-T patients (late second decade and older), with appropriate age- and sex-matched control participant data, to provide a more comprehensive insight of GM changes with age. We predict more pronounced GM changes would be observed in an older A-T cohort, as suggested from reported post-mortem findings.[93]

In terms of WM, we show changes associated with a number of cerebellar-corticomotor pathways, predominately within the left hemisphere in our A-T subjects. The localisation of changes to the dominant hemisphere is not clear. Post-mortem studies, in general, have not focused on neurodegenerative laterality. In one study, haemorrhagic lesions in left occipital WM were recorded in a 26-year-old male A-T patient.[91] In a recent similar study of Friedreich's ataxia using TBSS and VBM, increased MD was observed in the WM underlying the left central sulcus, among other general findings. A decrease in FA in the left superior cerebellar peduncle correlated with clinical severity.[180] Whether the localised WM changes in the left hemisphere are cohort specific or reflect more early degenerative changes in young A-T patients is unclear. Despite clinical observations of extensive WM neurodegeneration in young A-T sufferers in our study cohort, no clear correlation has been seen between this clinical observation and our imaging findings.

We also show a significant reduction in FA in the cerebral peduncles and WM of the internal capsule, particularly involving the left posterior limb of the internal capsule and corona radiata in the left cerebral hemisphere in A-T patients. These findings were not reflected in structural T2-weighted axial scans (Figure 3.4, Appendices), indicating the sensitivity and specificity of dMRI for delineating WM degeneration. Our radiological findings in general do not reflect past imaging observations in cerebral pathological conditions in A-T.[158] As seen from clinical observations of our A-T cohort, A-T neuropathology can be heterogeneous in nature among different patients, irrespective of age;[82-84] therefore, disease characteristics may differ from cohort to cohort.

Multisite studies with larger cohorts of A-T subjects may provide improved insight into the degeneration of WM pathways and the neurological variability associated with the disease. To broaden our perspective of the impact of mutation in the ATM gene, the temporal trajectories of WM and GM changes with age should be further investigated, particularly in older patients, because this

important information is yet to be established in A-T. In addition to this, serial evaluation of WM and GM changes with age in individual A-T subjects should be investigated in the future to understand whether these changes are caused by degeneration or delayed WM and GM maturation. Together, with VBM results, our TBSS findings support a mechanism of degeneration within the cerebellum, propagating to corticomotor regions along the length of the cortico-cerebellar motor pathways.

Future studies should also investigate degeneration of motor pathways that involve subcortical structures such as the basal ganglia, which are known to be involved with motor disorders. Basal ganglia pathological conditions were not explicitly seen in our study, despite the array of A-T characteristics observed in our clinical observations (Table 3.1); however, abnormalities in this structure have been previously recorded both in post-mortem study[92] and in radiological findings,[155] particularly in older patients. As we have already mentioned, our particular A-T cohort consisted of very young patients; therefore, future work in A-T should include older A-T subjects as well as younger patients to provide an age-specific timeline of neuropathology in A-T.

This study has a number of limitations, the foremost being the small number of A-T participants to undergo analysis and impact on our findings. Australia has seen fewer than 50 cases of A-T overall,[181] with our clinic being the only research clinic nationally, specialising in health care for 11 of those A-T patients, representing 22% of the national population. The group-wise analysis strategies employed in this study also make it difficult to fully understand the heterogeneity of patterns of degeneration across A-T subjects. In our clinic, we observed heterogeneity of movement disorders in each patient (Table 3.1), which suggests that A-T affects not only cerebellar tracts but many other motor circuits. The extent of multiple affected areas of the brain and their sequence of development will only be realised with much larger collaborative studies across multiple research sites.[182]

Future dMRI studies could also employ probabilistic tractography to delineate WM fibre tracts, to allow the connectivity and integrity of specific WM pathways linking multiple brain regions to be assessed.[160, 161] Such technology has been used in a number of ataxic conditions to study cerebellar-corticomotor networks[22, 25, 28] and are urgently required to fully understand the impact of ATM gene mutation and loss in connectivity of A-T motor circuits.

CHAPTER 4

Motor pathway degeneration in young ataxia-telangiectasia patients: A diffusion tractography study

This chapter includes the third manuscript published during PhD candiature in *NeuroImage Clinical* in 2015. The paper details diffusion tractography and along tract analysis of corticomotor cerebellar and corticospinal motor tracts in A-T patients and healthy control participants, under the second aim of the PhD project, to 'investigate if A-T neuropathy is localised to the cerebellum or extends to the entire motor cortex in select WM pathways in A-T'.

The paper highlights the ability to compute WM integrity quantitatively (FA and MD) at consistent intervals along tract length to provide a comprehensive view of WM microstructure variation by brain region in A-T patients. In addition, general degeneration, identification of structural differences and assessment of connectivity between cerebral and cerebellar regions of selected A-T motor tracts were assessed in this paper using WM tract streamline count, tract volume and apparent fibre density (AFD), respectively.

As first author of this paper, I collected, analysed and interpreted the data and drafted and edited the manuscript. My co-authors Stephen Rose, Kerstin Pannek, James Doecke and Lee Reid contributed to the computational analysis and interpretation of results. My co-authors Kate Sinclair, Simona Fiori and Martin Lavin contributed to the clinical interpretation of results. All co-authors provided critical revision of the article.

Motor pathway degeneration in young ataxia-telangiectasia patients: A diffusion tractography study

Ishani Sahama, Kate Sinclair, Simona Fiori, James Doecke, Kerstin Pannek, Lee Reid, Martin Lavin and Stephen Rose

NeuroImage Clinical 2015;9:206-215. DOI: 10.1016/j.nicl.2015.08.007

Submitted: 22 May 2015
Revised: 17 July 2015
Accepted: 13 August 2015
Available online: 20 August 2015
Journal impact factor (at publication): 2.526

Abstract

Our understanding of the effect of ataxia-telangiectasia mutated gene mutations on brain structure and function is limited. In this study, white matter motor pathway integrity was investigated in ataxia-telangiectasia patients using diffusion MRI and probabilistic tractography. Diffusion MRI were obtained from 12 patients (age range: 7-22 years, mean: 12 years) and 12 typically developing age-matched participants (age range 8-23 years, mean: 13 years). White matter fibre tracking and whole tract statistical analyses were used to assess quantitative fractional anisotropy and mean diffusivity differences along the cortico-ponto-cerebellar, cerebellar-thalamo-cortical, somatosensory and lateral corticospinal tract length in patients using a linear mixed effects model. White matter tract streamline number and apparent fibre density in patient and control tracts were also assessed. Reduced fractional anisotropy along all analysed patient tracts were observed (p<0.001). Mean diffusivity was significantly elevated in anterior tract locations but was reduced within cerebellar peduncle regions of all patient tracts (p<0.001). Reduced tract streamline number and tract volume in the left and right corticospinal and somatosensory tracts were observed in patients (p<0.006). In addition, reduced apparent fibre density in the left and right corticospinal and right somatosensory tracts (p<0.006) occurred in patients. Whole tract analysis of the corticomotor, corticospinal and somatosensory pathways in ataxia-telangiectasia showed significant white matter degeneration along the entire

length of motor circuits, highlighting that ataxia-telangiectasia gene mutation impacts the cerebellum and multiple other motor circuits in young patients.

Introduction

The autosomal recessive neurodegenerative disorder ataxia-telangiectasia (A-T) occurs in approximately 3 per million live births.[1] ATM (ataxia-telangiectasia mutated) gene mutations give rise to this multisystem disorder[2, 3] which is characterised by progressive cerebellar ataxia, immunodeficiency, sinopulmonary infections, oculocutaneous telangiectasia [4, 5] and elevated serum alpha-fetoprotein levels.[6] The protein kinase ATM, a key player in the cellular response to DNA damage is activated by DNA double-stranded breaks.[7, 8] The ATM protein is also involved in the response to oxidative damage, being activated by oxidative stress[9] and may have a more general role in cell homeostasis. Activated ATM phosphorylates a multitude of proteins controlling various cellular processes, specifically cell cycle checkpoint pathways[10] and DNA repair.[8] ATM gene mutations are linked to increased radiosensitivity both in A-T patients[11, 12] and in patient cells in culture.[13, 14] The cause of death in most A-T patients is lymphoreticular malignancy or recurrent chronic respiratory infections.[4, 5]

To date, conventional T1- and T2-weighted MRI imaging studies have highlighted hallmark neuropathological features, namely progressive cerebellar atrophy, in A-T (reviewed in Sahama[15]). From a radiological perspective this has been useful, however such studies provide limited insight into neurodegeneration and its association with loss of connectivity in multiple neural networks. Recently, we reported volume reductions in cortical motor regions in children with A-T using voxel-based morphometry (VBM) applied to structural MRI data.[183] Furthermore we observed WM structural changes within the cerebellum, cerebellar peduncles and in motor regions traversing the posterior limb of the internal capsule using diffusion MRI (dMRI) and tract-based spatial statistics (TBSS).[183] In this approach, diffusion tensor imaging (DTI) was used to measure the preferred direction of water diffusion along WM fibre tracts.[18] DTI provides quantitative measures of diffusion anisotropy, such as fractional anisotropy (FA), which is thought to reflect axonal WM fibre degeneration.[37, 160, 161] Mean diffusivity (MD), a quantitative measure of the mean motion of water considered in all directions, can be used to interrogate pathological cerebral tissue changes, such as demyelination.[57] Typically, decreases in FA, and increases in MD reflect WM fibre degeneration (reviewed in Beaulieu[37]).

Although voxel-wise analyses of FA and MD in A-T patients identify altered WM integrity,[183] a limitation of this approach is that it does not provide information about specific WM pathways

affected by neurodegenerative changes. When DTI is used in conjunction with probabilistic tractography algorithms, probabilistic maps of specific fibre tracts can be generated, enabling the connectivity of pathways linking multiple brain regions to be interrogated. [160, 161]

DTI and fibre tracking have been applied to study cerebellar - corticomotor networks in a number of ataxic conditions[21-28] other than A-T. Although histopathological evidence for collective atrophy in pontocerebellar pathways,[87] altered evoked potentials and myelinated fibre loss in spinal cord sensory pathways,[4, 88, 93, 94, 97, 184, 185] and demyelination of corticospinal tracts (CST) have been reported in A-T,[87, 89] these findings relate to post-mortem studies, usually at the end stages of disease. dMRI studies that employ probabilistic tractography to analyse WM pathway integrity and connectivity to multiple brain regions is urgently required to fully understand the impact of the ATM gene mutation on A-T motor circuits.

To this end, the present study employed the use of an 'along tract' statistical approach,[65] whereby diffusion imaging metrics (FA and MD) were measured along the length of lateral CST, somatosensory, cortico-ponto-cerebellar (CPC) and cerebellar-thalamo-cortical (CTC) tracts in young A-T and typically developing age-matched participants. Compared to standard 'tract-averaged' tractography, which provides one averaged FA and MD value per tract (reviewed in Colby[65]), the along tract protocol calculates FA and MD values at consistent intervals along the entire tract length, thereby providing a comprehensive view of the anatomical variation in WM integrity along neural pathways.

In addition to whole tract analysis, A-T WM tract streamline count, tract volume and apparent fibre density (AFD) were analysed in this study. Tract streamline counts can be used to detect general degeneration of A-T tracts. Tract volume measures the total voxel volume of all voxels belonging to the tract pathway of interest and when normalised to the intracranial volume (ICV), can provide an informed insight into hemisphere-specific WM changes.[186] Similarly, AFD, a tract specific measure derived from the fibre orientation distribution (FOD), allows identification of structural differences along single fibre bundles and assessment of connectivity between two anatomical regions that encompass a specific tract.[66] Using whole tract analysis, WM tract streamline count, tract volume and AFD measures, we present novel findings depicting loss in WM integrity along the entire tract length of CPC, CTC, somatosensory and CST pathways in A-T.

Methods

Participants

MRI data were acquired from 12 patients with A-T (age mean SD: 12±5.34; age range: 7-22 years, 6 Males) and 12 healthy, age-matched typically developing participants (age mean SD: 12.67±5.28; age range 8-23 years, 4 Males). All patients have been clinically diagnosed with A-T, according to the recent World Health Organisation recommendations[166] including genetic testing. Informed consent was given by all subjects and parents in accordance with our Human Ethics Institutional Review Board and the Declaration of Helsinki.

Clinical scoring

The A-T Neuro Examination Scale Toolkit (A-T NEST), which was refined from a quantitative 10-point scale,[167] was used to clinically observe A-T patients. This scaling system is a sensitive tool that specifically accounts for the multi-dimensional complexity and heterogeneity of A-T neurological deficits (personal communication with Dr. Thomas Crawford, Professor of Neurology and Paediatrics at the John Hopkins Hospital).

Image acquisition

MRI data were acquired using a 3T MRI scanner (Siemens Trio, Erlangen, Germany) with TQ gradients (45 mT/m, slew rate 200 T/m/s), using a 12-element Tim head array. A 0.9 mm isotropic 3D T1 Magnetisation Prepared Rapid Gradient Echo (MPRAGE) sequence was used to acquire a high-resolution structural image. The imaging parameters were: field of view 23×23×17.3 cm; TR/TE/TI 1900/2.32/900 ms; flip angle 9º; and matrix size 192×512×512×1 cm. Diffusion MRI acquisition consisted of a High Angular Resolution Diffusion Imaging (HARDI) sequence with the following parameters: 60 axial slices; 2.5 mm slice thickness; field of view 30×30 cm; TR/TE 9500/116 ms; and acquisition matrix 128×128, resulting in an in-plane resolution of 2.34×2.34 mm. To reduce susceptibility distortions, parallel imaging with an acceleration factor of 2 was employed. Sixty-four diffusion-weighted images were acquired at b = 3,000 s mm^{-2}, along with one minimally diffusion-weighted image (b = 0). The acquisition time for the diffusion dataset was 9:40 minutes. Two 2-dimensional gradient-recalled echo images (36 axial slices; 3 mm slice thickness with 0.75 mm gap; field of view 19.2×19.2 cm; TR/TE1/TE2 488/4.92/7.38 ms; acquisition matrix 64×64) were used to acquire a field map for diffusion data, to assist distortion correction due to susceptibility inhomogeneity.

Diffusion processing

Diffusion-weighted images were corrected for subject motion by identifying head movement within volumes using the discontinuity index and subsequently using the Fit Model to All Measurements (FMAM) method to correct movement between volumes.[172] Susceptibility distortions were corrected using the field map employing FMRIB's Utility for Geometrically Unwarping EPIs (FUGUE)[187] and Phase Region Expanding Labeller for Unwrapping Discrete Estimates (PRELUDE)[188] in raw image space (both contained within FMRIB's Software Library (FSL)),[169] with signal intensity correction.[189] Motion artefacts were identified and replaced using Detection and Replacement of Outliers Prior to Resampling (DROP-R),[171] modified from the originally proposed method to incorporate an outlier detection technique suitable for high b-value diffusion data.[175] Using the corrected data, the fibre orientation distribution (FOD) was estimated using the constrained spherical deconvolution (CSD) method within the MRtrix package (https://github.com/jdtournier/mrtrix3).[58] MRtrix was also used to generate FA and MD maps.

Tractography

Probabilistic tractography was performed using MRtrix3. To extract WM fibre tracks of interest, anatomically constrained tractography (ACT)[63] was performed. T1 co-registration to the diffusion imaging series, and subsequent FSL BET/FAST/FIRST processing on structural data as per the MRtrix3 'act_anat_prepare_fsl' script were conducted to produce a 'five tissue types' mask, to generate whole brain tractograms comprising fifty million streamlines.[59] Whole brain tractograms were subsequently processed using the Spherical-deconvolution Informed Filtering of Tractograms (SIFT) procedure introduced in MRtrix3, resulting in twenty-five million streamlines,[64] to reduce false positive streamlines. The MRtrix package was used to select regions-of-interest (ROIs) to enable extraction of the CPC, CTC, CST and somatosensory fibre tracks from SIFTed whole brain tractograms. ROIs, particularly for the CST and somatosensory tracts, were identified using established target regions specific to children[190, 191] and verified manually by an expert child neurologist (SF). *Reliability of ROI placement within and between subjects was determined by manual selection of ROIs for each subject, followed by careful expert cross-checking of ROI accuracy and placement.* ROIs were placed in the precentral and postcentral gyri and spinal cord for CST, postcentral gyrus and spinal cord for the somatosensory tracts and cerebral hemispheres and opposing medial cerebellar peduncle and superior cerebellar peduncle regions for the CPC and CTC tracts, respectively (Figure 4.1).

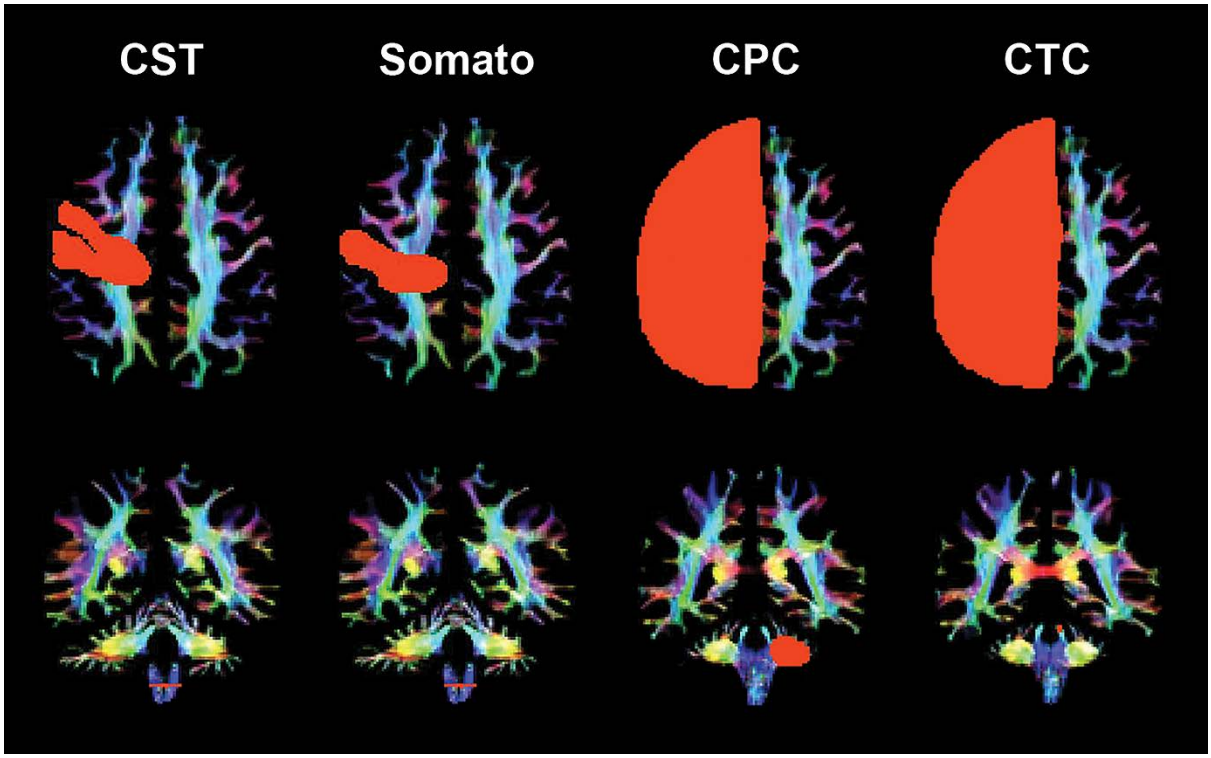

Figure 4.1. Region of Interest (ROI) placement for representative somatosensory motor cortex tracts for a control participant (age 23): Corticospinal (CST), somatosensory (Somato), cortico-ponto-cerebellar (CPC) and cerebellar-thalamo-cortical (CTC) tract ROIs in the cerebral cortex (first row) and cerebellar peduncles (second row). Colouration is based on the direction of water diffusion (Blue: ascending-descending diffusion; Red: left-right diffusion; Green: anterior-posterior diffusion).

Along Tract Statistical analysis

Quantitative tractography metrics (FA and MD) were derived using whole tract methodology. Motor circuits were defined according to 'start' and 'end' ROIs (visualised in Figure 4.1 first and second rows respectively) and cropped at 'end' ROIs to ensure similar tract length of all tracts within the circuit. Further removal of spurious tracts was achieved by rejecting 10% of the longest tracts in motor circuits. FA and MD were sampled by automated segmentation of individual tracts into 20 locations (bins) of equal streamline point count to ensure minimal data variance in metrics along the tract. This approach ensures anatomically coincident bins to be sampled along each tract of interest for each participant. FA and MD values within one patient were statistically compared to a corresponding age-matched control at each bin along each tract, using a linear mixed effects model. Bin location along the tract was associated with an anatomical landmark in individual patients to pinpoint WM changes by brain region in A-T. P-values less than or equal to 0.001 were considered statistically significant after *p*-value alpha adjustment for 40 multiple tests of hypotheses based on bin number (20) and condition (control or patient (2)) per bin, equating to the evaluation of individual bins in each subject group. In addition, MD values in all control and patient ROIs at the level of the

cerebral motor cortex (parietal cortex) and the cerebellar peduncles were computed using the 'fslstats' command, part of FSL[169] to cross-check MD values in selected corticomotor pathways. P-values less than or equal to 0.005 were considered statistically significant for this analysis after *p*-value alpha adjustment for 11 multiple tests of hypotheses, corresponding to the total number of ROIs selected. All statistical analyses and data visualisation were performed using the R statistical environment.[192]

WM Tract Streamline Number, Tract Volume and AFD Statistical analysis

As tensor based diffusivity measures are voxel-average quantities and not tract specific in voxels containing complex fibre architecture, streamline number, tract volume and AFD metrics were also investigated in this study. Streamline number, tract volume and AFD in A-T and control participants were calculated and averaged based on patient or control condition per tract due to the small number of subjects undergoing analysis. Tract volume was derived using the 'fslstats' command, part of FSL[169] and normalised based on ICV.[186] At high diffusion gradient b-values, the AFD is proportional to the intra-axonal volume of axons associated with that FOD lobe.[66] Summing the AFD integral for all FOD lobes associated with the tract streamlines enables generation of a measure related to the total intra-axonal tract volume. The AFD integral is normalised by dividing by the mean streamline length to yield a measure proportional to tract cross sectional area, and can be used to compare tract specific degeneration in A-T participants and age-matched control participants. AFD values (corrected and uncorrected for partial volume effects) were calculated using the 'afdconnectivity' command in MRtrix3 (https://github.com/jdtournier/mrtrix3). Parametric test assumptions of homogeneity of variance and normal distribution were assessed and confirmed prior to all statistical analyses. Statistical differences in streamline number, tract volume and AFD between patient and control conditions were computed using an independent t-test and visualised using the R statistical environment.[192] Streamline number, tract volume and AFD measures were considered significant after *p*-value alpha adjustment for 8 multiple tests of hypotheses based on number of tracts analysed ($p<0.006$).

Results

Clinical observations

Heterogenous ataxia and movement disorder were observed in A-T patients, irrespective of age. Clinical scores in four young patients depicted advanced WM degeneration, with variations in ataxic mobility (walking and standing) and neuropathy, the absence of ankle, knee and bicep tendon reflexes and loss of proprioception in the extremities (Patients 2, 7, 9 and 11, (7-10) years of age, Table 4.1, Appendices).

Whole Tract Analysis of Control and Patient WM Tracts

Lateral CST, CPC, CTC and somatosensory tracts descend from the cerebral motor cortex at the level of the parietal lobe to the cerebellar peduncles collectively, connecting these two regions. Compared to motor pathways in age-matched controls, A-T CST and somatosensory pathways display a morphological thinning of tracts at the level of the thalamus in the coronal view. In addition, A-T CPC and CTC pathways display morphological thinning of tracts in the cerebellum at the position of the medial cerebellar peduncles (Figure 4.2).

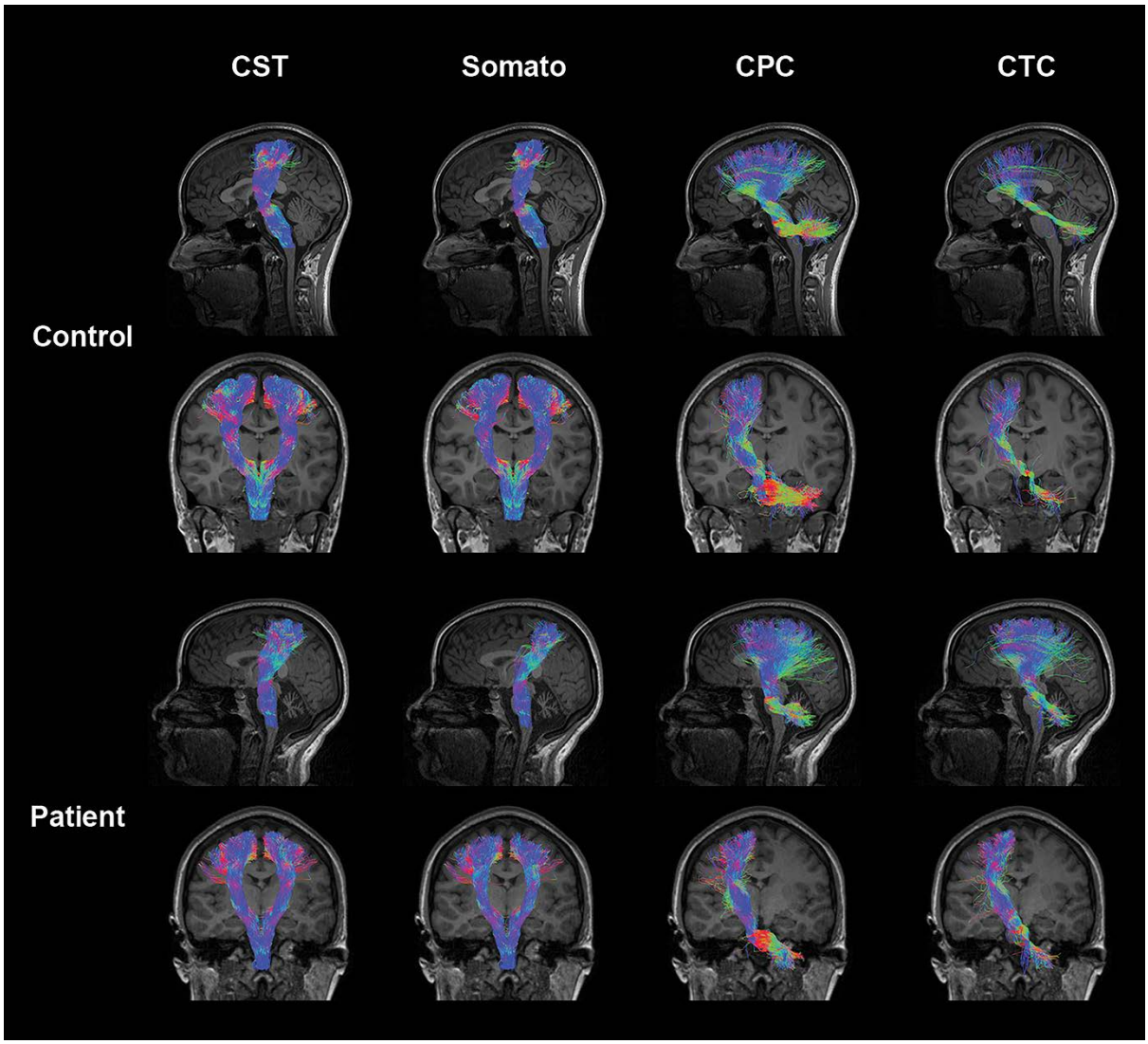

Figure 4.2. Somatosensory motor tracts in a representative control and ataxia-telangiectasia (A-T) subject (age 23): Control tracts are displayed in the first and second rows comprising the left sagittal (first row) tracts, left and right coronal (second row) corticospinal (CST) and somatosensory tracts, and left coronal (second row) cortico-ponto-cerebellar (CPC) and cerebellar-thalamo-cortical (CTC) tracts. Patient tracts are displayed in the third and fourth rows comprising the left sagittal (third row) tracts, left and right coronal (fourth row) CST and somatosensory tracts, and left coronal (fourth row)

CPC and CTC tracts. Colouration of tracts is based on the direction of water diffusion (Blue: ascending-descending diffusion; Red: left-right diffusion; Green: anterior-posterior diffusion).

Significant FA reductions along the lateral CST, CPC, CTC and somatosensory tracts were observed collectively in A-T patients compared to controls (p<0.001, Figure 4.3, for all tracts). Areas of non-significant FA changes in the left CTC at 5%, 11% and 32% of the tract length and in the right CTC at 0% and 5% of the tract length were observed in A-T (Figure 4.3, denoted by 'N'). A general decrease in average FA magnitude (approximated to two decimal places and averaged across age) between control and patient groups was observed along all analysed corticomotor tracts (Table 4.2, Appendices).

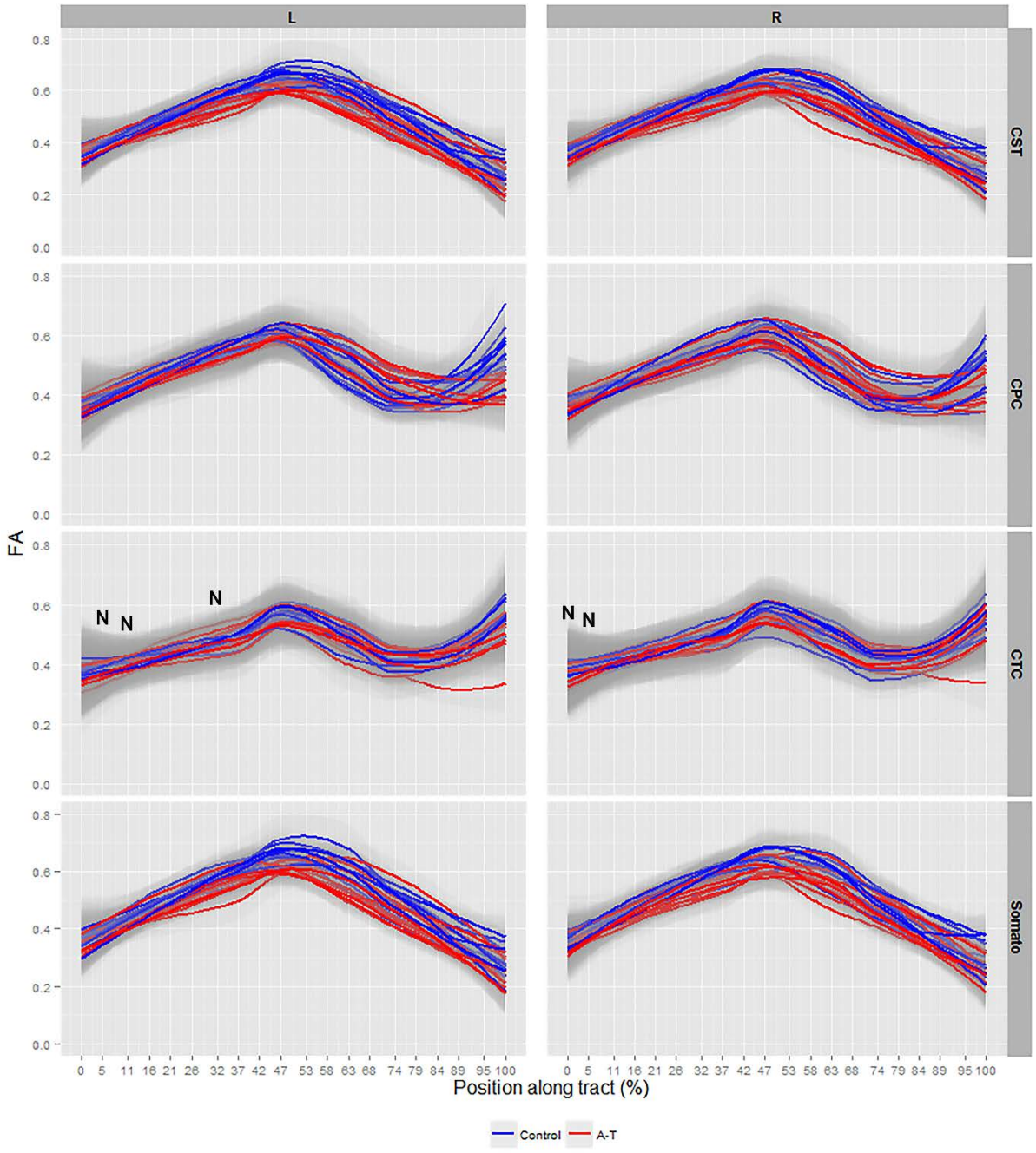

Figure 4.3. Smooth estimates of the average fractional anisotropy (FA) of all controls (blue) and patients (red) are plotted versus position from tract origin (cerebral motor cortex (0%) – cerebellar peduncles (100%)), faceted by tract name (Corticospinal (CST), somatosensory (Somato), Cortico-ponto-cerebellar (CPC), Cerebellar-thalamo-cortical (CTC)) and hemisphere (Left (L.) and Right (R.) ± pointwise 99% confidence range (light grey shading)). Tract position at 0-5% represents precentral and postcentral gyrus layers, at 47-58% represents thalamic layers in all tracts and at 95-100% represents the spinal cord in CST and somatosensory tracts, and position of the medial cerebellar and superior cerebellar peduncles connecting the brainstem and cerebellum for the CPC and CTC tracts, respectively. 'N' denotes tract locations with non-significant values.

A significant increase in MD in all A-T WM pathways was recorded at the level of the cerebral cortex (0%-50% of tract length), however, a paradoxical decrease in MD was observed at the level of the cerebellar peduncles (50%-100% of tract length) in all tracts (p<0.001, Figure 4.4). To cross-check the decrease in MD, a cross-examination of ROIs at the cerebral (precentral and postcentral gyrus) and cerebellar peduncle levels in patients and controls was conducted and revealed neither an increase nor decrease in MD at the cerebral and cerebellar levels in these ROIs respectively, in patients (data not shown). In addition, static change in average MD magnitude (approximated to two decimal places and averaged across age) between the control and patient groups was observed along all analysed corticomotor tracts (Table 4.2, Appendices). Areas of non-significant MD change in the right CPC tract at 32% of the tract length and in the right CTC tract at 0% and 37% of the tract length were observed in patients (Figure 4.4, denoted by 'N').

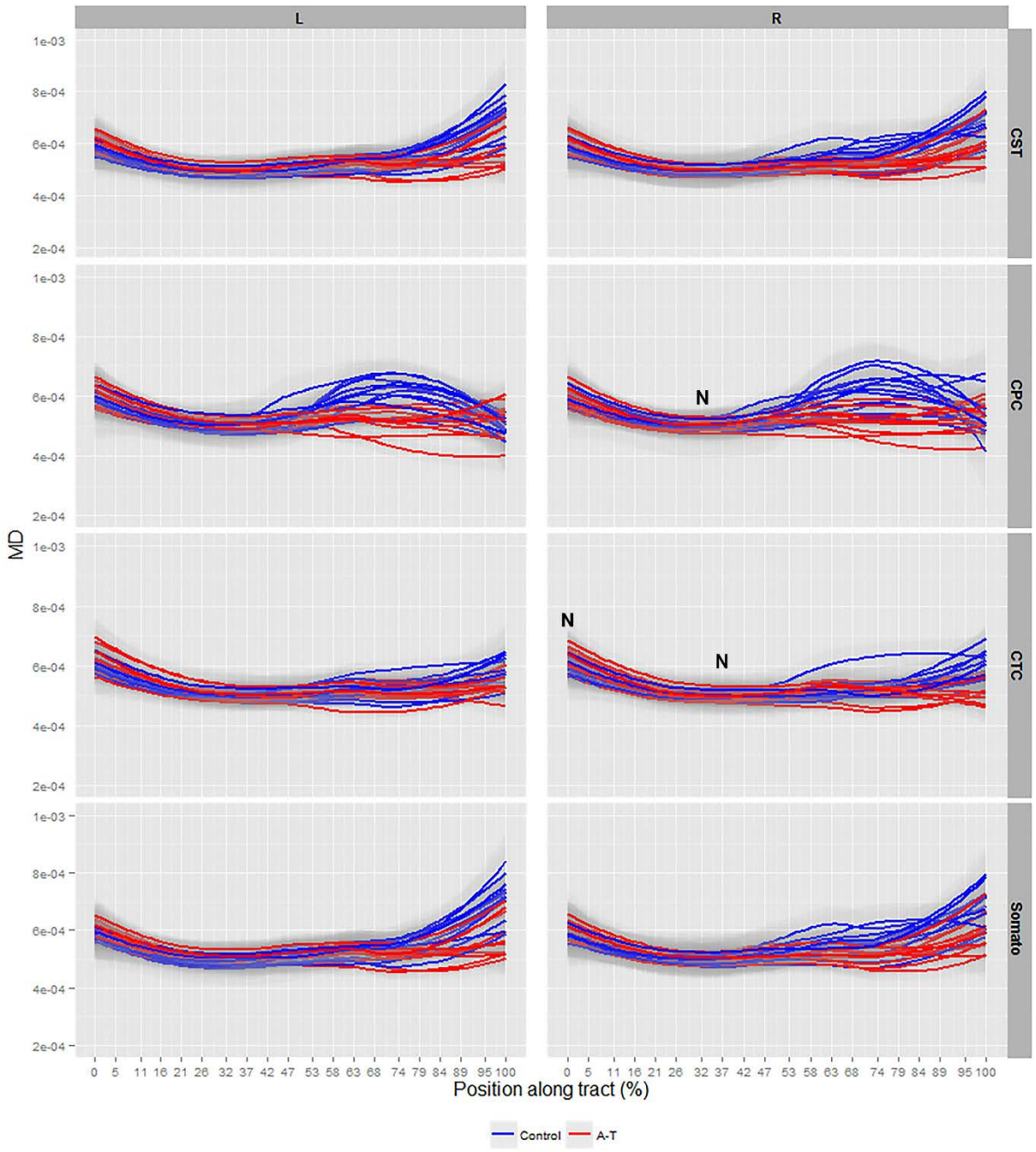

Figure 4.4. Smooth estimates of the average mean diffusivity (MD) of all controls (blue) and patients (red) are plotted versus position from tract origin (cerebral motor cortex (0%) – cerebellar peduncles (100%)), faceted by tract name (Corticospinal (CST), somatosensory (Somato), Cortico-ponto-cerebellar (CPC), Cerebellar-thalamo-cortical (CTC)) and hemisphere (Left (L.) and Right (R.) ± pointwise 99% confidence range (light grey shading)). Tract position at 0-5% represents precentral and postcentral gyrus layers, at 47-58% represents thalamic layers in all tracts and at 95-100% represents the spinal cord in CST and somatosensory tracts, and position of the medial cerebellar and superior cerebellar peduncles connecting the brainstem and cerebellum for the CPC and CTC tracts, respectively. 'N' denotes tract locations with non-significant values.

Streamline Number and Tract Volume Analysis

Reduced streamline number in the left and right CST and right somatosensory tracts was observed in A-T patients (p<0.006, Figure 4.5A). Tract volume reductions were observed in the left CTC, left somatosensory, right CPC and right CST A-T tracts (p<0.006, Figure 4.5C).

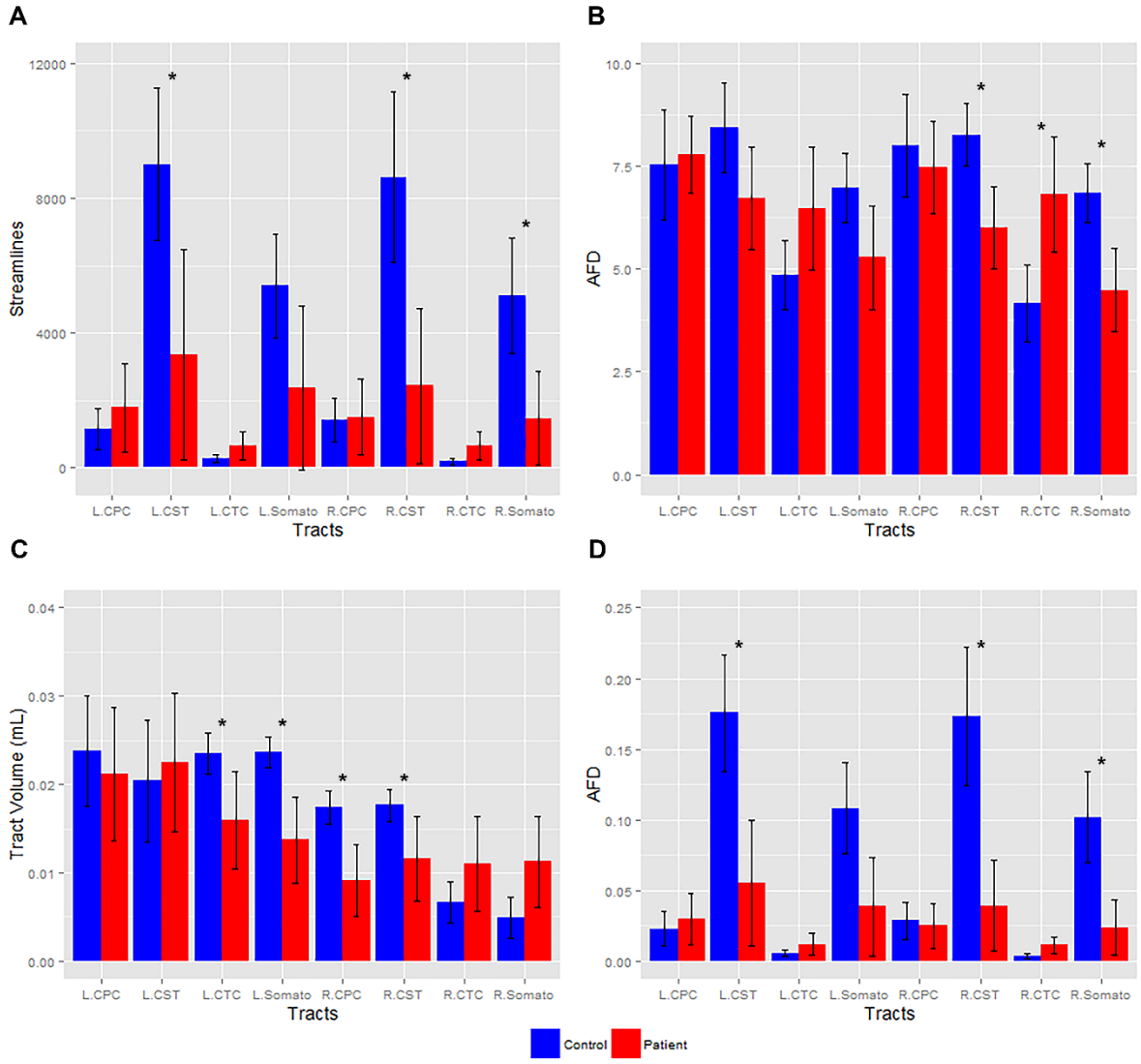

Figure 4.5. Number of white matter (WM) streamlines, tract volume and apparent fibre density (AFD) in control and patient tracts: A) Mean number of streamlines in WM tracts (Corticospinal (CST), somatosensory (Somato), Cortico-ponto-cerebellar (CPC), Cerebellar-thalamo-cortical (CTC)) (Left (L.) and Right (R.) ± pointwise 95% confidence interval) is plotted with significance (*, p<0.006). B) The mean AFD in WM tracts (Left (L.) and Right (R.) ± pointwise 95% confidence interval) is plotted with significance (*, p<0.006). C) The mean tract volume (mL) in WM tracts (Left (L.) and Right (R.) ± pointwise 95% confidence interval) is plotted with significance (*, p<0.006). D) The mean AFD in WM tracts (Left (L.) and Right (R.) ± pointwise 95% confidence interval) corrected for partial volume effects is plotted with significance (*, p<0.006).

AFD Analysis

Reductions in fibre integrity in the right CST and somatosensory tracts in A-T subjects were observed compared to controls (p<0.006, Figure 4.5B). Reductions in fibre integrity in the left and right CST and right somatosensory tracts in A-T subjects were also observed when corrected for partial volume effects (p<0.006, Figure 4.5D). Although not reaching a level of significance, the left CST (Figure 4.5B), left somatosensory and right CPC tracts (Figure 4.5B and D) displayed a trend towards reduced integrity in A-T subjects. Higher AFD was found in the right CTC tracts in A-T (p<0.006, Figure 4.5B), however this result was not significant in partial volume corrected data (Figure 4.5D), suggesting the influence of small streamline numbers delineating in this pathway.

Discussion

dMRI and probabilistic tractography have not yet been applied to A-T despite its use in investigating cerebellar WM degeneration in multi-spectrum ataxic disorders.[22, 25, 28] In this study, WM microstructural analysis of cerebellar-corticomotor and corticospinal pathways was conducted in a sizeable A-T cohort using an appropriate analysis pipeline. Specifically, anatomical variation in WM integrity along motor tract length was demonstrated for the first time in A-T.

Neurodegeneration of the lateral CST, CPC, CTC and somatosensory tracts along tract length was collectively observed among all A-T patients in this study. Analysis of FA and MD differences along the whole tract resulted in p-values with a magnitude of less than or equal to 10^{-6} (data not shown), indicating significant neurodegenerative change among A-T corticomotor and corticospinal tracts compared to age-matched control participants. FA reductions in the cerebral cortex, cerebellar and spinal cord regions suggest involvement of these areas in young A-T patients, and provide an insight into the advanced state of neuropathy, absence of reflexes (ankle, knee and bicep tendons) and proprioception observed in the extremities of these patients. While cerebellar degeneration is a well-established finding in A-T, structural changes in the cerebral motor cortex and spinal cord, particularly in histopathological studies, have been confined mainly to older A-T patients (reviewed in Sahama[15]) and sparingly in young patients.[88, 157] Cerebral abnormalities in structural MRI studies have also been observed largely in adult A-T patients,[145, 158, 193] however exceptional cases in early A-T have been noted.[157] Our current findings of cerebellar, somatosensory and spinal cord neurodegeneration, and our previous observations of reduced grey matter density in A-T motor regions,[183] provide evidence that the thalamus, precentral gyrus and postcentral gyrus are likely affected in our young A-T patient cohort. To our knowledge, involvement of these cortical areas has not previously been reported in imaging studies in A-T, however reduced metabolism in the fusiform gyrus of the cerebral cortex has been observed using ^{18}F-FDG PET imaging.[194]

In contrast to MD findings in neurodegenerative conditions (reviewed in Beaulieu[37]), a marked decrease in MD at the cerebellar peduncles was observed for all A-T tracts in this study, despite the lack of MD differences at the cerebral and cerebellar ROIs in patients and controls (data not shown), and the static change in average MD magnitude across patient age in corticomotor pathways. MD reductions have previously been reported during the hyperacute stages of ischemic stroke. In stroke, MD reduction has been postulated to be caused by cell swelling, where post ischemic energy failure causes sodium (Na+), potassium (K+)-ATPase transmembrane pump failure, inducing loss of ion homeostasis, excitatory amino acid release and water influx from extracellular to intracellular cell space (reviewed in Jones[195]). Such marked changes in ion homeostasis are unlikely to occur in A-T, since A-T neurons differentiated from induced pluripotent stem cells display similar voltage-gated potassium and sodium currents and action potential discharge as healthy neurons. Nevertheless, defective neuronal growth associated protein and potassium channel-interacting protein expression was observed in that study.[196] In a recent study, neural progenitors differentiated from olfactory neurosphere-derived cells in A-T patients were defective in neurite formation, neurite number and length.[197] In addition, a mouse model of A-T displayed decreases in the duration of calcium and sodium firing in Purkinje cells, with the presence of progressive calcium deficit despite normal resting membrane potential, input resistance or anomalous rectification (potassium currents) in cells. Calcium deficits were caused by decreases in calcium currents and were related to cell death in other tested mutant mice.[198] While these findings do not provide evidence for an imbalance in ion homeostasis in A-T neurons, they nevertheless indicate A-T neuronal cell abnormalities which could fit with MD reduction in the A-T cerebellum and spinal cord in the current study. MD reductions in A-T may also be markers of neurodegeneration, as restricted and hindered diffusion have been reported to decrease the apparent diffusivity of water,[199, 200] particularly where acute Wallerian degeneration is involved.[201] Currently, it is unclear whether neurodegeneration in A-T involves Wallerian degeneration in associated corticomotor pathways. Future use of longitudinal studies to track neurodegeneration in patients from early age to chronic disease states may allow the clarification of such degenerative involvement. Nevertheless, cell death in cerebellar regions is prevalent in A-T and are correlated with MD reductions, as are astrocyte reactivity and microglial/macrophage activation within the cerebral cortex.[200] Therefore MD reductions in this study may also reflect chronic oxidative stress-induced Purkinje cell death, thought to be the primary cause of neurodegeneration, as a consequence of failure to actively regulate oxidative stress levels in the A-T cerebellum (reviewed in Sahama[15]). Overall, the unpredictable combination of demyelination, axon loss, gliosis, and inflammation in individual A-T patients may result in competing influences of quantitative DTI metrics in brain regions. To improve DTI metric specificity in A-T, a combination

of multiple imaging measures (e.g., T1, T2, magnetisation transfer, perfusion, fast/slow diffusion)[57] is required.

Reductions in WM tract streamline number, tract volume and AFD measures coincided with FA reduction in robust WM tracts, in particular, in the left and right CST and somatosensory tracts in A-T. AFD connectivity and streamline number are highly related to one another when ACT and SIFT protocols are used, however, the localisation of neurodegenerative changes to the right hemisphere in A-T is unprecedented. Previously, we reported significant cerebellar-corticomotor pathway changes localised to only the left cerebral hemisphere in A-T using a different analysis technique, namely TBSS,[42, 44] with no clear correlation to clinical observations.[183] TBSS is a voxel-wise analysis technique that is less specific to probing the integrity of individual WM pathways. Although we reported only significant changes in FA and MD within left hemispheric WM pathways, we did observe similar changes within corresponding right hemisphere WM (uncorrected) that did not reach a level of statistical significance. The observation of both left and right hemisphere WM motor tract involvement in the current analysis may indicate the added sensitivity of the more specific along tract analysis approach. In structural imaging, there is little evidence of right cerebral laterality in A-T, particularly in the present A-T cohort (data not shown), however, post-mortem studies have recorded lesions exclusive to the right thalamus[88] and right temporal WM.[91] Localised WM maturation in the control population may also contribute to the laterality observed in streamline number and AFD metrics in our A-T patients. Indeed, voxel-wise analysis and DTI imaging in healthy children and adults have revealed increased FA and decreased MD with increasing age in the right temporal lobe[202] and right inferior longitudinal fasciculus.[203] These observations however, are cohort specific, thus WM tract streamline number and AFD laterality in this study may also be specific to our patient cohort.

Low streamline numbers in control and A-T CPC and CTC tracts highlight the challenge of robustly defining these pathways using dMRI acquisition schemes suitable for clinical populations (less than 10 minute scan time). Given this limitation, some caution needs to be observed when deferring information about degeneration processes occurring within these pathways. It should be noted that only streamlines hitting both cerebellar and cortical targets were included in this study. Many streamlines projecting from the cerebellum failed to project into the motor cortex and therefore has the potential for biasing streamline number analyses. Clearly, larger cohorts are needed to better define integrity of these motor pathways.

The primary limitation of this study is the small A-T cohort that underwent analysis and impacted on the findings. Fewer than 50 A-T cases have been reported in Australia overall,[181] with this study's clinical population recruited from the only research clinic nationally, specialising in health care for an estimated 54% of the national A-T population. In addition, the use of non-sedated MRI scanning in this study has restricted the age range of patients to age 6 and above. To understand the extent of multiple affected brain areas and their sequence of development in early and advanced A-T, larger collaborative studies across multiple research sites[182] are required. Another significant limitation is the inability of dMRI to accurately resolve crossing fibre tracts in complex WM architecture.[54] Specifically, multiple fibres that cross within each voxel provide unintuitive quantitative DTI measures. Indeed, in neurodegenerative conditions, increased anisotropy can be observed in regions of crossing fibres,[55] and is observed in average FA magnitude values per bin in the present study. In the cases of Wallerian degeneration, almost no change in diffusion anisotropy can be detected where degenerated pathways cross other tracts.[56] The use of a higher order model can resolve multiple crossing fibres within each voxel[58] and can improve the accuracy of tract delineations with tractography however, paradoxical changes in FA and MD (calculated using the diffusion tensor model), as seen in the measure of A-T WM integrity in the present study, can confound interpretation of results. Multiple imaging metrics in combination with higher order models allow complex neurodegenerative processes in A-T to be interpreted comprehensively thus streamline number, tract volume and AFD measures were introduced in this study to obtain a broader understanding of the neurological processes that contribute to A-T neurodegeneration.

In future, investigation of the cerebro-olivocerebellar and cerebro-reticular cerebellar pathways is required in A-T due to involvement of the inferior olives[87-90, 94] and the medullary reticular formation[88] in the disease. The dorsal spinocerebellar tracts in A-T[88, 95] also warrant further investigation but were excluded in the current study due to insufficient tract length in brain MRI for whole tract analysis. In future, spinal cord MRI could be employed to effectively capture these tracts in their entirety for analysis.

CHAPTER 5

Serial investigation of neurodegeneration in young ataxia-telangiectasia patients

This chapter includes the fourth manuscript produced during PhD candidature, which was submitted for review to *Paediatric Neurology* in 2015. The report details a longitudinal dMRI study of A-T imaging data acquired over the three year course of this project. This study addresses the third aim of the project, to 'investigate if A-T neuropathy is localised to the cerebellum or extends to the entire motor cortex in serial study of patients'.

The paper highlights the use of a sensitive TBSS and VBM procedure to quantitatively assess whole brain WM integrity (FA and MD) and GM volume between A-T T1 and dMRI data sets between years one and two, one and three and two and three in patients, respectively. The paper also highlights serial volumetric analysis of the basal ganglia, thalamus and cerebellum and serial ROI analysis of the medial cerebellar peduncle (MCP) and posterior limb of the internal capsule (PLIC), that represent areas of corticomotor and corticospinal pathway degeneration in A-T patients, respectively (Chapter 3). Overall, this paper attempts to provide a complete picture of the neurodegenerative progression in A-T patients over two years of study, an outcome that has not been attempted before using diffusion MRI.

As first author of this paper, I collected, analysed and interpreted the data and drafted and edited the manuscript. My co-author Jurgen Fripp contributed to the data processing. My co-authors Stephen Rose and Kerstin Pannek contributed to the interpretation of results. My co-authors Kate Sinclair and Martin Lavin contributed to the clinical interpretation of results. All co-authors critically revised the article.

Serial investigation of neurodegeneration in young ataxia-telangiectasia patients

Ishani Sahama, Kate Sinclair, Jurgen Fripp, Kerstin Pannek, Martin Lavin and Stephen Rose

Submitted: 26 August 2015
Journal impact factor (presently): 1.695

Abstract

Although progressive ataxia and oculomotor apraxia are well-recognised clinical features of ataxia-telangiectasia, very little is known about neurodegenerative changes over time within key brain structures known to be associated with motor function and control in this disease. To investigate these changes, serial structural and diffusion-weighted MRI data were acquired from 10 ataxia-telangiectasia patients (4 male: age range: 6-16 years). Corticomotor white matter microstructure and volumetric change of the caudate, putamen, thalamus, and cerebellum were quantitatively measured over a period of two years. Despite progressive loss of motor function in some participants (3/10 patients), based on a group-wise paired t-test analysis, we found no significant white matter microscopic or volumetric changes within these brain regions. This finding highlights that within a cohort of young patients with well-established patterns of cerebellar atrophy on MRI at baseline, progressive degeneration of thalamic, cerebellar, basal ganglia regions as well as corticomotor cerebellar white matter microstructural changes occur at a surprisingly slow rate. This finding has implications for our understanding of early neurodegenerative change and potential benefit of the use of neuroprotective or neural-restorative therapies for ataxia-telangiectasia.

Introduction

Ataxia-telangiectasia (A-T) is a neurodegenerative disorder marked by progressive cerebellar ataxia, immunodeficiency, sinopulmonary infections, oculocutaneous telangiectasia[4, 5] and elevated serum alpha-fetoprotein levels.[6] The multi-system characteristics of this autosomal recessive condition are caused by the ATM (ataxia-telangiectasia mutated) gene mutations.[2, 3] Recurrent chronic respiratory infections and lung complications resulting therefrom, as well as lymphoid malignancy[4, 5] are the causes of death in A-T.

To date, imaging studies in A-T have involved T1- and T2-weighted structural imaging that are useful from a radiological perspective, but provide limited insight into neurodegeneration and loss of multiple neural network connectivity in A-T. A-T neurodegeneration can be probed using appropriate analysis pipelines. Recently, we have shown that diffusion and structural MRI uncovers grey matter (GM) volume reductions in cortical motor regions and white matter (WM) structural changes in the cerebellum, anterior/posterior horns of the medulla, cerebral peduncles and posterior limb of the internal capsule (PLIC) in children with A-T compared to age-matched typically developing children.[183] Diffusion tensor imaging (DTI) in this analysis enabled the quantification of the preferred diffusion direction (diffusion anisotropy) of water along WM fibre tracts,[18] using fractional anisotropy (FA) and mean diffusivity (MD) measures, the former of which is thought to reflect axonal WM fibre degeneration,[37, 160, 161] and the latter of which measures mean water motion in all directions.[57] Decreases in FA and increases in MD reflect WM fibre degeneration (reviewed in Beaulieu[37]) and together, infer pathological changes in cerebral tissue, such as demyelination.[57]

Although progressive loss of motor function is well recognised in A-T, there is limited information about volumetric and WM microstructural changes to key brain structures known to be associated with motor function and control from an imaging perspective. To improve our understanding of the patterns of neurodegenerative change in A-T patients over time, we employ a series of voxel-wise and region-of-interest (ROI) analyses of diffusion MRI (dMRI) data to track WM integrity of key corticospinal and corticomotor cerebellar pathways in this study. In addition, volumetric analysis of cerebellar, and a number of subcortical brain regions (caudate, putamen and thalamus) are quantitatively assessed over a two year period using structural MRI. Overall, this study probes the pattern and magnitude of GM and WM neurodegenerative trajectories, which are important considerations for future development and application of neuroprotective or neural-restorative therapies in A-T.

Methods

Participants

MRI data were acquired once per year over two years from 10 A-T patients (4 male: age range: 6-16 years). Five patients did not provide data in year 2 (time point 3) of this study. All patients were clinically diagnosed with human A-T in accordance with the recent World Health Organisation recommendations[166] including genetic testing. All parents of young patients gave informed consent as per the Human Ethics Institutional Review Board and the Declaration of Helsinki.

Clinical assessment

Neurological deficits were quantitatively assessed using the A-T Neuro Examination Scale Toolkit (A-T NEST).[167] The A-T NEST accounts for the multi-dimensional nature of A-T characteristics and compensates for the disease's complexity and heterogeneity, making for an effective and sensitive method to precisely measure A-T neurological deficits.

Image acquisition

A 3T MRI scanner (Siemens Trio, Erlangen, Germany) with TQ gradients (45 mT/m, slew rate 200 T/m/s) and 12-element Tim head array was used to acquire MRI images. High-resolution structural images were acquired using a 0.9 mm isotropic 3D T1 Magnetisation Prepared Rapid Gradient Echo (MPRAGE) sequence. T2-weighted structural images were acquired for radiological assessment using the T2 Half Fourier Acquisition Single Shot Turbo Spin Echo (HASTE) sequence. The imaging parameters were: field of view 23×23×17.3 cm; TR/TE/TI 1900/2.32/900 ms; flip angle 9º; matrix size 192×512×512×1 cm. The following parameters in the High Angular Resolution Diffusion Imaging (HARDI) sequence were used to acquire diffusion images: 60 axial slices; 2.5 mm slice thickness; field of view 30×30 cm; TR/TE 9500/116 ms; acquisition matrix 128×128, resulting in an in-plane resolution of 2.34×2.34 mm. Susceptibility distortions were reduced by employing an acceleration factor of 2 to parallel imaging. Sixty-four diffusion-weighted images were acquired at b = 3,000 s mm^{-2}, along with one minimally diffusion-weighted image (b = 0). The diffusion dataset acquisition time was 9:40 minutes. A field map for diffusion data, using two 2-dimensional gradient-recalled echo images (36 axial slices; 3 mm slice thickness with 0.75 mm gap; field of view 19.2×19.2 cm; TR/TE1/TE2 488/4.92/7.38 ms; acquisition matrix 64×64) was used to correct for distortions due to susceptibility inhomogeneity.

Diffusion processing

Head movement within diffusion-weighted image volumes were identified using the discontinuity

index[168] and movement between volumes was corrected using the Fit Model to All Measurements (FMAM) method.[172] FMRIB's Utility for Geometrically Unwarping EPIs (FUGUE)[187] and Phase Region Expanding Labeller for Unwrapping Discrete Estimates (PRELUDE)[188] (both contained within FMRIB's Software Library (FSL))[169] were employed in raw image space, with signal intensity correction[189] to correct for susceptibility distortions using the field map. The Detection and Replacement of Outliers Prior to Resampling (DROP-R)[171] method modified to include an outlier detection technique suitable for high b-value diffusion data,[175] was used to identify and replace motion artefacts. The fibre orientation distribution (FOD) was estimated in the corrected diffusion data using the constrained spherical deconvolution (CSD) method within the MRtrix package (https://github.com/jdtournier/mrtrix3).[58, 59] MRtrix was also used to generate FA and MD maps.

Voxel-based analysis of diffusion MRI

WM microstructure between MRI data time points was interrogated using the advanced Normalisation Tools (ANTS)-Group-wise Voxel-based analysis, based on group-wise registration using the ANTS registration software.[204] This analysis is similar to our previous tract-based spatial statistics (TBSS) analysis[183] however, skeleton projection is omitted, providing greater sensitivity in detecting WM microstructural changes across subjects.[204] Permutation testing with 5,000 iterations (group-wise paired t-test), correcting for multiple comparisons in space using threshold-free cluster enhancement was conducted using the 'randomise' program included in FSL.[178]

Region of interest analysis of diffusion MRI

WM microstructure between MRI data time points was further interrogated by creating group-wise FA (1) and MD (1) templates (2 total) of all serial data using whole brain voxel-wise methodology,[204] and manually selecting regions of interest (ROIs) in the medial cerebellar peduncle (MCP) and PLIC of these templates to represent corticomotor cerebellar and corticospinal pathways, respectively (Figure 5.1A). Subsequently, ROIs were projected to each patient's FA and MD data set, to calculate mean FA and MD values. Time point differences of FA and MD in each ROI were statistically assessed using a paired t-test and visualised using the R statistical environment.[192] Statistical significance was conferred at $p<0.004$ after p-value alpha adjustment for 12 multiple tests of hypotheses based on the number of ROIs (4) and time point comparisons (3).

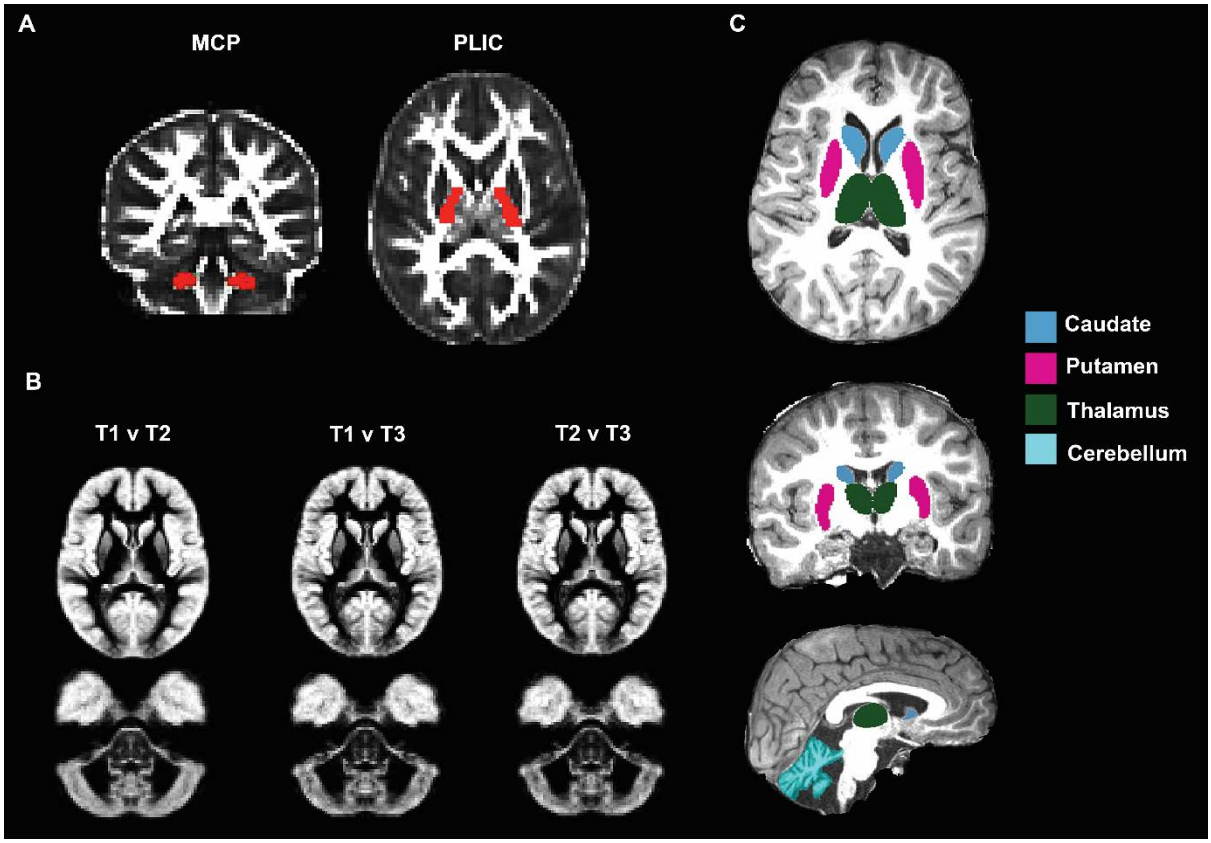

Figure 5.1. A) Regions of interest (ROIs: depicted in red) of the left and right medial cerebellar peduncle (MCP) and posterior limb of the internal capsule (PLIC) are overlaid on the ataxia-telangiectasia (A-T) patient fractional anisotropy (FA) template. B) Grey matter (GM) template of patient data set comparisons (time points 1 versus 2 (T1 v T2), time points 1 versus 3 (T1 v T3) and time points 2 versus 3 (T2 v T3), respectively) in the mid-cerebral (z-axis=39) and mid-cerebellar (z-axis=15) plane. C) Structural T1-weighted images in the axial (first row), coronal (second row) and sagittal (third row) planes of an 8-year-old A-T patient brain with automated segmentation of the caudate, putamen, thalamus and cerebellum in cerebral and cerebellar hemispheres are presented.

Voxel-based morphometry of structural MRI

Grey matter changes between MRI data time points in A-T were analysed with FSL-Voxel Based Morphometry (VBM)[40] an optimised protocol[41] carried out with FSL tools,[42] as per our previous analysis (4-dimensional GM templates are pictured in Figure 5.1B).[183] Permutation testing with 5,000 iterations (group-wise paired t-test), correcting for multiple comparisons in space using threshold-free cluster enhancement[178] was conducted using the ‘randomise’ program included in FSL.

Volumetric analysis of deep GM structures

To perform volumetric analysis of select deep GM areas, FMRIB's Integrated Registration and Segmentation Tool (FIRST), a model-based segmentation and registration tool[47] was used to segment

the caudate, putamen and thalamus in both hemispheric locations (Figure 5.1C). Due to the sensitivity of the cerebellum in image resolution[48] manual cerebellar segmentation was conducted, by creating a group-wise T1 template of all patient T1 data,[204] manually selecting the cerebellum on this template (Figure 5.1C) and subsequently projecting the selection onto each patient T1 data set for volumetric computation. Time point differences in mask volume for all selected structures were statistically assessed using a paired t-test and visualised using the R statistical environment.[192] Statistical significance was conferred at $p<0.002$ after p-value alpha adjustment for 21 multiple tests of hypotheses based on the number of selected structures (7) and time point comparisons (3).

Results

Baseline and serial anatomical MRI

As shown in Figure 5.2, T1 and T2-weighted MRI scans acquired at baseline revealed heterogeneous patterns of cerebellar atrophy, independent of patient age. Serial T2-weighted images acquired over the duration of the study are also presented and show little, if any progressive cerebellar atrophy over this period (Figure 5.2). Ventricular enlargement, indicative of general WM degeneration, was also not observed (data not shown).

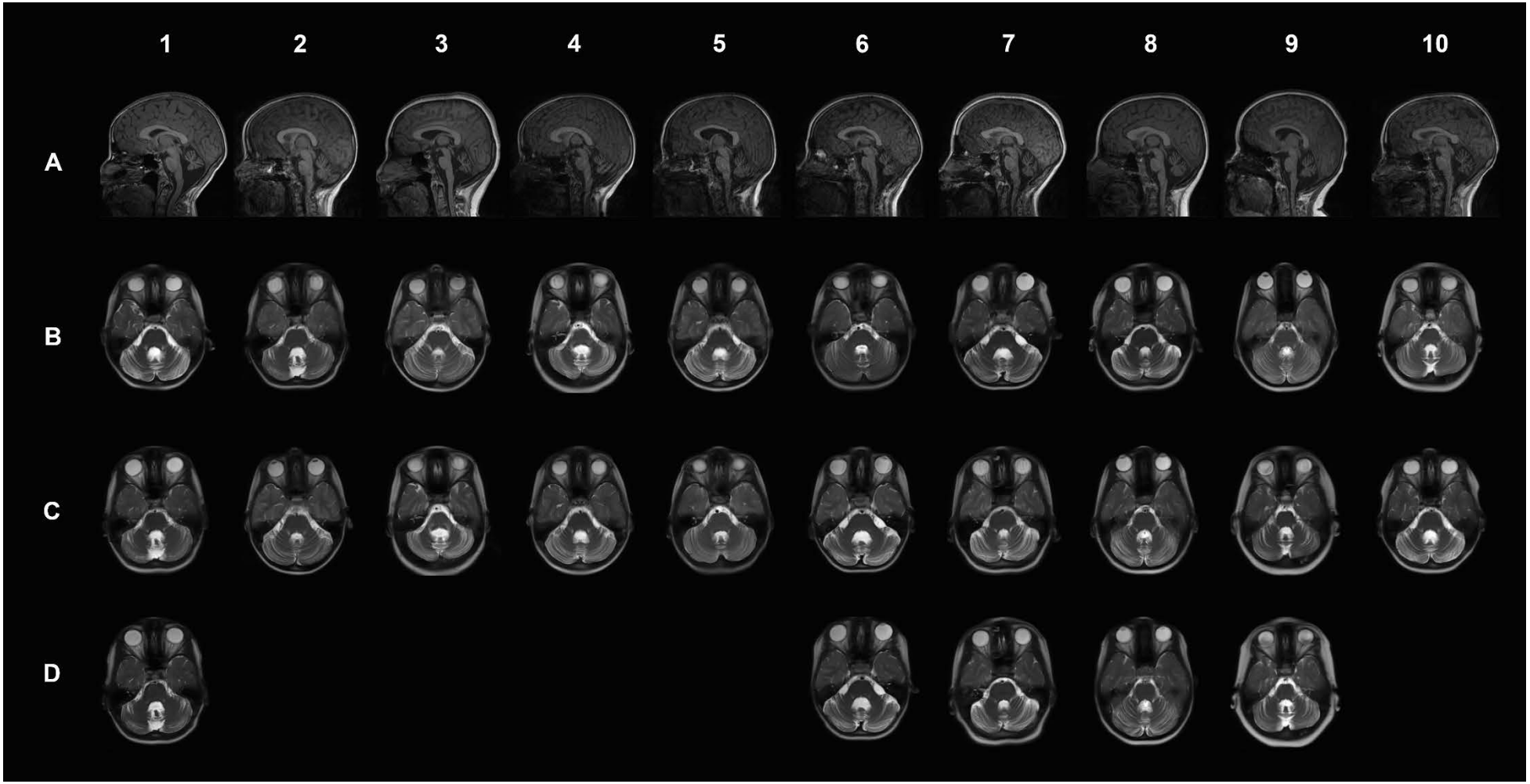

Figure 5.2. A) Structural T1-weighted images of all ataxia-telangiectasia (A-T) patients at base line (time point 1) in the sagittal plane. B) Structural T2-weighted images of the mid-cerebellar level (z-axis=5) of all A-T patients at baseline in the axial plane. C) Structural T2-weighted images of the mid-

cerebellar level (z-axis=5) of all A-T patients at time point 2 in the axial plane. D) Structural T2-weighted images of the mid-cerebellar level (z-axis=5) of all A-T patients (where data was available) at time point 3 in the axial plane.

Neurological assessments

Patient demographics including AT-NEST score are given in Table 5.1. Clinical observations over the two year period indicated heterogeneous patterns in motor dysfunction. Ataxia, movement disorder and communication sub-scoring were highly heterogeneous and independent of age. The A-T NEST scores indicated marked/mixed neuropathy, with a loss of ankle, knee and bicep tendon reflexes and loss of proprioception in toes for 3 of the 10 patients (patients 2, 4 and 8 between time points 1 and 2, Table 5.1). These patients presented with a decrease in walking, standing and hand tapping ability over a one year time span.

Table 5.1. Summary of A-T NEST clinical observations by time point

			Ataxia[a]						**Movement Disorder**[b]			**Communication**[c]					
			Walking			**Standing**			**Hand Tapping**			**Articulation**			**Response Time**		
Patient	**Age***	**Gender**	T1	T2	T3	T1	T2	T3	T1	T2	T3	T1	T2	T3	T1	T2	T3
1	16	M	0	0		0	0		2			0	0(3)		0	0	
2	7	F	6	1		4	4		3	2		2	1		2	1	
3	12	F	1(5)	1		2(5)	0		N/A	2		0	2			1	
4	9	M	4	1		4(7)	1		1	2		1	0		1	1	
5	6	M	4(5)	5		4(5)	6(7)		N/A	2		1	1			1	
6	9	M	3(5)	1	1	2(5)	2(7)	0	N/A	2	2	0	1	0		1	1
7	14	F	1(5)	0	0	1(5)	0	0	N/A	1	2	0	1	0		1	1
8	7	F	5	3	2	4	5	3	3	3	2	2	1(3)	1(3)	1	1	1
9	8	F	2	2	1	2	2	0	2	2	1	1	1(3)	1(3)	0	1	1
10	10	F	4	4		3	4		2	2		1	1		1	1	

[a] Maximum score for each subcategory is 6.

[b] Maximum score for each subcategory is 5.

[c] Maximum score for each subcategory is 2.

‘()’ Corresponds to a change of maximum score in the clinical assessment at the given time point juncture.

‘T1-T3’ corresponds to time points 1-3.

‘N/A’ corresponds to data that was collected in a different format to the listed clinical activity.

*Age is listed at the time of the first MRI scan (T1).

Grey fill corresponds to the absence of clinical scores.

WM microstructural changes

Group-wise analyses of registered FA and MD maps employing an optimised voxel-based approach[204] across time points revealed no significant whole brain changes in anisotropy measures, after correction for multiple comparisons. No significant differences in FA or MD measures in MCP and PLIC ROIs were observed between any time point after correction for multiple comparisons. Anisotropy measures for the MCP and PLIC ROI analysis are given in Table 5.2.

Table 5.2. Summary statistics of Volumetric and White Matter Microstructural Analysis

Area	Hemisphere	Time Point	Mean Volume (mm^3)	SD	SE	p value	Time point Comparison
Cerebellum		1	106693.37	13892.87	3587.12	0.76	1v2
	W	2	106379.98	14100.63	3640.77	0.88	2v3
		3	106154.86	12772.47	4039.01	0.91	1v3
Caudate	L	1	3331.11	689.89	178.13	0.30	1v2
	L	2	3278.65	756.50	195.33	0.03	2v3
	L	3	3497.88	434.80	137.50	0.01	1v3
	R	1	3590.44	736.76	190.23	0.82	1v2
	R	2	3576.88	887.30	229.10	0.54	2v3
	R	3	3788.89	582.65	184.25	0.39	1v3
		1	6921.55	1412.79	364.78	0.52	1v2
	W	2	6855.54	1622.74	418.99	0.21	2v3
		3	7286.77	995.14	314.69	0.12	1v3
Putamen	L	1	4145.85	1089.51	281.31	0.75	1v2
	L	2	4219.66	1075.62	277.72	0.32	2v3
	L	3	4134.40	807.59	255.38	0.80	1v3
	R	1	4084.15	986.07	254.60	0.06	1v2
	R	2	4350.66	1016.60	262.48	0.19	2v3
	R	3	4334.96	611.32	193.32	0.09	1v3
		1	8229.99	2053.12	530.11	0.18	1v2
	W	2	8570.33	2086.09	538.63	0.27	2v3
		3	8469.37	1409.03	445.57	0.08	1v3
Thalamus	L	1	6206.55	1050.24	271.17	0.07	1v2
	L	2	6363.87	1153.97	297.96	0.40	2v3

	L	3	6692.96	509.36	161.07	0.03	1v3
	R	1	6023.06	1016.84	262.55	0.62	1v2
	R	2	6011.90	1063.06	274.48	0.12	2v3
	R	3	6473.90	417.37	131.98	0.18	1v3
	W	1	12229.61	2051.74	529.76	0.38	1v2
		2	12375.77	2204.62	569.23	0.18	2v3
		3	13166.86	908.50	287.29	0.08	1v3

ROI	Hemisphere	Time Point	Mean FA	SD	SE	p value	Time point Comparison
MCP	L	1	0.48	0.03	0.01	0.92	1v2
	L	2	0.48	0.04	0.01	0.05	2v3
	L	3	0.51	0.01	0.00	0.01	1v3
	R	1	0.49	0.04	0.01	0.12	1v2
	R	2	0.51	0.04	0.01	0.99	2v3
	R	3	0.50	0.03	0.01	0.24	1v3
PLIC	L	1	0.51	0.02	0.01	0.87	1v2
	L	2	0.51	0.03	0.01	0.21	2v3
	L	3	0.47	0.04	0.01	0.04	1v3
	R	1	0.51	0.02	0.00	0.82	1v2
	R	2	0.50	0.03	0.01	0.75	2v3
	R	3	0.49	0.04	0.01	0.15	1v3

ROI	Hemisphere	Time Point	Mean MD (mm^2/s)	SD	SE	p value	Time point Comparison
MCP	L	1	0.001	0.000	0.000	0.827	1v2
	L	2	0.001	0.000	0.000	0.022	2v3
	L	3	0.000	0.000	0.000	0.050	1v3
	R	1	0.001	0.000	0.000	0.298	1v2
	R	2	0.000	0.000	0.000	0.565	2v3
	R	3	0.000	0.000	0.000	0.097	1v3
PLIC	L	1	0.001	0.000	0.000	0.080	1v2
	L	2	0.001	0.000	0.000	0.154	2v3
	L	3	0.000	0.000	0.000	0.099	1v3
	R	1	0.001	0.000	0.000	0.030	1v2
	R	2	0.001	0.000	0.000	0.236	2v3

	R	3	0.000	0.000	0.000	0.107	1v3

‘FA’ corresponds to Fractional Anisotropy.

‘L’ corresponds to Left Hemisphere.

‘MCP’ refers to Medial Cerebellar Peduncle.

‘MD’ corresponds to Mean Diffusivity.

‘PLIC’ refers to Posterior Limb of the Internal Capsule.

‘R’ corresponds to Right Hemisphere.

‘ROI’ corresponds to Region of Interest.

‘SD’ refers to Standard Deviation.

‘SE’ refers to Standard Error of the Mean.

‘v’ refers to ‘Versus’.

‘W’ corresponds to the whole brain structure without hemispheric separation.

GM volumetric changes

Group-wise analyses of registered cortical and subcortical GM regions on structural MRI revealed no significant whole brain GM changes. Volumetric measures for the thalamus, basal ganglia striatum and cerebellum for the three time points are listed in Table 5.2. No significant change in volume of these structures were found over the studied two year period, after correction for multiple comparisons.

Discussion

Radiological MRI assessment of children with A-T has established heterogeneous patterns of cerebellar atrophy independent of age (reviewed in Sahama[15]). In a previous study comparing A-T and age-matched typically developing children, we have shown that degeneration is not confined to the cerebellum, but involves atrophy of cortical motor regions and loss in white matter integrity within the anterior/posterior horns of the medulla, cerebral peduncles and PLIC.[183] To date, very little is known about progressive neurodegenerative disease in young A-T patients. With the development of new neuroprotective and neural-restorative therapies for A-T,[205, 206] it is important to understand the pattern and magnitude of neurodegenerative processes to gauge the best window of opportunity for therapy administration.

Despite clear patterns of cerebellar atrophy in our young A-T cohort, rigorous voxel-wise and ROI analyses of WM integrity in corticomotor cerebellar and corticospinal pathways and volumetric analysis of the thalamus, basal ganglia and cerebellum in the youngest patients (6 years of age),

revealed very little, if any, degeneration as a whole, over a period of two years. This finding was surprising given the established, and in some cases, significant atrophy present in baseline images. In terms of clinical measures, three of the ten patients showed marked reduction in clinical motor performance scores, however the small number of subjects precluded any statistical analysis within this subgroup of patients. The presence of progressive cerebellar atrophy is minimal, and reflects the findings of the voxel-wise and ROI analyses.

The lack of significant A-T neurodegeneration in this young cohort over a two year period also leads to interesting questions regarding the timing of degenerative onset associated with mutation of the ATM gene. Extensive cerebellar atrophy is present in our youngest patients, however little, if any, degeneration is observed or quantitatively measurable using MRI for a follow-up period of two years. It may be speculated that for some patients, significant cerebellar degeneration must occur well before 5 years of age. Clearly not only the anatomical pattern, but the magnitude and rate of neurodegeneration is also highly heterogeneous in patients with A-T. Acquiring MRI data from very young age at clinical diagnosis (2 years of age in our A-T clinics) to chronic disease state presents many challenges. Collaborative studies across multiple research sites[182] are urgently required to achieve this goal.

There are a number of limitations in this study, the first being the prevalence of involuntary head motion artefact during non-sedated MRI scanning of patients. For the analysis of dMRI data, we implemented an automated robust pre-processing pipeline to detect and correct for image artefacts caused by head motion and image distortions. Automated analysis and careful manual cross-checking of all deep GM and cerebellar structural volumes were also conducted to ensure a high level of accuracy in these measures.

The A-T NEST clinical scoring system was employed in this serial study to assess clinical functional measures. The limitation of this system is the incomplete status of clinical tasks during patient examination, which provides a difficult tracking medium for neurodegeneration. To date, the A-T NEST scoring system is under development and has yet to be used in large A-T clinical studies with other clinical ataxic measures.

Further study limitations include the restricted size and age range of the patient cohort and the investigated time period that did not allow the very early developmental sequence of A-T neurodegeneration from clinical diagnosis to be observed. It should be noted that in Australia, there are fewer than 50 cases of A-T overall, with our clinic being the only research clinic nationally,

specialising in health care for an estimated 54% of the Australian A-T population (children and young adults) overall.

Trajectories of normal development for cortical and subcortical structures from typically developing children for comparison with A-T patients over this time frame would have been beneficial. In typically developing children over this age range, increased microstructural development (increased FA and decreased MD) within WM motor pathways[202, 207, 208] with concomitant increase in cortical and subcortical volumes[209-211] are reported. These trends were not reflected in our A-T cohort, indicating a complex mechanism involving compromised neurodevelopment and slow degeneration of WM and GM motor regions.

In conclusion, this study has revealed that within a cohort of young A-T patients with well-established patterns of cerebellar atrophy in MRI at baseline, progressive degeneration of thalamic, cerebellar, basal ganglia regions and corticomotor cerebellar WM microstructural changes occur at a surprisingly slow rate. This finding has implications for the initiation of potential new neuroprotective and neural-restorative therapies at the earliest stages before significant neurodegeneration has occurred in A-T patients.

CHAPTER 6

Discussion and Conclusions

Novel Contributions

A series of novel developments have been made in this thesis in the purpose of applying high-resolution MRI and diffusion-weighted imaging modalities to analyse the structural integrity of whole brain WM and GM structure, and corticomotor WM pathways in young A-T patients. The three aims of this thesis, which were to:

1. assess whole brain cortex and subcortical WM and GM morphological changes between A-T patients and typically developing participants

2. investigate if A-T neuropathy is localised to the cerebellum or extends to the entire motor cortex in select WM pathways in A-T

3. investigate if A-T neuropathy is localised to the cerebellum or extends to the entire motor cortex in serial study of patients

were addressed in a series of four scientific papers. The initial review paper (Chapter 2) was integral to the project in that it defined knowledge gaps in MRI imaging modalities in A-T. The second publication (Chapter 3) allowed key areas of neurodegeneration in A-T, namely the cerebral motor cortex and cerebellum, to be specified from anatomical and histopathological information highlighted in the review paper. These anatomical specifications and the whole brain imaging findings of the A-T cohort in Chapter 3 drove further specification of key corticomotor-cerebellar WM pathways that connect the cerebral motor cortex and cerebellum in A-T patients in the third publication featured in

Chapter 4. The comprehensive WM microstructure analysis of the aforementioned pathways in Chapter 4 indicated that the neurodegenerative effect among young A-T patients in this study is large, and that multiple areas ranging from the parietal cortex (precentral and postcentral gyrus), to the cerebellar peduncles (for corticomotor cerebellar pathways) and spinal cord (for corticospinal pathways), were involved in A-T neurodegeneration. Finally in Chapter 5, structural and diffusion-weighted MRI imaging were applied to map serial WM microstructure and GM volumetric changes of select corticomotor-cerebellar ROIs defined in Chapter 4. Longitudinal degeneration of thalamic, cerebellar, basal ganglia regions and corticomotor cerebellar WM microstructure changes were not found among the young A-T cohort over the studied time period however, well-established patterns of cerebellar atrophy in MRI at baseline were observed, indicating slow degeneration among patients, and the potential for new neuroprotective and neural-restorative therapies at the earliest stages of A-T neurodegeneration.

Future work

Spinal Cord studies

Histopathological spinal cord studies among A-T patients are limited to post-mortem study, typically at the end stages of disease (reviewed in Sahama[15] (Chapter 2)), whereas imaging studies of the A-T spinal cord are limited to morphological T1 and T2-weighted structural imaging. In future, studies utilising dMRI and probabilistic tractography methods need to be conducted in A-T to visualise the extent of spinal cord WM microstructure degeneration among patients at early and advanced disease states. Indeed, the use of spinal cord imaging modalities have been attempted in cervical spinal cord studies in healthy adult populations,[212-214] yielding largely reproducible results for DTI metrics. In addition, DTI metrics can also be determined at specific cervical cord levels (i.e. C3-C7) and correlated to clinical motor and sensory functions using appropriate clinical rating systems[213] to comprehensively analyse WM microstructure, similar to tract segmentation and quantitative DTI measurement conducted in Chapter 4 of this thesis.

International collaborative studies

A general limitation of this project was the small number of A-T participants to undergo analysis and impact on the findings. In Australia, there have been fewer than 50 cases of A-T reported overall,[181] with the clinical population used in Chapters 3-5 of this thesis recruited from the only research clinic nationally, specialising in health care for an estimated 54% of the national population of patients. To understand and explore the extent of multiple affected areas of the brain and their sequence of development in early and advanced A-T, larger collaborative studies across multiple research sites[182] is required.

Animal studies

In this project, older A-T patients (above 22 years of age) were not available for study. In this respect, animal models can be used to observe advanced disease states and chronic pathology in A-T. An established A-T mouse model has been used previously in A-T studies however, neurodegeneration is largely absent in this model (reviewed in Lavin[215]). In contrast, a novel A-T rat model, developed by Prof. Martin Lavin from the University of Queensland Centre for Clinical Research, provides a feasible medium to study the advanced stages of A-T neurodegeneration. Initial investigation of structural T1 images in three rat model strains (ATM gene Knock Out (ATM KO, representing the classic A-T phenotype), ATM gene missense mutated (representing the variant A-T phenotype with milder neurological symptoms than classic A-T) and wild type Fisher F344 background rat phenotype) revealed marked atrophy of the molecular cell layer and deep cerebellar layer of the ATM KO strain compared to the control (Figure 6.1). The cerebellum of the ATM missense mutated animal was visually similar to the control, reflecting the milder phenotype of the ATM missense mutated strain compared to the ATM KO strain (Figure 6.1).

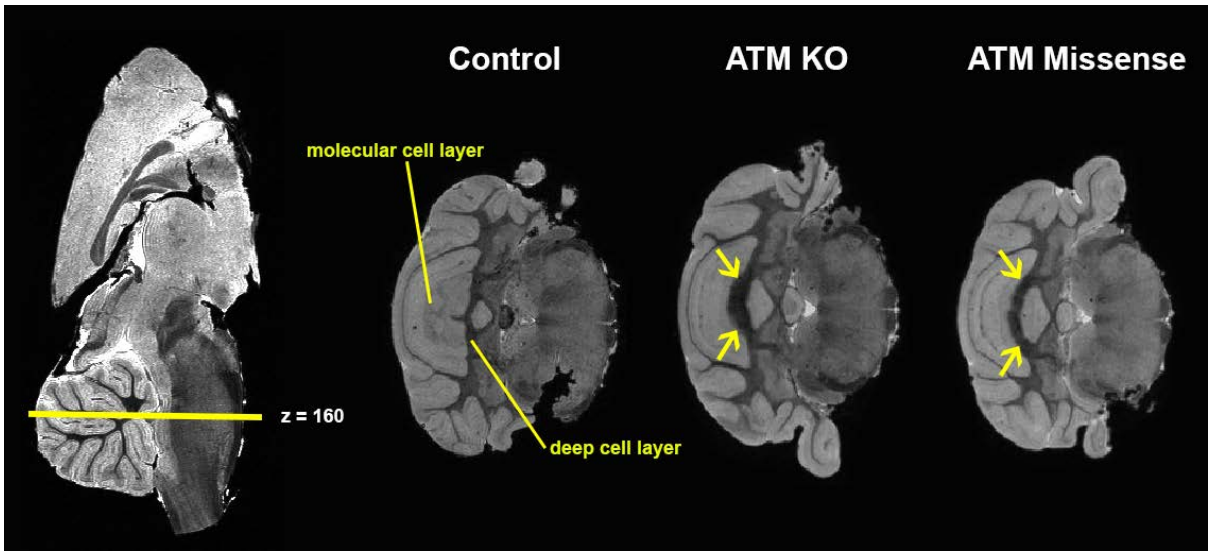

Figure 6.1. Axial mid-cerebellar T1 structural images of control, ataxia-telangiectasia mutated gene knock out (ATM KO) and ATM missense mutated rat strains. Images were taken at mid-cerebellar level to illustrate molecular cell layers and deep cerebellar layers of the pictured animals and atrophy observed in these layers (arrows).

In future, whole brain analysis and probabilistic tractography analysis of the corticomotor-cerebellar and corticospinal pathways should be conducted in the animal model (rats) to comprehensively observe chronic A-T neurodegeneration in the absence of older A-T patients for study.

Other imaging studies

High-resolution T1 structural images

Despite the use of comprehensive pre-processing protocols to detect and correct for motion artefact in raw diffusion MRI images in A-T, improved image quality and subsequently, improved grey and white matter contrast in structural MRI images enable detailed analysis of A-T neurodegeneration using structural and volumetric analyses (i.e. cortical segmentation and VBM), and delineation of neural pathways using probabilistic tractography based methods. In this project, MPRAGE imaging sequences were used to collect high-resolution T1 structural images of A-T patients (Chapters 3-5). The MPRAGE sequence provides superior grey and white matter contrast and image quality than T1-weighted spin-echo sequences,[216] which were also used in this project.

Recently, a modification of the MPRAGE sequence to provide better image quality in T1 structural data has given rise to the MP2RAGE imaging sequence.[217] The MP2RAGE sequence will prove useful in imaging studies in A-T patients due to improved reproducibility and tissue contrast in deep GM regions compared to MPRAGE T1 structural images.[218] Segmentation of key deep grey matter areas of interest in A-T, namely the caudate, putamen (striatum of the basal ganglia) and grey matter regions of the thalamus have been found to be significantly larger in MP2RAGE than in MPRAGE structural images,[218] indicating the superior contrast of deep GM structures afforded by the MP2RAGE acquisition protocol. In addition, a quantitative high-resolution T1 map is also acquired in the MP2RAGE image acquisition process[218] that can be used for quantitative morphometric neuroimaging.[219] Specifically, this map can be superimposed on target brain regions in A-T[220] to provide markers of subtle microstructural damage.[221] This feature of the MP2RAGE imaging sequence adds further viability to distinguishing ROIs for volumetric analysis in the A-T brain (Chapter 5), despite poor image quality and the difficulty with which to isolate these structures manually from A-T brain images. It should be noted however that there is preferential bias for ROI selection in MP2RAGE images when selecting ROIs in the averaged T1 map,[218] therefore this limitation should be considered when distinguishing GM areas using MP2RAGE in future A-T study. Lastly, MP2RAGE sequences in A-T can also be used to capture GM pathology in the spinal cord, a key aspect of the A-T neurodegenerative phenotype (reviewed in Sahama[15] (Chapter 2)).

Positron Emission Tomography

Positron Emission Tomography (PET) is a non-invasive imaging modality that uses systemically administered tracers labelled with positron emitting isotopes in brain imaging.[222, 223] PET imaging has been used in a number of neurodegenerative conditions such as cerebellar ataxia[224] and spinocerebellar ataxia.[225-227] In recent years, PET has been extended to the study of A-T, through

general patient work-up[228] and through PET and 18F-fluorodeoxyglucose (FDG) use where brain glucose metabolism, a marker of brain function, was measured in ten adult A-T patients. This study uncovered lower glucose metabolism in the A-T cerebellum compared to controls and asymptomatic relatives (siblings), and significant inter-subject metabolic variability in the cerebellar vermis and brain.[194] These findings reflect cerebellar pathology that has been reported in histopathological A-T studies (reviewed in Sahama[15] (Chapter 2)) as well as the extensive heterogeneity of A-T neurodegeneration and clinical presentation, as seen in the A-T cohort used for this project.

Despite the advances in A-T neuroimaging presented in the aforementioned paper, MRI imaging was excluded from this study due to poor image quality and unsuitability for coregistration purposes.[194] The work highlighted in this thesis has utilised a robust analysis pipeline to acquire MRI images and conduct dMRI analyses to interrogate neurodegeneration in A-T patients comprehensively, thus future use of conjoint structural MRI, dMRI and PET studies in A-T is an attractive option to effectively analyse key areas of neurodegeneration among A-T patients. Indeed, in spinocerebellar ataxia case studies, the use of MRI volumetry and multitracer PET studies have been used to identify metabolic and atrophic brain changes in patients,[229] as well as presymptomatic markers of neurodegeneration, particularly in regards to striatal-dopaminergic dysfunction in patients.[225] The use of PET-MR hybrid modalities allow the imaging of PET tracers, MRI contrast agents or MRI-detectable metabolites in correlation to the anatomy, as well as providing improved soft-tissue contrast and reduced ionising radiation levels compared to PET-CT modalities,[230-232] therefore the use of PET-MR imaging would prove useful in a radiosensitive cohort such as A-T.

The involvement of dopaminergic-striatal systems have been described in A-T. From an imaging perspective, decreased bilateral binding of the cerebral dopamine-D2-receptor in the striatum of the basal ganglia has been recorded in a young A-T patient using single-photon emission computed tomography.[233] The use of PET imaging would be useful in confirming this finding in the A-T cohort used in this project. In particular, the demonstrated sensitivity of PET imaging in effectively detecting early neuronal impairment, such as reduced postsynaptic dopaminergic levels in unaffected mutation carriers of ataxia,[225] and before preclinical stages of neurodegenerative disease,[234, 235] as well as highlighting cerebellar metabolic changes in asymptomatic individuals[229] or genetic carriers[194] of A-T could prove useful. Underlying pathophysiological mechanisms specific to A-T can also be effectively pinpointed by sensitive PET analysis of dopaminergic functions,[236, 237] and can also be used in conjunction with robust clinical rating scales[225, 238] and clinical tasks[239] to effectively correlate clinical severity with functional impairment among patients.

PET imaging can also be used in clinical trials to assess activation and deactivation patterns in the cerebral motor cortex and cerebellum, to understand motor performance changes with treatment among A-T patients. This methodology has been attempted in young children with cerebral palsy to assess the safety and efficacy of therapeutic allogeneic umbilical cord blood potentiated with recombinant human erythropoietin, in improving motor and cognitive dysfunction among patients,[240] and also in Multiple-System-Atrophy Parkinson-type patients, in assessing the efficacy of the antibiotic minocycline, in reducing the progression of neurodegeneration among patients.[241] A recent development in A-T drug discovery highlights the use of encapsulated dexamethasone sodium phosphate (DSP) in autologous erythrocytes (EryDex) among A-T patients, which is devoid of the characteristic long-term steroid side effects and allows for slow release of dexamethasone for up to one month after initial dosing.[205, 206] The recently conducted EryDex trial in A-T assessed the effect of the drug in improving A-T neurological symptoms and adaptive behaviour among patients however, concurrent tracking of neurological improvement among patients using imaging modalities was largely absent. PET imaging in this trial could contribute to a better understanding of the neurological improvement at the cortical motor level in the A-T brain. It should be noted that although PET imaging has been used among young patients in clinical pilot studies,[228] PET poses a significant radioactive risk in A-T patients (reviewed in Sahama[15] (Chapter 2)), therefore to manage this risk, PET studies in A-T should be attempted in adult patients.

Functional MRI

The use of functional MRI (fMRI) in analysing motor performance changes during therapeutic treatment in A-T (i.e. EryDex trial), could provide further insights into the neurological improvements of young A-T patients, without exposure to ionising radiation. fMRI was first used in A-T to track motor performance changes caused by Betamethasone among patients.[133] In this study, six A-T patients received a 10-day cycle of oral betamethasone and fMRI analysis was conducted over the course of the study. Voxel-based comparisons were used to highlight an increase in the number of activated motor cortex voxels under the on-therapy condition compared with cortical activity under baseline conditions in patients. Changes in motor performance in treated A-T patients correlated with an increase in activation of relevant cortical areas, indicating motor performance improvement with betamethasone treatment.[133] fMRI modalities have also been used in Friedrich's ataxia and spinocerebellar ataxia to assess cerebellar cortex and nuclei function[242] and assess the functional re-organisation of cortical and sub-cortical brain regions, specifically the cortico-cerebellar,[243-245] cortico-striatal and parieto-frontal loops, arising from cerebellar pathology.[244] Future clinical trials in A-T should implement fMRI analyses to map the functional re-organisation of cortico-cerebellar and

corticospinal pathways, to track neurological improvements with continued use of therapeutic compounds in young A-T patients.

References

1. Woods CG, Bundey SE, Taylor AM. Unusual features in the inheritance of ataxia telangiectasia. Hum Genet 1990;84(6):555-562.

2. Gatti RA, Berkel I, Boder E, et al. Localization of an ataxia-telangiectasia gene to chromosome 11q22-23. Nature 1988;336(6199):577-580.

3. Savitsky K, Bar-Shira A, Gilad S, et al. A single ataxia telangiectasia gene with a product similar to PI-3 kinase. Science 1995;268(5218):1749-1753.

4. Boder E, Sedgwick RP. Ataxia-telangiectasia; a familial syndrome of progressive cerebellar ataxia, oculocutaneous telangiectasia and frequent pulmonary infection. Pediatrics 1958;21(4):526-554.

5. Dunn HG, Meuwissen H, Livingstone CS, Pump KK. ATAXIA-TELANGIECTASIA. Canadian Medical Association journal 1964;91:1106-1118.

6. Waldmann TA, McIntire KR. Serum-alpha-fetoprotein levels in patients with ataxia-telangiectasia. Lancet 1972;2(7787):1112-1115.

7. Lavin MF. Ataxia-telangiectasia: from a rare disorder to a paradigm for cell signalling and cancer. Nature reviews Molecular cell biology 2008;9(10):759-769.

8. Shiloh Y, Ziv Y. The ATM protein kinase: regulating the cellular response to genotoxic stress, and more. Nature reviews Molecular cell biology 2013;14(4):197-210.

9. Guo Z, Kozlov S, Lavin MF, Person MD, Paull TT. ATM activation by oxidative stress. Science 2010;330(6003):517-521.

10. Beamish H, Williams R, Chen P, Lavin MF. Defect in multiple cell cycle checkpoints in ataxia-telangiectasia postirradiation. The Journal of biological chemistry 1996;271(34):20486-20493.

11. Gotoff SP, Amirmokri E, Liebner EJ. Ataxia telangiectasia. Neoplasia, untoward response to x-irradiation, and tuberous sclerosis. Am J Dis Child 1967;114(6):617-625.

12. Morgan JL, Holcomb TM, Morrissey RW. Radiation reaction in ataxia telangiectasia. Am J Dis Child 1968;116(5):557-558.

13. Taylor AM, Harnden DG, Arlett CF, et al. Ataxia telangiectasia: a human mutation with abnormal radiation sensitivity. Nature 1975;258(5534):427-429.

14. Chen PC, Lavin MF, Kidson C, Moss D. Identification of ataxia telangiectasia heterozygotes, a cancer prone population. Nature 1978;274(5670):484-486.

15. Sahama I, Sinclair K, Pannek K, Lavin M, Rose S. Radiological imaging in ataxia telangiectasia: a review. Cerebellum 2014;13(4):521-530.

16. Sood S, Gupta A, Tsiouris AJ. Advanced magnetic resonance techniques in neuroimaging: diffusion, spectroscopy, and perfusion. Seminars in roentgenology 2010;45(2):137-146.

17. Einstein A. On the movement of small particles suspended in stationary liquids required by the molecular-kinetic theory of heat. Annalen der Physik 1905;17(16):549-560.

18. Basser PJ, Mattiello J, LeBihan D. Estimation of the effective self-diffusion tensor from the NMR spin echo. Journal of magnetic resonance Series B 1994;103(3):247-254.

19. Stejskal EOOaT, J. E. . E. Spin diffusion measurements: Spin echoes in the presence of a time-dependent field gradient. The Journal of Chemical Physics 1965;42(1):288.

20. Pannek K, Guzzetta A, Colditz PB, Rose SE. Diffusion MRI of the neonate brain: acquisition, processing and analysis techniques. Pediatric radiology 2012;42(10):1169-1182.

21. Yoon B, Kim JS, Lee KS, Kim BS, Chung SR, Kim YI. Early pathological changes in the cerebellum of patients with pure cerebellar syndrome demonstrated by diffusion-tensor imaging. European neurology 2006;56(3):166-171.

22. Habas C, Cabanis EA. Anatomical parcellation of the brainstem and cerebellar white matter: a preliminary probabilistic tractography study at 3 T. Neuroradiology 2007;49(10):849-863.

23. Kitamura K, Nakayama K, Kosaka S, et al. Diffusion tensor imaging of the cortico-ponto-cerebellar pathway in patients with adult-onset ataxic neurodegenerative disease. Neuroradiology 2008;50(4):285-292.

24. Ying SH, Landman BA, Chowdhury S, et al. Orthogonal diffusion-weighted MRI measures distinguish region-specific degeneration in cerebellar ataxia subtypes. Journal of neurology 2009;256(11):1939-1942.

25. Pagani E, Ginestroni A, Della Nave R, et al. Assessment of brain white matter fiber bundle atrophy in patients with Friedreich ataxia. Radiology 2010;255(3):882-889.

26. Rizzo G, Tonon C, Valentino ML, et al. Brain diffusion-weighted imaging in Friedreich's ataxia. Movement disorders : official journal of the Movement Disorder Society 2011;26(4):705-712.

27. Solodkin A, Peri E, Chen EE, Ben-Jacob E, Gomez CM. Loss of intrinsic organization of cerebellar networks in spinocerebellar ataxia type 1: correlates with disease severity and duration. Cerebellum 2011;10(2):218-232.

28. Prodi E, Grisoli M, Panzeri M, et al. Supratentorial and pontine MRI abnormalities characterize recessive spastic ataxia of Charlevoix-Saguenay. A comprehensive study of an Italian series. European journal of neurology : the official journal of the European Federation of Neurological Societies 2013;20(1):138-146.

29. Basser PJ, Mattiello J, LeBihan D. MR diffusion tensor spectroscopy and imaging. Biophysical journal 1994;66(1):259-267.

30. Jones DK, Horsfield MA, Simmons A. Optimal strategies for measuring diffusion in anisotropic systems by magnetic resonance imaging. Magn Reson Med 1999;42(3):515-525.

31. Jones DK. The effect of gradient sampling schemes on measures derived from diffusion tensor MRI: a Monte Carlo study. Magn Reson Med 2004;51(4):807-815.

32. Jeurissen B, Tournier JD, Dhollander T, Connelly A, Sijbers J. Multi-tissue constrained spherical deconvolution for improved analysis of multi-shell diffusion MRI data. Neuroimage 2014;103:411-426.

33. Basser PJ, Pierpaoli C. Microstructural and physiological features of tissues elucidated by quantitative-diffusion-tensor MRI. Journal of magnetic resonance Series B 1996;111(3):209-219.

34. Pajevic S, Pierpaoli C. Color schemes to represent the orientation of anisotropic tissues from diffusion tensor data: application to white matter fiber tract mapping in the human brain. Magn Reson Med 1999;42(3):526-540.

35. Rose SE, Chen F, Chalk JB, et al. Loss of connectivity in Alzheimer's disease: an evaluation of white matter tract integrity with colour coded MR diffusion tensor imaging. Journal of neurology, neurosurgery, and psychiatry 2000;69(4):528-530.

36. Pierpaoli C, Jezzard P, Basser PJ, Barnett A, Di Chiro G. Diffusion tensor MR imaging of the human brain. Radiology 1996;201(3):637-648.

37. Beaulieu C. The basis of anisotropic water diffusion in the nervous system - a technical review. NMR Biomed 2002;15(7-8):435-455.

38. Mori S, Zhang J. Principles of diffusion tensor imaging and its applications to basic neuroscience research. Neuron 2006;51(5):527-539.

39. Della Nave R, Ginestroni A, Diciotti S, Salvatore E, Soricelli A, Mascalchi M. Axial diffusivity is increased in the degenerating superior cerebellar peduncles of Friedreich's ataxia. Neuroradiology 2011;53(5):367-372.

40. Douaud G, Smith S, Jenkinson M, et al. Anatomically related grey and white matter abnormalities in adolescent-onset schizophrenia. Brain 2007;130(Pt 9):2375-2386.

41. Good CD, Johnsrude IS, Ashburner J, Henson RN, Friston KJ, Frackowiak RS. A voxel-based morphometric study of ageing in 465 normal adult human brains. Neuroimage 2001;14(1 Pt 1):21-36.

42. Smith SM, Jenkinson M, Woolrich MW, et al. Advances in functional and structural MR image analysis and implementation as FSL. Neuroimage 2004;23 Suppl 1:S208-219.

43. Simon TJ, Ding L, Bish JP, McDonald-McGinn DM, Zackai EH, Gee J. Volumetric, connective, and morphologic changes in the brains of children with chromosome 22q11.2 deletion syndrome: an integrative study. Neuroimage 2005;25(1):169-180.

44. Smith SM, Jenkinson M, Johansen-Berg H, et al. Tract-based spatial statistics: voxelwise analysis of multi-subject diffusion data. Neuroimage 2006;31(4):1487-1505.

45. Jones DK, Symms MR, Cercignani M, Howard RJ. The effect of filter size on VBM analyses of DT-MRI data. Neuroimage 2005;26(2):546-554.

46. Sommer M, Koch MA, Paulus W, Weiller C, Buchel C. Disconnection of speech-relevant brain areas in persistent developmental stuttering. Lancet 2002;360(9330):380-383.

47. Patenaude B, Smith SM, Kennedy DN, Jenkinson M. A Bayesian model of shape and appearance for subcortical brain segmentation. Neuroimage 2011;56(3):907-922.

48. Jenkinson M. Cerebellar volume. In; 2011.

49. Bach M, Laun FB, Leemans A, et al. Methodological considerations on tract-based spatial statistics (TBSS). Neuroimage 2014;100:358-369.

50. Conturo TE, Lori NF, Cull TS, et al. Tracking neuronal fiber pathways in the living human brain. Proceedings of the National Academy of Sciences of the United States of America 1999;96(18):10422-10427.

51. Mori S, Crain BJ, Chacko VP, van Zijl PC. Three-dimensional tracking of axonal projections in the brain by magnetic resonance imaging. Annals of neurology 1999;45(2):265-269.

52. Basser PJ, Pajevic S, Pierpaoli C, Duda J, Aldroubi A. In vivo fiber tractography using DT-MRI data. Magn Reson Med 2000;44(4):625-632.

53. Jeurissen B, Leemans A, Tournier JD, Jones DK, Sijbers J. Investigating the prevalence of complex fiber configurations in white matter tissue with diffusion magnetic resonance imaging. Human brain mapping 2013;34(11):2747-2766.

54. Jones DK. Studying connections in the living human brain with diffusion MRI. Cortex; a journal devoted to the study of the nervous system and behavior 2008;44(8):936-952.

55. Douaud G, Jbabdi S, Behrens TE, et al. DTI measures in crossing-fibre areas: increased diffusion anisotropy reveals early white matter alteration in MCI and mild Alzheimer's disease. Neuroimage 2011;55(3):880-890.

56. Pierpaoli C, Barnett A, Pajevic S, et al. Water diffusion changes in Wallerian degeneration and their dependence on white matter architecture. Neuroimage 2001;13(6 Pt 1):1174-1185.

57. Alexander AL, Lee JE, Lazar M, Field AS. Diffusion tensor imaging of the brain. Neurotherapeutics : the journal of the American Society for Experimental NeuroTherapeutics 2007;4(3):316-329.

58. Tournier JD, Calamante F, Connelly A. Robust determination of the fibre orientation distribution in diffusion MRI: non-negativity constrained super-resolved spherical deconvolution. Neuroimage 2007;35(4):1459-1472.

59. Tournier JD, Calamante F, Connelly A. MRtrix: Diffusion tractography in crossing fiber regions. International Journal of Imaging Systems and Technology 2012;22(1):53-66.

60. Tuch DS, Reese TG, Wiegell MR, Makris N, Belliveau JW, Wedeen VJ. High angular resolution diffusion imaging reveals intravoxel white matter fiber heterogeneity. Magn Reson Med 2002;48(4):577-582.

61. Rose S, Guzzetta A, Pannek K, Boyd R. MRI structural connectivity, disruption of primary sensorimotor pathways, and hand function in cerebral palsy. Brain connectivity 2011;1(4):309-316.

62. Tournier JD, Calamante F, Gadian DG, Connelly A. Direct estimation of the fiber orientation density function from diffusion-weighted MRI data using spherical deconvolution. Neuroimage 2004;23(3):1176-1185.

63. Smith RE, Tournier JD, Calamante F, Connelly A. Anatomically-constrained tractography: improved diffusion MRI streamlines tractography through effective use of anatomical information. Neuroimage 2012;62(3):1924-1938.

64. Smith RE, Tournier JD, Calamante F, Connelly A. SIFT: Spherical-deconvolution informed filtering of tractograms. Neuroimage 2013;67:298-312.

65. Colby JB, Soderberg L, Lebel C, Dinov ID, Thompson PM, Sowell ER. Along-tract statistics allow for enhanced tractography analysis. Neuroimage 2012;59(4):3227-3242.

66. Raffelt D, Tournier JD, Rose S, et al. Apparent Fibre Density: a novel measure for the analysis of diffusion-weighted magnetic resonance images. Neuroimage 2012;59(4):3976-3994.

67. Swift M, Morrell D, Cromartie E, Chamberlin AR, Skolnick MH, Bishop DT. The incidence and gene frequency of ataxia-telangiectasia in the United States. Am J Hum Genet 1986;39(5):573-583.

68. Louis-Bar M. Confin Neurol 1941;4(32).

69. Watters D, Khanna KK, Beamish H, et al. Cellular localisation of the ataxia-telangiectasia (ATM) gene product and discrimination between mutated and normal forms. Oncogene 1997;14(16):1911-1921.

70. Cornforth MN, Bedford JS. On the nature of a defect in cells from individuals with ataxia-telangiectasia. Science 1985;227(4694):1589-1591.

71. Jaspers NG, de Wit J, Regulski MR, Bootsma D. Abnormal regulation of DNA replication and increased lethality in ataxia telangiectasia cells exposed to carcinogenic agents. Cancer research 1982;42(1):335-341.

72. Jaspers NG, Gatti RA, Baan C, Linssen PC, Bootsma D. Genetic complementation analysis of ataxia telangiectasia and Nijmegen breakage syndrome: a survey of 50 patients. Cytogenet Cell Genet 1988;49(4):259-263.

73. Pandita TK, Hittelman WN. The contribution of DNA and chromosome repair deficiencies to the radiosensitivity of ataxia-telangiectasia. Radiation research 1992;131(2):214-223.

74. Higurashi M, Conen PE. In vitro chromosomal radiosensitivity in "chromosomal breakage syndromes". Cancer 1973;32(2):380-383.

75. Paterson MC, Smith BP, Lohman PH, Anderson AK, Fishman L. Defective excision repair of gamma-ray-damaged DNA in human (ataxia telangiectasia) fibroblasts. Nature 1976;260(5550):444-447.

76. Lehman AR, Stevens S. The production and repair of double strand breaks in cells from normal humans and from patients with ataxia telangiectasia. Biochim Biophys Acta 1977;474(1):49-60.

77. Cox R, Hosking GP, Wilson J. Ataxia telangiectasia. Evaluation of radiosensitivity in cultured skin fibroblasts as a diagnostic test. Arch Dis Child 1978;53(5):386-390.

78. Taylor AM, Rosney CM, Campbell JB. Unusual sensitivity of ataxia telangiectasia cells to bleomycin. Cancer research 1979;39(3):1046-1050.

79. Vincent RA, Jr., Sheridan RB, 3rd, Huang PC. DNA strained breakage repair in ataxia telangiectasia fibroblast-like cells. Mutation research 1975;33(2-3):357-366.

80. Houldsworth J, Lavin MF. Effect of ionizing radiation on DNA synthesis in ataxia telangiectasia cells. Nucleic acids research 1980;8(16):3709-3720.

81. Foray N, Priestley A, Alsbeih G, et al. Hypersensitivity of ataxia telangiectasia fibroblasts to ionizing radiation is associated with a repair deficiency of DNA double-strand breaks. International journal of radiation biology 1997;72(3):271-283.

82. Perlman S, Becker-Catania S, Gatti RA. Ataxia-telangiectasia: diagnosis and treatment. Seminars in pediatric neurology 2003;10(3):173-182.

83. Chun HH, Gatti RA. Ataxia-telangiectasia, an evolving phenotype. DNA repair 2004;3(8-9):1187-1196.

84. Huang Y, Yang L, Wang JC, et al. Twelve Novel Atm Mutations Identified in Chinese Ataxia Telangiectasia Patients. Neuromolecular Medicine 2013;15(3):536-540.

85. de Graaf AS, de Jong G, Kleijer WJ. An early-onset recessive cerebellar disorder with distal amyotrophy and, in two patients, gross myoclonia: a probable ataxia telangiectasia variant. Clinical neurology and neurosurgery 1995;97(1):1-7.

86. Watanabe M, Sugai Y, Concannon P, et al. Familial spinocerebellar ataxia with cerebellar atrophy, peripheral neuropathy, and elevated level of serum creatine kinase, gamma-globulin, and alpha-fetoprotein. Annals of neurology 1998;44(2):265-269.

87. Verhagen MM, Martin JJ, van Deuren M, et al. Neuropathology in classical and variant ataxia-telangiectasia. Neuropathology : official journal of the Japanese Society of Neuropathology 2012;32(3):234-244.

88. De Leon GA, Grover WD, Huff DS. Neuropathologic changes in ataxia-telangiectasia. Neurology 1976;26(10):947-951.

89. Agamanolis DP, Greenstein JI. Ataxia-telangiectasia. Report of a case with Lewy bodies and vascular abnormalities within cerebral tissue. Journal of neuropathology and experimental neurology 1979;38(5):475-489.

90. Amromin GD, Boder E, Teplitz R. Ataxia-telangiectasia with a 32 year survival. A clinicopathological report. Journal of neuropathology and experimental neurology 1979;38(6):621-643.

91. Monaco S, Nardelli E, Moretto G, Cavallaro T, Rizzuto N. Cytoskeletal pathology in ataxia-telangiectasia. Clinical neuropathology 1988;7(1):44-46.

92. Terplan KL, Krauss RF. Histopathologic brain changes in association with ataxia-telangiectasia. Neurology 1969;19(5):446-454.

93. Sourander P, Bonnevier JO, Olsson Y. A case of ataxia-telangiectasia with lesions in the spinal cord. Acta neurologica Scandinavica 1966;42(3):354-366.

94. Stritch SJ. Pathological findings in three cases of ataxia-telangiectasia. J Neurol Neurosurg Pyschiatr 1966;29:489–499.

95. Solitare GB, Lopez VF. Louis-bar's syndrome (ataxia-telangiectasia). Neuropathologic observations. Neurology 1967;17(1):23-31.

96. Solitare GB. Louis-Bar's syndrome (ataxia-telangiectasia). Anatomic considerations with emphasis on neuropathologic observations. Neurology 1968;18(12):1180-1186.

97. Aguilar MJ, Kamoshita S, Landing BH, Boder E, Sedgwick RP. Pathological observations in ataxia-telangiectasia. A report of five cases. Journal of neuropathology and experimental neurology 1968;27(4):659-676.

98. Itatsu Y, Uno Y. An autopsy case of ataxia-telangiectasia. Acta pathologica japonica 1969;19(2):229-239.

99. Paula-Barbosa MM, Ruela C, Tavares MA, Pontes C, Saraiva A, Cruz C. Cerebellar cortex ultrastructure in ataxia-telangiectasia. Annals of neurology 1983;13(3):297-302.

100. Larnaout A, Belal S, Ben Hamida C, Ben Hamida M, Hentati F. Atypical ataxia telangiectasia with early childhood lower motor neuron degeneration: a clinicopathological observation in three siblings. Journal of neurology 1998;245(4):231-235.

101. Goodman WN, Cooper WC, Kessler GB, Fischer MS, Gardner MB. Ataxia-telangiectasia. A report of two cases in siblings presenting a picture of progressive spinal muscular atrophy. Bulletin of the Los Angeles neurological societies 1969;34(1):1-22.

102. Soares HD, Morgan JI, McKinnon PJ. Atm expression patterns suggest a contribution from the peripheral nervous system to the phenotype of ataxia-telangiectasia. Neuroscience 1998;86(4):1045-1054.

103. Quick KL, Dugan LL. Superoxide stress identifies neurons at risk in a model of ataxia-telangiectasia. Annals of neurology 2001;49(5):627-635.

104. Oka A, Takashima S. Expression of the ataxia-telangiectasia gene (ATM) product in human cerebellar neurons during development. Neuroscience letters 1998;252(3):195-198.

105. Gorodetsky E, Calkins S, Ahn J, Brooks PJ. ATM, the Mre11/Rad50/Nbs1 complex, and topoisomerase I are concentrated in the nucleus of Purkinje neurons in the juvenile human brain. DNA repair 2007;6(11):1698-1707.

106. Yi M, Rosin MP, Anderson CK. Response of fibroblast cultures from ataxia-telangiectasia patients to oxidative stress. Cancer Lett 1990;54(1-2):43-50.

107. Reichenbach J, Schubert R, Schindler D, Muller K, Bohles H, Zielen S. Elevated oxidative stress in patients with ataxia telangiectasia. Antioxidants & redox signaling 2002;4(3):465-469.

108. Rotman G, Shiloh Y. Ataxia-telangiectasia: is ATM a sensor of oxidative damage and stress? BioEssays : news and reviews in molecular, cellular and developmental biology 1997;19(10):911-917.

109. Barlow C, Dennery PA, Shigenaga MK, et al. Loss of the ataxia-telangiectasia gene product causes oxidative damage in target organs. Proceedings of the National Academy of Sciences of the United States of America 1999;96(17):9915-9919.

110. Takao N, Li Y, Yamamoto K. Protective roles for ATM in cellular response to oxidative stress. FEBS letters 2000;472(1):133-136.

111. Chen P, Peng C, Luff J, et al. Oxidative stress is responsible for deficient survival and dendritogenesis in purkinje neurons from ataxia-telangiectasia mutated mutant mice. The Journal of neuroscience : the official journal of the Society for Neuroscience 2003;23(36):11453-11460.

112. Blough NV, Zafiriou OC. Reaction of superoxide with nitric oxide to form peroxonitrite in alkaline aqueous solution. Inorganic Chemistry 1985;24(22):3502-3504.

113. Beckman JS, Beckman TW, Chen J, Marshall PA, Freeman BA. Apparent hydroxyl radical production by peroxynitrite: implications for endothelial injury from nitric oxide and superoxide. Proceedings of the National Academy of Sciences of the United States of America 1990;87(4):1620-1624.

114. Reliene R, Fischer E, Schiestl RH. Effect of N-acetyl cysteine on oxidative DNA damage and the frequency of DNA deletions in atm-deficient mice. Cancer research 2004;64(15):5148-5153.

115. Schubert R, Erker L, Barlow C, et al. Cancer chemoprevention by the antioxidant tempol in Atm-deficient mice. Human molecular genetics 2004;13(16):1793-1802.

116. Gueven N, Luff J, Peng C, Hosokawa K, Bottle SE, Lavin MF. Dramatic extension of tumor latency and correction of neurobehavioral phenotype in Atm-mutant mice with a nitroxide antioxidant. Free radical biology & medicine 2006;41(6):992-1000.

117. Reliene R, Schiestl RH. Antioxidant N-acetyl cysteine reduces incidence and multiplicity of lymphoma in Atm deficient mice. DNA repair 2006;5(7):852-859.

118. Ito K, Takubo K, Arai F, et al. Regulation of reactive oxygen species by Atm is essential for proper response to DNA double-strand breaks in lymphocytes. Journal of immunology (Baltimore, Md : 1950) 2007;178(1):103-110.

119. Reliene R, Schiestl RH. Experimental antioxidant therapy in ataxia telangiectasia. Clinical medicine Oncology 2008;2:431-436.

120. Reliene R, Fleming SM, Chesselet MF, Schiestl RH. Effects of antioxidants on cancer prevention and neuromotor performance in Atm deficient mice. Food and chemical toxicology : an international journal published for the British Industrial Biological Research Association 2008;46(4):1371-1377.

121. Mercer JR, Yu E, Figg N, et al. The mitochondria-targeted antioxidant MitoQ decreases features of the metabolic syndrome in ATM+/-/ApoE-/- mice. Free radical biology & medicine 2012;52(5):841-849.

122. Fearnhead HO, Chwalinski M, Snowden RT, Ormerod MG, Cohen GM. Dexamethasone and etoposide induce apoptosis in rat thymocytes from different phases of the cell cycle. Biochemical pharmacology 1994;48(6):1073-1079.

123. Yan M, Qiang W, Liu N, Shen J, Lynn WS, Wong PK. The ataxia-telangiectasia gene product may modulate DNA turnover and control cell fate by regulating cellular redox in lymphocytes. FASEB journal : official publication of the Federation of American Societies for Experimental Biology 2001;15(7):1132-1138.

124. Yan M, Kuang X, Qiang W, et al. Prevention of thymic lymphoma development in Atm-/- mice by dexamethasone. Cancer research 2002;62(18):5153-5157.

125. Kuang X, Yan M, Liu N, et al. Control of Atm-/- thymic lymphoma cell proliferation in vitro and in vivo by dexamethasone. Cancer chemotherapy and pharmacology 2005;55(3):203-212.

126. Buoni S, Zannolli R, Sorrentino L, Fois A. Betamethasone and improvement of neurological symptoms in ataxia-telangiectasia. Archives of neurology 2006;63(10):1479-1482.

127. Broccoletti T, Del Giudice E, Amorosi S, et al. Steroid-induced improvement of neurological signs in ataxia-telangiectasia patients. European journal of neurology : the official journal of the European Federation of Neurological Societies 2008;15(3):223-228.

128. Zannolli R, Buoni S, Betti G, et al. A randomized trial of oral betamethasone to reduce ataxia symptoms in ataxia telangiectasia. Movement disorders : official journal of the Movement Disorder Society 2012;27(10):1312-1316.

129. Russo I, Cosentino C, Del Giudice E, et al. In ataxia-teleangiectasia betamethasone response is inversely correlated to cerebellar atrophy and directly to antioxidative capacity. European Journal of Neurology 2009;16(6):755-759.

130. Broccoletti T, Del Giudice E, Cirillo E, et al. Efficacy of very-low-dose betamethasone on neurological symptoms in ataxia-telangiectasia. European journal of neurology : the official journal of the European Federation of Neurological Societies 2011;18(4):564-570.

131. Gatti RA, Vinters HV. Cerebellar pathology in ataxia-telangiectasia: the significance of basket cells. Kroc Foundation series 1985;19:225-232.

132. Gatti RA, Perlman S. A proposed bailout for A-T patients? European journal of neurology : the official journal of the European Federation of Neurological Societies 2009;16(6):653-655.

133. Quarantelli M, Giardino G, Prinster A, et al. Steroid treatment in Ataxia-Telangiectasia induces alterations of functional magnetic resonance imaging during prono-supination task. European journal of paediatric neurology : EJPN : official journal of the European Paediatric Neurology Society 2013;17(2):135-140.

134. Scharnetzky M, Kohlschutter A, Krtsch H. Computerized tomographic findings in a case of ataxia-telangiectasia (Louis-Bar syndrome). Neuropediatrics 1980;11(4):384-387.

135. Meshram CM, Sawhney IM, Prabhakar S, Chopra JS. Ataxia telangiectasia in identical twins: unusual features. Journal of neurology 1986;233(5):304-305.

136. Wong V, Yu YL, Chan-Lui WY, Woo E, Yeung CY. Ataxia telangiectasia in Chinese children. A clinical and electrophysiological study. Clinical neurology and neurosurgery 1987;89(3):137-144.

137. de Jonge J, Tijssen CC. Ataxia telangiectasia in a brother and sister at older age. Clinical neurology and neurosurgery 1988;90(3):279-281.

138. Kryst T, Kozlowski P, Walecki J, Gajkowski K. Cerebellar atrophy diagnosed by computed tomography and clinical data. Acta radiologica Supplementum 1986;369:396-398.

139. Wick MC, Kremser C, Frischauf S, Wick G. In vivo molecular imaging of vascular stress. Cell stress & chaperones 2008;13(3):263-273.

140. Golay X, Jiang H, van Zijl PC, Mori S. High-resolution isotropic 3D diffusion tensor imaging of the human brain. Magn Reson Med 2002;47(5):837-843.

141. Pajevic S, Aldroubi A, Basser PJ. A continuous tensor field approximation of discrete DT-MRI data for extracting microstructural and architectural features of tissue. Journal of magnetic resonance (San Diego, Calif : 1997) 2002;154(1):85-100.

142. Dafni H, Landsman L, Schechter B, Kohen F, Neeman M. MRI and fluorescence microscopy of the acute vascular response to VEGF165: vasodilation, hyper-permeability and lymphatic uptake, followed by rapid inactivation of the growth factor. NMR Biomed 2002;15(2):120-131.

143. Demaerel P, Kendall BE, Kingsley D. Cranial CT and MRI in diseases with DNA repair defects. Neuroradiology 1992;34(2):117-121.

144. Farina L, Uggetti C, Ottolini A, et al. Ataxia-telangiectasia: MR and CT findings. Journal of computer assisted tomography 1994;18(5):724-727.

145. Sardanelli F, Parodi RC, Ottonello C, et al. Cranial MRI in ataxia-telangiectasia. Neuroradiology 1995;37(1):77-82.

146. Ciemins JJ, Horowitz AL. Abnormal white matter signal in ataxia telangiectasia. AJNR American journal of neuroradiology 2000;21(8):1483-1485.

147. Opeskin K, Waterston J, Nirenberg A, Hare WS. Ataxia telangiectasia with long survival. Journal of clinical neuroscience : official journal of the Neurosurgical Society of Australasia 1998;5(4):471-473.

148. Kamiya M, Yamanouchi H, Yoshida T, et al. Ataxia telangiectasia with vascular abnormalities in the brain parenchyma: report of an autopsy case and literature review. Pathology international 2001;51(4):271-276.

149. Huang KY, Shyur SD, Wang CY, Shen EY, Liang DC. Ataxia telangiectasia: report of two cases. Journal of microbiology, immunology, and infection = Wei mian yu gan ran za zhi 2001;34(1):71-75.

150. Tavani F, Zimmerman RA, Berry GT, Sullivan K, Gatti R, Bingham P. Ataxia-telangiectasia: the pattern of cerebellar atrophy on MRI. Neuroradiology 2003;45(5):315-319.

151. Firat AK, Karakas HM, Firat Y, Yakinci C. Quantitative evaluation of brain involvement in ataxia telangiectasia by diffusion weighted MR imaging. European journal of radiology 2005;56(2):192-196.

152. Lin DD, Crawford TO, Lederman HM, Barker PB. Proton MR spectroscopic imaging in ataxia-telangiectasia. Neuropediatrics 2006;37(4):241-246.

153. Wallis LI, Griffiths PD, Ritchie SJ, Romanowski CA, Darwent G, Wilkinson ID. Proton spectroscopy and imaging at 3T in ataxia-telangiectasia. AJNR American journal of neuroradiology 2007;28(1):79-83.

154. Habek M, Brinar VV, Rados M, Zadro I, Zarkovic K. Brain MRI abnormalities in ataxia-telangiectasia. The neurologist 2008;14(3):192-195.

155. Kieslich M, Hoche F, Reichenbach J, et al. Extracerebellar MRI-lesions in ataxia telangiectasia go along with deficiency of the GH/IGF-1 axis, markedly reduced body weight, high ataxia scores and advanced age. Cerebellum 2010;9(2):190-197.

156. Al-Maawali A, Blaser S, Yoon G. Diagnostic approach to childhood-onset cerebellar atrophy: a 10-year retrospective study of 300 patients. J Child Neurol 2012;27(9):1121-1132.

157. Chung EO, Bodensteiner JB, Noorani PA, Schochet SS. Cerebral White-Matter Changes Suggesting Leukodystrophy in Ataxia Telangiectasia. Journal of Child Neurology 1994;9(1):31-35.

158. Lin DD, Barker PB, Lederman HM, Crawford TO. Cerebral Abnormalities in Adults with Ataxia-Telangiectasia. AJNR American journal of neuroradiology 2013.

159. JH M. Text of Child Neurology. 4th ed ed. Philadelphia: Lea & Febiger, 1990.

160. Ciccarelli O, Behrens TE, Altmann DR, et al. Probabilistic diffusion tractography: a potential tool to assess the rate of disease progression in amyotrophic lateral sclerosis. Brain 2006;129(Pt 7):1859-1871.

161. Johansen-Berg H, Rushworth MF. Using diffusion imaging to study human connectional anatomy. Annual review of neuroscience 2009;32:75-94.

162. Zalesky A, Akhlaghi H, Corben LA, et al. Cerebello-cerebral connectivity deficits in Friedreich ataxia. Brain structure & function 2013.

163. Nissenkorn A, Hassin-Baer S, Lerman SF, Levi YB, Tzadok M, Ben-Zeev B. Movement disorder in ataxia-telangiectasia: treatment with amantadine sulfate. J Child Neurol 2013;28(2):155-160.

164. Mizoguchi K, Yokoo H, Yoshida M, Tanaka T, Tanaka M. Amantadine increases the extracellular dopamine levels in the striatum by re-uptake inhibition and by N-methyl-D-aspartate antagonism. Brain research 1994;662(1-2):255-258.

165. Blanpied TA, Clarke RJ, Johnson JW. Amantadine inhibits NMDA receptors by accelerating channel closure during channel block. The Journal of neuroscience : the official journal of the Society for Neuroscience 2005;25(13):3312-3322.

166. Notarangelo L, Casanova JL, Fischer A, et al. Primary immunodeficiency diseases: an update. The Journal of allergy and clinical immunology 2004;114(3):677-687.

167. Crawford TO, Mandir AS, Lefton-Greif MA, et al. Quantitative neurologic assessment of ataxia-telangiectasia. Neurology 2000;54(7):1505-1509.

168. Nam H, Park HJ. Distortion correction of high b-valued and high angular resolution diffusion images using iterative simulated images. Neuroimage 2011;57(3):968-978.

169. Jenkinson M, Beckmann CF, Behrens TE, Woolrich MW, Smith SM. FSL. Neuroimage 2012;62(2):782-790.

170. Sled JG, Zijdenbos AP, Evans AC. A nonparametric method for automatic correction of intensity nonuniformity in MRI data. IEEE transactions on medical imaging 1998;17(1):87-97.

171. Morris D, Nossin-Manor R, Taylor MJ, Sled JG. Preterm neonatal diffusion processing using detection and replacement of outliers prior to resampling. Magn Reson Med 2011;66(1):92-101.

172. Bai Y, Alexander P. Model-based registration to correct for motion between acquisitions in diffusion MR imaging. IEEE International Symposium on Biomedical Imaging: From Nano to Macro; 2008.

173. Rohde GK, Barnett AS, Basser PJ, Marenco S, Pierpaoli C. Comprehensive approach for correction of motion and distortion in diffusion-weighted MRI. Magn Reson Med 2004;51(1):103-114.

174. Leemans A, Jones DK. The B-matrix must be rotated when correcting for subject motion in DTI data. Magn Reson Med 2009;61(6):1336-1349.

175. Pannek K, Raffelt D, Bell C, Mathias JL, Rose SE. HOMOR: higher order model outlier rejection for high b-value MR diffusion data. Neuroimage 2012;63(2):835-842.

176. Andersson JLR, Jenkinson M, Smith S. Non-linear optimisation
FMRIB Technial Report TR07JA1. Oxford, United Kingdom: FMRIB Centre; 2007.

177. Andersson JLR, Jenkinson M, Smith S. Non-linear registration, aka Spatial normalisation. FMRIB technical report TR07JA2 from www.fmrib.ox.ac.uk/analysis/techrep: FMRIB; 2007.

178. Smith SM, Nichols TE. Threshold-free cluster enhancement: addressing problems of smoothing, threshold dependence and localisation in cluster inference. Neuroimage 2009;44(1):83-98.

179. Hua K, Zhang J, Wakana S, et al. Tract probability maps in stereotaxic spaces: analyses of white matter anatomy and tract-specific quantification. Neuroimage 2008;39(1):336-347.

180. Della Nave R, Ginestroni A, Tessa C, et al. Brain white matter tracts degeneration in Friedreich ataxia. An in vivo MRI study using tract-based spatial statistics and voxel-based morphometry. Neuroimage 2008;40(1):19-25.

181. Miles J. A charity that begins at home. In: The Courier-Mail; 2011.

182. Anscombe C. New technology could shed light on treatment of rare genetic condition. In: Health News; 2013.

183. Sahama I, Sinclair K, Fiori S, Pannek K, Lavin M, Rose S. Altered corticomotor-cerebellar integrity in young ataxia telangiectasia patients. Movement disorders : official journal of the Movement Disorder Society 2014;29(10):1289-1298.

184. Dunn HG. Nerve conduction studies in children with Friedreich's ataxia and ataxia-telangiectasia. Dev Med Child Neurol 1973;15(3):324-337.

185. Scarpini C, Mondelli M, Guazzi GC, Federico A. Ataxia-telangiectasia: somatosensory, brainstem auditory and motor evoked potentials in six patients. Dev Med Child Neurol 1996;38(1):65-73.

186. Kamson DO, Juhasz C, Chugani HT, Jeong JW. Novel diffusion tensor imaging technique reveals developmental streamline volume changes in the corticospinal tract associated with leg motor control. Brain & development 2015;37(4):370-375.

187. Jenkinson M. Fast, automated, N-dimensional phase-unwrapping algorithm. Magn Reson Med 2003;49(1):193-197.

188. Jenkinson M, Wilson JL, Jezzard P. Perturbation method for magnetic field calculations of nonconductive objects. Magn Reson Med 2004;52(3):471-477.

189. Jones DK. Precision and accuracy in diffusion tensor magnetic resonance imaging. Topics in magnetic resonance imaging : TMRI 2010;21(2):87-99.

190. Kamali A, Kramer LA, Frye RE, Butler IJ, Hasan KM. Diffusion tensor tractography of the human brain cortico-ponto-cerebellar pathways: a quantitative preliminary study. Journal of magnetic resonance imaging : JMRI 2010;32(4):809-817.

191. Kumar A, Juhasz C, Asano E, et al. Diffusion tensor imaging study of the cortical origin and course of the corticospinal tract in healthy children. AJNR American journal of neuroradiology 2009;30(10):1963-1970.

192. Team RC. R: A language and environment for statistical computing. . In. Vienna, Austria: R Foundation for Statistical Computing; 2014.

193. Hoche F, Frankenberg E, Rambow J, et al. Cognitive phenotype in ataxia-telangiectasia. Pediatric neurology 2014;51(3):297-310.

194. Volkow ND, Tomasi D, Wang GJ, Studentsova Y, Margus B, Crawford TO. Brain glucose metabolism in adults with ataxia-telangiectasia and their asymptomatic relatives. Brain 2014;137(Pt 6):1753-1761.

195. Jones D. Diffusion MRI: Theory, Methods and Applications. New York: Oxford University Press, 2011.

196. Carlessi L, Fusar Poli E, Bechi G, et al. Functional and molecular defects of hiPSC-derived neurons from patients with ATM deficiency. Cell death & disease 2014;5:e1342.

197. Stewart R, Kozlov S, Matigian N, et al. A patient-derived olfactory stem cell disease model for ataxia-telangiectasia. Human molecular genetics 2013;22(12):2495-2509.

198. Chiesa N, Barlow C, Wynshaw-Boris A, Strata P, Tempia F. Atm-deficient mice Purkinje cells show age-dependent defects in calcium spike bursts and calcium currents. Neuroscience 2000;96(3):575-583.

199. Le Bihan D. Molecular diffusion, tissue microdynamics and microstructure. NMR Biomed 1995;8(7-8):375-386.

200. Tuor UI, Morgunov M, Sule M, et al. Cellular correlates of longitudinal diffusion tensor imaging of axonal degeneration following hypoxic-ischemic cerebral infarction in neonatal rats. NeuroImage Clinical 2014;6:32-42.

201. Musson R, Romanowski C. Restricted diffusion in Wallerian degeneration of the middle cerebellar peduncles following pontine infarction. Polish journal of radiology / Polish Medical Society of Radiology 2010;75(4):38-43.

202. Qiu D, Tan LH, Zhou K, Khong PL. Diffusion tensor imaging of normal white matter maturation from late childhood to young adulthood: voxel-wise evaluation of mean diffusivity, fractional anisotropy, radial and axial diffusivities, and correlation with reading development. Neuroimage 2008;41(2):223-232.

203. Schmithorst VJ, Wilke M, Dardzinski BJ, Holland SK. Correlation of white matter diffusivity and anisotropy with age during childhood and adolescence: a cross-sectional diffusion-tensor MR imaging study. Radiology 2002;222(1):212-218.

204. Schwarz CG, Reid RI, Gunter JL, et al. Improved DTI registration allows voxel-based analysis that outperforms tract-based spatial statistics. Neuroimage 2014;94:65-78.

205. Chessa L, Leuzzi V, Plebani A, et al. Intra-erythrocyte infusion of dexamethasone reduces neurological symptoms in ataxia teleangiectasia patients: results of a phase 2 trial. Orphanet journal of rare diseases 2014;9:5.

206. Leuzzi V, Micheli R, D'Agnano D, et al. Positive effect of erythrocyte-delivered dexamethasone in ataxia-telangiectasia. Neurology(R) neuroimmunology & neuroinflammation 2015;2(3):e98.

207. Olson EA, Collins PF, Hooper CJ, Muetzel R, Lim KO, Luciana M. White matter integrity predicts delay discounting behavior in 9- to 23-year-olds: a diffusion tensor imaging study. Journal of cognitive neuroscience 2009;21(7):1406-1421.

208. Lebel C, Gee M, Camicioli R, Wieler M, Martin W, Beaulieu C. Diffusion tensor imaging of white matter tract evolution over the lifespan. Neuroimage 2012;60(1):340-352.

209. Bergfield KL, Hanson KD, Chen K, et al. Age-related networks of regional covariance in MRI gray matter: reproducible multivariate patterns in healthy aging. Neuroimage 2010;49(2):1750-1759.

210. Taki Y, Hashizume H, Thyreau B, et al. Linear and curvilinear correlations of brain gray matter volume and density with age using voxel-based morphometry with the Akaike information criterion in 291 healthy children. Human brain mapping 2013;34(8):1857-1871.

211. Taki Y, Thyreau B, Kinomura S, et al. A longitudinal study of age- and gender-related annual rate of volume changes in regional gray matter in healthy adults. Human brain mapping 2013;34(9):2292-2301.

212. Van Hecke W, Leemans A, Sijbers J, Vandervliet E, Van Goethem J, Parizel PM. A tracking-based diffusion tensor imaging segmentation method for the detection of diffusion-related changes of the cervical spinal cord with aging. Journal of magnetic resonance imaging : JMRI 2008;27(5):978-991.

213. Chang Y, Jung TD, Yoo DS, Hyun JK. Diffusion tensor imaging and fiber tractography of patients with cervical spinal cord injury. Journal of neurotrauma 2010;27(11):2033-2040.

214. Brander A, Koskinen E, Luoto TM, et al. Diffusion tensor imaging of the cervical spinal cord in healthy adult population: normative values and measurement reproducibility at 3T MRI. Acta radiologica (Stockholm, Sweden : 1987) 2014;55(4):478-485.

215. Lavin MF. The appropriateness of the mouse model for ataxia-telangiectasia: Neurological defects but no neurodegeneration. DNA repair 2013;12(8):612-619.

216. Brant-Zawadzki M, Gillan GD, Nitz WR. MP RAGE: a three-dimensional, T1-weighted, gradient-echo sequence--initial experience in the brain. Radiology 1992;182(3):769-775.

217. Marques JP, Kober T, Krueger G, van der Zwaag W, Van de Moortele PF, Gruetter R. MP2RAGE, a self bias-field corrected sequence for improved segmentation and T1-mapping at high field. Neuroimage 2010;49(2):1271-1281.

218. Okubo G, Okada T, Yamamoto A, et al. MP2RAGE for deep gray matter measurement of the brain: A comparative study with MPRAGE. Journal of magnetic resonance imaging : JMRI 2015.

219. Fujimoto K, Polimeni JR, van der Kouwe AJ, et al. Quantitative comparison of cortical surface reconstructions from MP2RAGE and multi-echo MPRAGE data at 3 and 7 T. Neuroimage 2014;90:60-73.

220. Strotmann B, Heidemann RM, Anwander A, et al. High-resolution MRI and diffusion-weighted imaging of the human habenula at 7 tesla. Journal of magnetic resonance imaging : JMRI 2014;39(4):1018-1026.

221. Simioni S, Amaru F, Bonnier G, et al. MP2RAGE provides new clinically-compatible correlates of mild cognitive deficits in relapsing-remitting multiple sclerosis. Journal of neurology 2014;261(8):1606-1613.

222. Mohan KK, Chugani DC, Chugani HT. Positron emission tomography in pediatric neurology. Seminars in pediatric neurology 1999;6(2):111-119.

223. Phelps M. PET: Physics, instrumentation, and scanners. PET: Molecular Imaging and Its Biological Applications
New York: Springer-Verlag, 2004.

224. Kaya N, Aldhalaan H, Al-Younes B, et al. Phenotypical spectrum of cerebellar ataxia associated with a novel mutation in the CA8 gene, encoding carbonic anhydrase (CA) VIII. American journal of medical genetics Part B, Neuropsychiatric genetics : the official publication of the International Society of Psychiatric Genetics 2011;156b(7):826-834.

225. Brockmann K, Reimold M, Globas C, et al. PET and MRI reveal early evidence of neurodegeneration in spinocerebellar ataxia type 17. Journal of nuclear medicine : official publication, Society of Nuclear Medicine 2012;53(7):1074-1080.

226. Oh JS, Oh M, Chung SJ, Kim JS. Cerebellum-specific 18F-FDG PET analysis for the detection of subregional glucose metabolism changes in spinocerebellar ataxia. Neuroreport 2014;25(15):1198-1202.

227. Tanji H, Nagasawa H, Hayashi T, et al. PET study in a patient with spinocerebellar degeneration before and after long-term administration of thyrotropin releasing hormone. Behavioural neurology 1996;9(3):171-175.

228. Sandlund JT, Hudson MM, Kennedy W, Onciu M, Kastan MB. Pilot study of modified LMB-based therapy for children with ataxia-telangiectasia and advanced stage high grade mature B-cell malignancies. Pediatric blood & cancer 2013.

229. Inagaki A, Iida A, Matsubara M, Inagaki H. Positron emission tomography and magnetic resonance imaging in spinocerebellar ataxia type 2: a study of symptomatic and asymptomatic individuals. European journal of neurology : the official journal of the European Federation of Neurological Societies 2005;12(9):725-728.

230. Catana C, Procissi D, Wu Y, et al. Simultaneous in vivo positron emission tomography and magnetic resonance imaging. Proceedings of the National Academy of Sciences of the United States of America 2008;105(10):3705-3710.

231. Delso G, Ziegler S. PET/MRI system design. European journal of nuclear medicine and molecular imaging 2009;36 Suppl 1:S86-92.

232. Schafer JF, Gatidis S, Schmidt H, et al. Simultaneous whole-body PET/MR imaging in comparison to PET/CT in pediatric oncology: initial results. Radiology 2014;273(1):220-231.

233. Koepp M, Schelosky L, Cordes I, Cordes M, Poewe W. Dystonia in ataxia telangiectasia: report of a case with putaminal lesions and decreased striatal [123I]iodobenzamide binding. Movement disorders : official journal of the Movement Disorder Society 1994;9(4):455-459.

234. van Oostrom JC, Dekker M, Willemsen AT, de Jong BM, Roos RA, Leenders KL. Changes in striatal dopamine D2 receptor binding in pre-clinical Huntington's disease. European journal of

neurology : the official journal of the European Federation of Neurological Societies 2009;16(2):226-231.

235. van Oostrom JC, Maguire RP, Verschuuren-Bemelmans CC, et al. Striatal dopamine D2 receptors, metabolism, and volume in preclinical Huntington disease. Neurology 2005;65(6):941-943.

236. Otsuka M, Ichiya Y, Kuwabara Y, et al. Striatal 18F-dopa uptake and brain glucose metabolism by PET in patients with syndrome of progressive ataxia. Journal of the neurological sciences 1994;124(2):198-203.

237. Wullner U, Reimold M, Abele M, et al. Dopamine transporter positron emission tomography in spinocerebellar ataxias type 1, 2, 3, and 6. Archives of neurology 2005;62(8):1280-1285.

238. Wang PS, Liu RS, Yang BH, Soong BW. Topographic brain mapping of the international cooperative ataxia rating scale. A positron emission tomography study. Journal of neurology 2007;254(6):722-728.

239. Mishina M, Senda M, Ishii K, Ohyama M, Kitamura S, Katayama Y. Cerebellar activation during ataxic gait in olivopontocerebellar atrophy: a PET study. Acta neurologica Scandinavica 1999;100(6):369-376.

240. Min K, Song J, Kang JY, et al. Umbilical cord blood therapy potentiated with erythropoietin for children with cerebral palsy: a double-blind, randomized, placebo-controlled trial. Stem cells (Dayton, Ohio) 2013;31(3):581-591.

241. Dodel R, Spottke A, Gerhard A, et al. Minocycline 1-year therapy in multiple-system-atrophy: effect on clinical symptoms and [(11)C] (R)-PK11195 PET (MEMSA-trial). Movement disorders : official journal of the Movement Disorder Society 2010;25(1):97-107.

242. Stefanescu MR, Dohnalek M, Maderwald S, et al. Structural and functional MRI abnormalities of cerebellar cortex and nuclei in SCA3, SCA6 and Friedreich's ataxia. Brain 2015;138(Pt 5):1182-1197.

243. Jayakumar PN, Desai S, Pal PK, Balivada S, Ellika S, Kalladka D. Functional correlates of incoordination in patients with spinocerebellar ataxia 1: a preliminary fMRI study. Journal of clinical neuroscience : official journal of the Neurosurgical Society of Australasia 2008;15(3):269-277.

244. Akhlaghi H, Corben L, Georgiou-Karistianis N, et al. A functional MRI study of motor dysfunction in Friedreich's ataxia. Brain research 2012;1471:138-154.

245. Georgiou-Karistianis N, Akhlaghi H, Corben LA, et al. Decreased functional brain activation in Friedreich ataxia using the Simon effect task. Brain and cognition 2012;79(3):200-208.

246. Chatterjee G, Chandel R, Kamble P. A rare case of ataxia telangiectasia with intracranial tumor; 2014 April 1, 2014.

247. Meneret A, Ahmar-Beaugendre Y, Rieunier G, et al. The pleiotropic movement disorders phenotype of adult ataxia-telangiectasia. Neurology 2014;83(12):1087-1095.

248. Nagasravani J, Chacham S, Narayan Reddy U, Narsing Rao J, Rao SP, Mahmood A. A rare case of ataxia telangiectasia in a 9-year-old female child. Pediatric neurology 2014;51(4):583-584.

249. Nakayama T, Sato Y, Uematsu M, et al. Myoclonic axial jerks for diagnosing atypical evolution of ataxia telangiectasia. Brain & development 2015;37(3):362-365.

Appendices

Table 2.2. Summary of CT/MRI studies in A-T (not included in Chapter 2)

Reference	Image type (CT/T1/T2/MRI)	Age Range (years)	Gender (M/F)	Major findings
Chatterjee and colleagues[246]	MRI	3	1/0	**Findings:** MRI shows a suprasellar tumour.
Hoche and colleagues[193]	MRI	4.35/14.02^	16/6	**Aims:** to examine neuropsychological changes in young A-T patients. **Findings:** MRI images (1.5T) were available in 14 of 22 patients and were taken in a sedated manner. MRI in the younger age group (average age: 4.35) revealed marked cerebellar atrophy. MRI in the older age group (average age: 14.02) revealed extracerebellar atrophy. Follow-up MRI was available for three patients (Patients 3, 4 and 9: maximum age range between scans 7-12.6 years of age) for retrospective analysis. Individual progress of signal changes and cerebellar atrophy in these three patients were recorded. Vermian atrophy (Patients 3 and 4) and increased signal in the dentate nucleus (Patients 3 and 9), cerebral cortex, red nucleus, substantia nigra (Patient 3),

				caudate nucleus, putamen and thalamus (Patient 9) were reported.
Meneret and colleagues[247]	MRI	N/A*	N/A*	**Findings:** out of MRI data for 12 patients (14 were recorded in this study overall), 10 displayed mild to severe isolated cerebellar atrophy. Patient 6 displayed normal MRI at 25 years of age. Patient 13 did not display cerebellar atrophy at age 20 however a few hyperintense T2 lesions were observed in the cerebral WM (genu of internal capsule and left superior cerebellar peduncle).
Nagasravani and colleagues[248]	MRI	9	0/1	**Findings:** prominent cerebellar folia with mild hypoplasia of the inferior cerebellar vermis.
Nakayama and colleagues[249]	MRI	12	0/1	**Findings:** moderate atrophy of the vermis and cerebellum.

* Ages and genders of patients at examination were not explicitly stated.[247]

^ Average ages of two age groups of patients were listed in the paper.[193]

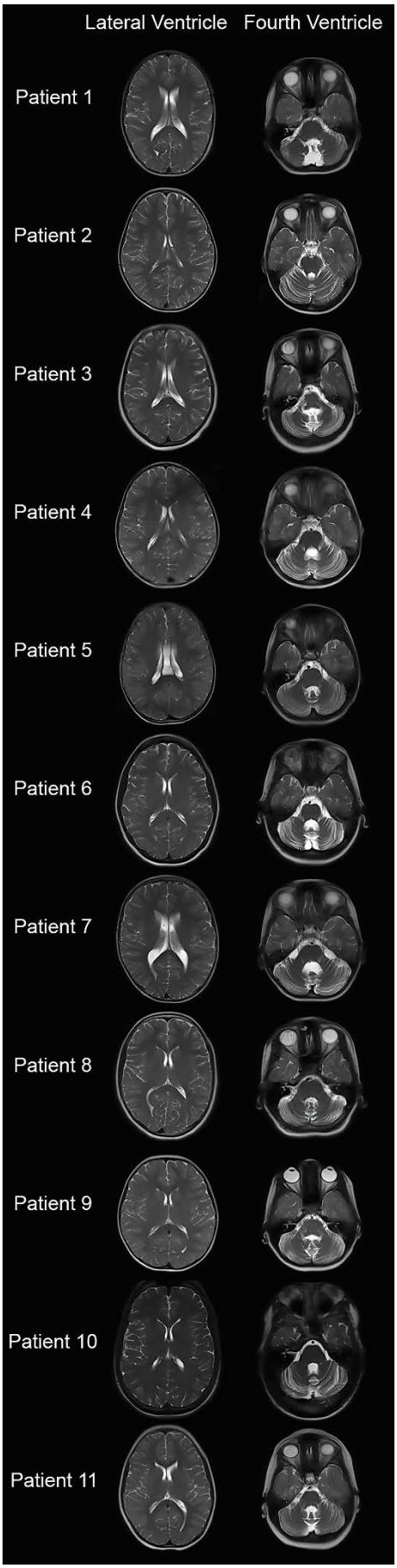
Lateral Ventricle
Fourth Ventricle
Patient 1
Patient 2
Patient 3
Patient 4
Patient 5
Patient 6
Patient 7
Patient 8
Patient 9
Patient 10
Patient 11

Figure 3.4 (Chapter 3). Axial T2-weighted MRI scans of the lateral ventricle and fourth ventricle in numbered ataxia-telangiectasia subjects.

Table 4.1. (Chapter 4) Summary of A-T NEST clinical observations of A-T patients

Patient	Age	Ataxia	Movement Disorder	Symptoms[b]
1	16	**Walking:** 0/6 **Standing:** 0/6	**Bradykinesia:** 2/6 **Hyperkinesia:** 16/16 **Dystonia:** 8/12	**Ataxia:** no support required for sitting but slight swaying is present. Vertical support required for standing and walking. **Movement Disorder:** dystonia in limb posturing is present with either social/cognitive or motor activation. **Neuropathy:** ankle tendon, bicep tendon and knee tendon reflexes are absent. Proprioception in toes are normal.
2	7	**Walking:** 6/6 **Standing:** 4/6	**Bradykinesia:** 3/6 **Hyperkinesia:** 13/16 **Dystonia:** N/A[+]	**Ataxia:** no support required for sitting but slight swaying is present. Sways when standing with feet together. Normal path width without corrective steps is taken with walking. **Neuropathy:** ankle tendon reflexes are absent. Bicep tendon and knee tendon reflexes are present. Proprioception in toes and vibration sense at ankles are present.
3	12	**Walking:** 1/5 **Standing:** 2+/5	**Bradykinesia:** 3.5/8 **Hyperkinesia:** 6/15 **Dystonia:** 10/14	**Ataxia:** sits with self-support of arms. Corrective steps taken when standing. Massive lateral support needed for walking. **Movement Disorder:** Retro-Colic spasms with motor or stance activation are present. Head/trunk posturing/tilt/turn is mild at rest

				and during movement/posture. Trunk posturing/tilt/turn is mild at rest and normal during movement/posture.
4	9	**Walking:** 4/6 **Standing:** 4/7	**Bradykinesia:** 1/6 **Hyperkinesia:** 10/16 **Dystonia:** 7/11	**Ataxia:** sits without support but sways markedly. Standing and walking requires no support but takes wide base or corrective stagger steps. **Movement Disorder:** at rest, distal/hand tremor and proximal (face/head/trunk) tremor is present. **Neuropathy:** proprioception is normal in toes, where movement sensibility is intact.
5	7	**Walking:** 5/6 **Standing:** 6/7	**Bradykinesia:** 2/6 **Hyperkinesia:** 10/16 **Dystonia:** 7/11	**Ataxia:** no support needed for sitting but displays slight/occasional swaying. Sways when standing with feet together. Walks at normal speed without support, with mild path deviations or corrective steps. **Movement Disorder:** at rest, face/head/trunk/distal limb tremor is present.
6	21	N/A[+]	N/A[+]	
7	10	**Walking:** 1/6 **Standing:** 2/7	**Bradykinesia:** 2/6 **Hyperkinesia:** 6/16 **Dystonia:** 8/11	**Ataxia:** no support needed for sitting but displays marked swaying. Standing and walking requires lateral support. **Movement Disorder:** tremor in the face/head/trunk/distal limbs are present with both

				social/cognitive and motor activation. **Neuropathy:** ankle tendon, bicep tendon and knee tendon reflexes are absent.
8	15	**Walking:** 0/6 **Standing:** 0/6	**Bradykinesia:** 1/6 **Hyperkinesia:** 13/16 **Dystonia:** 6/11	**Ataxia:** no support needed for sitting but displays marked swaying. Standing and walking require vertical support. **Movement Disorder:** tremor in the face/head/trunk and dystonia in limb posturing is present with social/cognitive and motor activation. **Neuropathy:** ankle tendon, bicep tendon and knee tendon reflexes are absent. Proprioception in toes have movement sensibility intact. Vibration sense in ankles is present.
9	7	**Walking:** 5/6 **Standing:** 4/6	**Bradykinesia:** 4/6 **Hyperkinesia:** 10/14* **Dystonia:** 8/12	**Ataxia:** no support needed for sitting but displays slight swaying. Sways when standing with feet together. Walks at normal speed without support, with mild path deviations or corrective steps. **Movement Disorder:** head and limb posturing is present with either social/cognitive or motor activation. **Neuropathy:** knee tendon reflexes are present. Ankle tendon reflexes are absent.

				Proprioception in toes is not completely absent.
10	22	**Walking:** 0/6 **Standing:** 0/6	**Bradykinesia:** 2/6 **Hyperkinesia:** 8/16 **Dystonia:** 3/12	**Ataxia:** no support needed for sitting but displays slight swaying. Standing and walking requires vertical support. **Movement Disorder:** at rest, distal limb movement is present. Tremor in the face/head/trunk is present with both social/cognitive and motor activation. Head and limb posturing is present with both social/cognitive and motor activation. **Neuropathy:** ankle tendon, bicep tendon and knee tendon reflexes are absent. Some vibration sense at ankles is intact.
11	8	**Walking:** 2/6 **Standing:** 2/6	**Bradykinesia:** 2/6 **Hyperkinesia:** N/A^{+} **Dystonia:** N/A^{+}	**Ataxia:** no support needed for sitting but displays marked swaying. No support needed for standing however corrective steps are taken. Walking requires some lateral support.
12	10	**Walking:** 4/6 **Standing:** 3+/6	**Bradykinesia:** 2/5* **Hyperkinesia:** 11/16 **Dystonia:** 6/11	**Ataxia:** no support needed for sitting or standing but sways markedly while sitting and requires corrective steps when walking. **Movement Disorder:** Retro-Colic spasms and distal/hand movement are present with either social/cognitive or motor or posture activation.

	Neuropathy: proprioception in toes is present, with rare position errors during clinical task. Plantar responses are normal.

* Clinical tests were incomplete.

+ Clinical scores were absent/not recorded.

Table 4.2. (Chapter 4) Summary of Corticomotor Tract Diffusion Tensor Metrics

Tract		Corticospinal										Cortico-Ponto-Cerebellar									
		Left					Right					Left					Right				
Bin(%)	Condition	N^	FA	SD#	MD	SD#	N^	FA	SD#	MD	SD#	N^	FA	SD#	MD	SD#	N^	FA	SD#	MD	SD#
0	Control	524578	0.32	0.11	0.0006	0.0001	500550	0.32	0.11	0.0006	0.0001	71044	0.31	0.10	0.0006	0.0001	87857	0.32	0.11	0.0006	0.0001
	Patient	176514	0.31	0.10	0.0006	0.0001	126239	0.32	0.10	0.0006	0.0001	98879	0.32	0.10	0.0006	0.0001	83869	0.32	0.10	0.0006	0.0001
5	Control	514884	0.43	0.10	0.0006	0.0001	491897	0.43	0.11	0.0006	0.0001	70175	0.43	0.11	0.0006	0.0001	86754	0.44	0.10	0.0006	0.0001
	Patient	179386	0.42	0.10	0.0006	0.0001	127326	0.43	0.11	0.0006	0.0001	99184	0.43	0.10	0.0006	0.0001	83791	0.44	0.09	0.0006	0.0001
11	Control	517077	0.47	0.09	0.0005	0.0000	493168	0.48	0.10	0.0005	0.0000	70223	0.47	0.11	0.0005	0.0000	86816	0.48	0.10	0.0005	0.0000
	Patient	178179	0.47	0.09	0.0005	0.0000	127663	0.49	0.09	0.0005	0.0000	98930	0.49	0.10	0.0005	0.0000	83772	0.48	0.09	0.0005	0.0000
16	Control	521351	0.47	0.10	0.0005	0.0000	497841	0.48	0.10	0.0005	0.0000	70794	0.45	0.10	0.0005	0.0000	87388	0.45	0.10	0.0005	0.0000
	Patient	178080	0.48	0.09	0.0005	0.0000	126982	0.50	0.10	0.0005	0.0000	99334	0.48	0.11	0.0005	0.0000	84205	0.47	0.10	0.0005	0.0000
21	Control	519892	0.46	0.10	0.0005	0.0000	495681	0.45	0.10	0.0005	0.0000	70559	0.42	0.10	0.0005	0.0000	87265	0.43	0.11	0.0005	0.0000
	Patient	177923	0.48	0.10	0.0005	0.0000	126956	0.49	0.10	0.0005	0.0000	99176	0.46	0.11	0.0005	0.0000	83735	0.43	0.10	0.0005	0.0000
26	Control	517905	0.48	0.11	0.0005	0.0000	494723	0.47	0.11	0.0005	0.0000	70443	0.45	0.11	0.0005	0.0001	87112	0.46	0.11	0.0005	0.0000
	Patient	178506	0.47	0.10	0.0005	0.0000	127540	0.47	0.09	0.0005	0.0000	99277	0.44	0.10	0.0005	0.0000	84152	0.43	0.10	0.0005	0.0000
32	Control	518613	0.56	0.10	0.0005	0.0000	495613	0.55	0.10	0.0005	0.0000	70486	0.51	0.11	0.0005	0.0000	87116	0.52	0.11	0.0005	0.0000
	Patient	177230	0.51	0.10	0.0005	0.0000	126529	0.51	0.10	0.0005	0.0000	98633	0.49	0.10	0.0005	0.0000	83519	0.48	0.11	0.0005	0.0000
37	Control	521073	0.62	0.08	0.0005	0.0000	497154	0.61	0.08	0.0005	0.0000	70727	0.58	0.09	0.0005	0.0000	87411	0.58	0.10	0.0005	0.0000
	Patient	178446	0.58	0.09	0.0005	0.0000	127127	0.57	0.09	0.0005	0.0000	99434	0.56	0.09	0.0005	0.0000	84122	0.56	0.09	0.0005	0.0000
42	Control	521858	0.65	0.07	0.0005	0.0000	497653	0.65	0.07	0.0005	0.0000	70888	0.62	0.08	0.0005	0.0000	87579	0.62	0.08	0.0005	0.0000
	Patient	177992	0.63	0.07	0.0005	0.0000	126885	0.62	0.07	0.0005	0.0000	99257	0.61	0.07	0.0005	0.0000	84199	0.62	0.08	0.0005	0.0000
47	Control	516949	0.67	0.07	0.0005	0.0000	493976	0.67	0.07	0.0005	0.0000	70310	0.62	0.09	0.0005	0.0000	86845	0.62	0.09	0.0005	0.0000
	Patient	178086	0.65	0.07	0.0005	0.0000	127072	0.64	0.07	0.0005	0.0000	98977	0.62	0.07	0.0005	0.0000	83584	0.63	0.08	0.0005	0.0000
53	Control	516429	0.66	0.10	0.0005	0.0000	493878	0.66	0.10	0.0005	0.0000	70179	0.59	0.10	0.0005	0.0001	86869	0.61	0.11	0.0005	0.0001
	Patient	178029	0.62	0.09	0.0005	0.0000	127437	0.61	0.09	0.0005	0.0000	98905	0.59	0.09	0.0005	0.0000	83765	0.61	0.09	0.0005	0.0000

58	Control	521858	0.64	0.12	0.0005	0.0001	497653	0.64	0.12	0.0005	0.0001	70888	0.56	0.12	0.0006	0.0001	87579	0.59	0.13	0.0006	0.0001
	Patient	177992	0.57	0.12	0.0005	0.0001	126885	0.56	0.11	0.0005	0.0001	99257	0.54	0.11	0.0005	0.0001	84199	0.57	0.12	0.0005	0.0001
63	Control	521073	0.62	0.13	0.0006	0.0001	497152	0.60	0.13	0.0006	0.0001	70727	0.51	0.14	0.0006	0.0001	87411	0.54	0.14	0.0006	0.0001
	Patient	178438	0.52	0.13	0.0006	0.0001	127127	0.50	0.12	0.0005	0.0001	99434	0.49	0.12	0.0006	0.0001	84122	0.50	0.13	0.0006	0.0001
68	Control	517220	0.58	0.13	0.0006	0.0001	493667	0.55	0.13	0.0006	0.0001	70278	0.45	0.15	0.0006	0.0001	86898	0.45	0.15	0.0006	0.0002
	Patient	178072	0.52	0.13	0.0006	0.0001	127176	0.51	0.12	0.0005	0.0001	98864	0.49	0.13	0.0005	0.0001	83731	0.47	0.13	0.0005	0.0001
74	Control	519299	0.49	0.12	0.0005	0.0001	496665	0.50	0.12	0.0005	0.0001	70650	0.37	0.13	0.0006	0.0002	87330	0.33	0.13	0.0006	0.0002
	Patient	177594	0.50	0.12	0.0005	0.0001	126893	0.51	0.11	0.0005	0.0001	99046	0.46	0.13	0.0005	0.0001	83934	0.43	0.12	0.0005	0.0001
79	Control	519892	0.41	0.10	0.0005	0.0001	495681	0.41	0.10	0.0005	0.0001	70559	0.32	0.10	0.0006	0.0002	87265	0.29	0.09	0.0006	0.0002
	Patient	177923	0.43	0.10	0.0005	0.0001	126956	0.44	0.09	0.0005	0.0001	99176	0.38	0.11	0.0005	0.0001	83727	0.34	0.10	0.0005	0.0001
84	Control	521351	0.37	0.09	0.0005	0.0001	497841	0.36	0.09	0.0006	0.0001	70794	0.34	0.10	0.0006	0.0001	87388	0.35	0.11	0.0006	0.0001
	Patient	178080	0.36	0.08	0.0005	0.0001	126982	0.38	0.09	0.0005	0.0001	99334	0.33	0.09	0.0005	0.0001	84200	0.33	0.10	0.0005	0.0001
89	Control	518471	0.35	0.09	0.0006	0.0001	495110	0.34	0.09	0.0006	0.0001	70430	0.39	0.11	0.0005	0.0001	87028	0.39	0.13	0.0006	0.0001
	Patient	177283	0.30	0.06	0.0006	0.0001	127016	0.34	0.11	0.0006	0.0001	98699	0.34	0.08	0.0005	0.0001	83556	0.36	0.09	0.0005	0.0001
95	Control	513490	0.32	0.08	0.0007	0.0001	489955	0.31	0.09	0.0007	0.0002	69968	0.49	0.14	0.0005	0.0001	86479	0.49	0.15	0.0006	0.0002
	Patient	180281	0.28	0.07	0.0006	0.0001	127971	0.29	0.08	0.0006	0.0001	99415	0.41	0.12	0.0006	0.0001	84002	0.40	0.13	0.0006	0.0002
100	Control	524578	0.34	0.09	0.0007	0.0001	500550	0.33	0.09	0.0007	0.0001	71044	0.57	0.13	0.0005	0.0001	87857	0.57	0.13	0.0005	0.0001
	Patient	176514	0.30	0.09	0.0007	0.0002	126239	0.32	0.10	0.0007	0.0002	98879	0.50	0.14	0.0005	0.0001	83869	0.48	0.13	0.0006	0.0002

^ ‘N’ refers to number of values sampled in each tract.

‘SD’ refers to Standard Deviation.

‘FA’ and ‘MD’ refers to average Fractional Anisotropy and Mean Diffusivity across all control participant/patient ages respectively.

‘Bin(%)’ refers to percentage of tract along the length of the target pathway.